Alenia
AEROSPAZIO
Space Division

Daimler-Benz Aerospace

Mercury Cornerstone

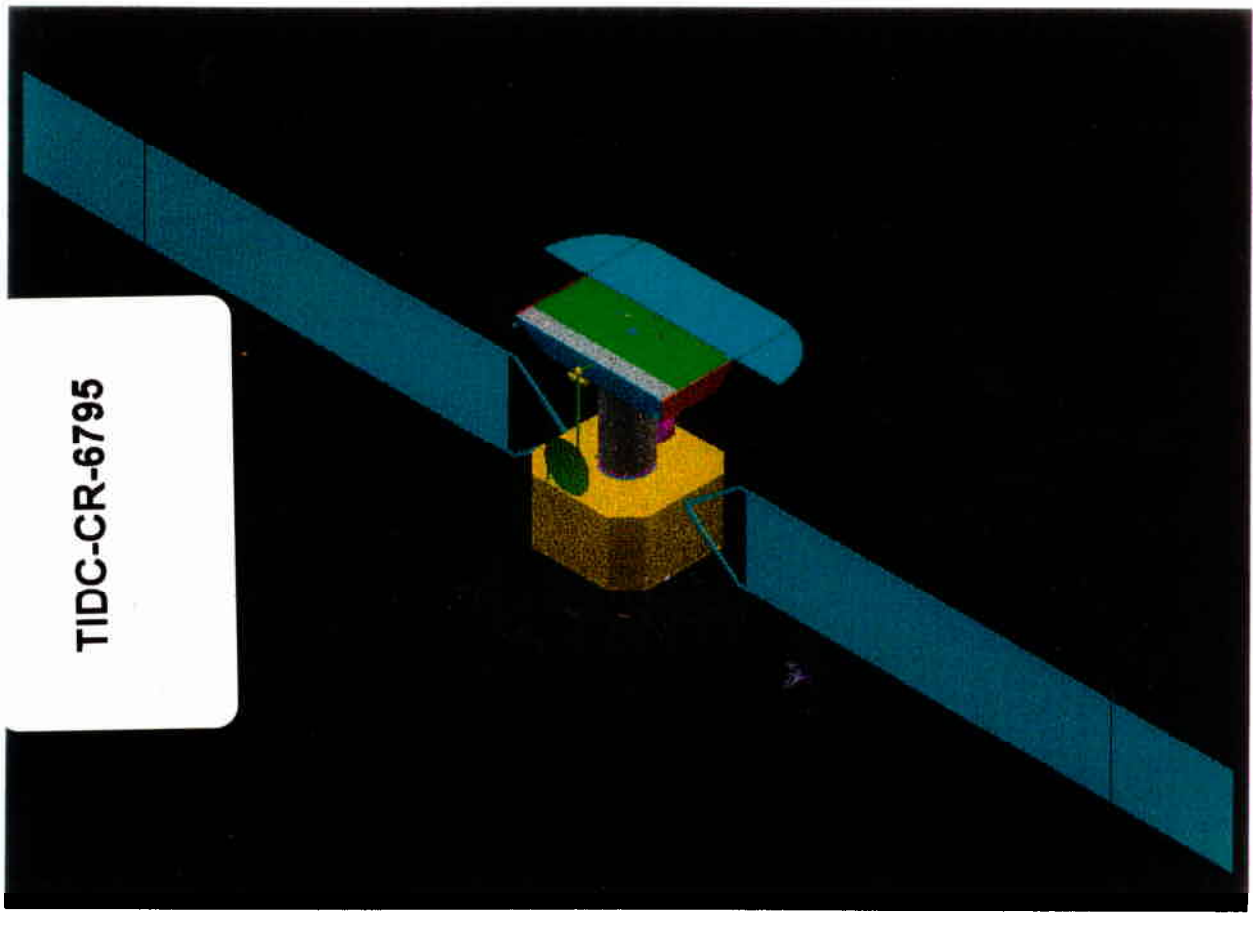

TIDC-CR-6795

System and Technology Study
Phase 1 Summary Report

ESA Contract 12559/97/NL/MS

ESTEC Study Manager: George E.N. Scoon
Alenia Study Manager: Alberto Anselmi

SD-RP-AI-0262 - November 1998

REPORT

TITLE : MERCURY CORNERSTONE SYSTEM AND TECHNOLOGY STUDY
PHASE 1 SUMMARY REPORT

DRL Item or D.R.D. No :

SIGNATURES AND APPROVALS ON ORIGINAL

PREPARED: STUDY TEAM

CHECKED : A. ANSELMI

APPROVED:

AUTHORIZED: I. BARRACO

APPROVALS:

STUDY MANAGER A. ANSELMI

DATA MANAGEMENT:

DOCUMENT CHANGE RECORD

ISSUE-DATE	REASONS FOR CHANGE	AFFECTED PARAGRAPHS
01 – 09 Nov. 1998		

TABLE OF CONTENTS

1. INTRODUCTION AND PHASE 1 OBJECTIVES

1.1 Scope of the System Study

This document provides a summary of the work performed as part of Phase 1 of the Mercury Cornerstone (MCS) System and Technology Study.

The Mercury Cornerstone is a mission to planet Mercury, under study by ESA as part of the Horizon 2000+ scientific programme plan, designed to improve our understanding of the planet and its surroundings by a wide variety of techniques, from remote sensing to particle and field detectors, as well as to conduct fundamental physics experiments by radio science.

The Mercury mission has already been addressed by ESA in a number of studies based on a ballistic transfer and a spinning satellite [Ref. 1, 2]. After the mission was included in the Cornerstone class, a new scenario characterised by transfer by electric propulsion delivering multiple satellite modules to Mercury orbit was developed [Ref. 3]. The principal features of the new mission scenario are :

- the cruise to Mercury will be executed by electric propulsion
- the Mercury Orbiter will be based on a three-axis stabilised platform in a low-altitude circular orbit, performing remote sensing experiments with high pointing accuracy
- the particle and fields experiments will be based on a separate spinning Subsatellite, released from the cruiser/Orbiter into a convenient eccentric orbit
- a Surface Package will be accommodated, to be released from the Cruiser/Orbiter to penetrate or land on Mercury.

The objective of the current study is to investigate this new scenario in greater detail, with particular regard to the design of the Electric Propulsion Stage and the thermal control of the 3-axis stabilised Mercury Orbiter [Ref. 4].

The overall study objectives are as follows.

- Establish the **feasibility of a large electric propulsion stage**, providing ≈ 1 N thrust to achieve transfer from Earth orbit to Mercury orbit in a time span of about two years. This task requires a feasibility study of both (a) the **thruster system**, with issues of thruster durability and reliability, thruster system configuration, and design of the electric power conditioning equipment, and (b) a large **solar array**, capable of providing on the order of 10 kW power near Earth, and operating in such diverse environments as deep space (in the cruise phase) and the vicinity of the sun and Mercury. Task (b), in turn, must address issues ranging from **solar cells** capable of providing high efficiency up to very high temperatures, to the design of panels capable of withstanding the harsh Mercury environment.
- Establish the feasibility of controlling the adverse environment at Mercury, with special regard to the very large thermal inputs from the sun (over 10 times the Solar Constant at 0.3 AU distance) and the planet (albedo and IR fluxes). In particular, the study must identify a **thermal design** capable of sustaining the experiment and systems operation on the 3-axis stabilised Orbiter platform (and the Subsatellite), and establish the required advances in thermal control technology and equipment. The high **radiation threats** and the effects on the solar cells and electronic equipment are another major subject of the environmental control.
- As a pre-requisite to the above, identify a **system configuration and operation principles** that will facilitate as much as possible the tasks of the thermal control, as well as meeting the payload and system requirements. An example is the attitude law in Mercury orbit, that must be designed so that enough radiating area is protected from the sun's and planet's radiation at all times, in order that heat can be rejected efficiently, while meeting constrains from the payload (e.g. viewing directions) and on-board equipment (e.g. antenna pointing at the Earth).

- Establish the feasibility of the particles and fields experiments, with their requirements of high **magnetic and electro-magnetic cleanliness**. In recognition of this challenge, these experiments are the payload of a separate Subsatellite, which makes the cleanliness tasks possible. Nevertheless, cleanliness requirements have a bearing on the global system design, as the experiments must share the Cruiser/Orbiter environment on the ground and during the cruise, to an extent that must be studied.
- Devise a realistic **mission profile**, ensuring that the multiple scientific goals are accomplished while meeting the various system and technology constraints as they will have been defined in the above studies. As part of that task, due account must be taken of the specific mission autonomy and protection concepts, appropriate to a planetary mission.
- Finally, produce **reference system architecture and subsystem designs**, to the extent necessary to establish a realistic programme planning and the associated cost estimate.

1.2 Objectives of Phase 1

The objectives of Phase 1 were as follows.

1) Develop a **reference mission profile**, including the cruise, approach, and operational orbits, incorporating the electric propulsion in a realistic and feasible scenario
2) Consolidate the understanding of the **reference payload** interface and operation requirements
3) Develop the design of the **electric propulsion stage,** comprising suitable thrusters and solar array
4) Develop design principles for **environment control in Mercury orbit,** with particular regard to thermal control of the 3-axis Orbiter and the spinning Subsatellite, as well as radiation control
5) Establish a **Reference system configuration & architecture**, comprising configuration of spacecraft elements (cruise stage, 3-axis Orbiter, Subsatellite, Hard Lander), attitude and communications strategies, and system block diagram, in order that the Phase 2 detailed design exercise can proceed on a solid basis.

1.3 Study Team and Study Plan

The study team includes Alenia and DASA with the responsibilities shown in Fig. 1.3-1. Moreover, consultancy contracts were started with CISE and ASE on the subject of solar cells and with SEP and MMS-UK on the subject of electric thrusters. For this report, DASA contributed chapters 3.2, 6-7-8-9, and 11; the remaining chapters were written by Alenia. The contributions of the consultants are included in the contents of the corresponding chapters.

The study was started on March 15, 1998 and, as is customary in ESA feasibility studies, is divided into three phases. Phase 1 was devoted to high-level system trade-offs, developed to the extent that a viable system architecture is proposed and critical technologies are identified. Phase 2 is to develop the selected architecture, with particular regard to the critical areas identified in Phase 1. Phase 3 will consolidate the programme plan and the cost estimate, already outlined in Phase 2, again with particular regard to critical areas and new technologies. Fig. 1.3-2 shows the overall study logic and Fig. 1.3-3 shows the current programme schedule.

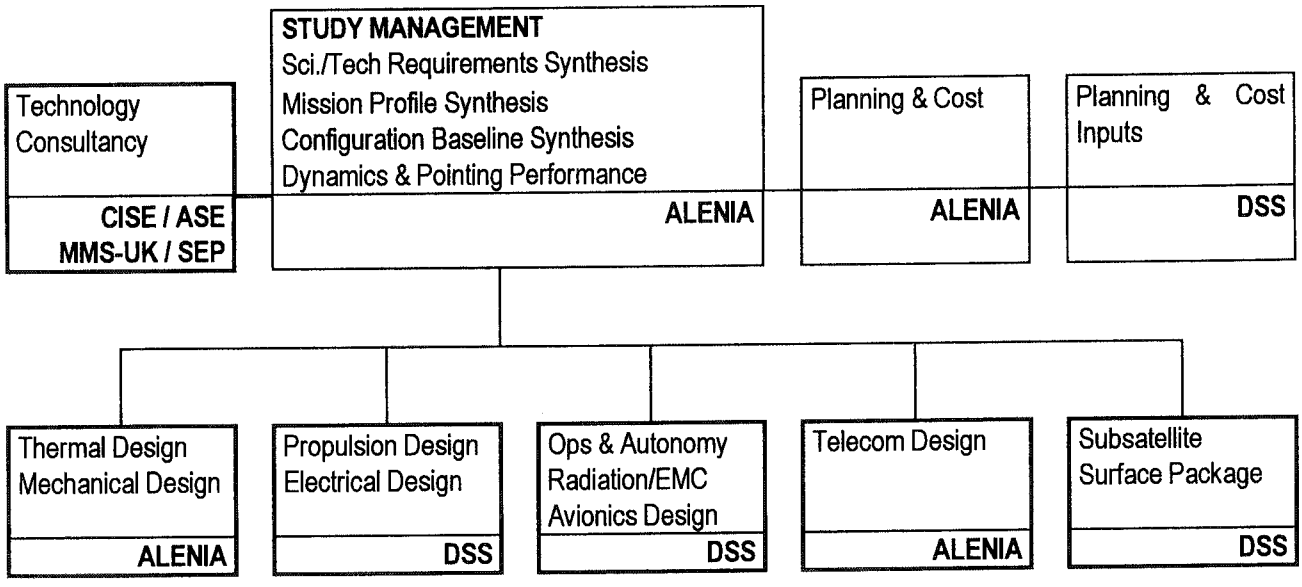

Figure 1.3-1 Task sharing and responsibilities

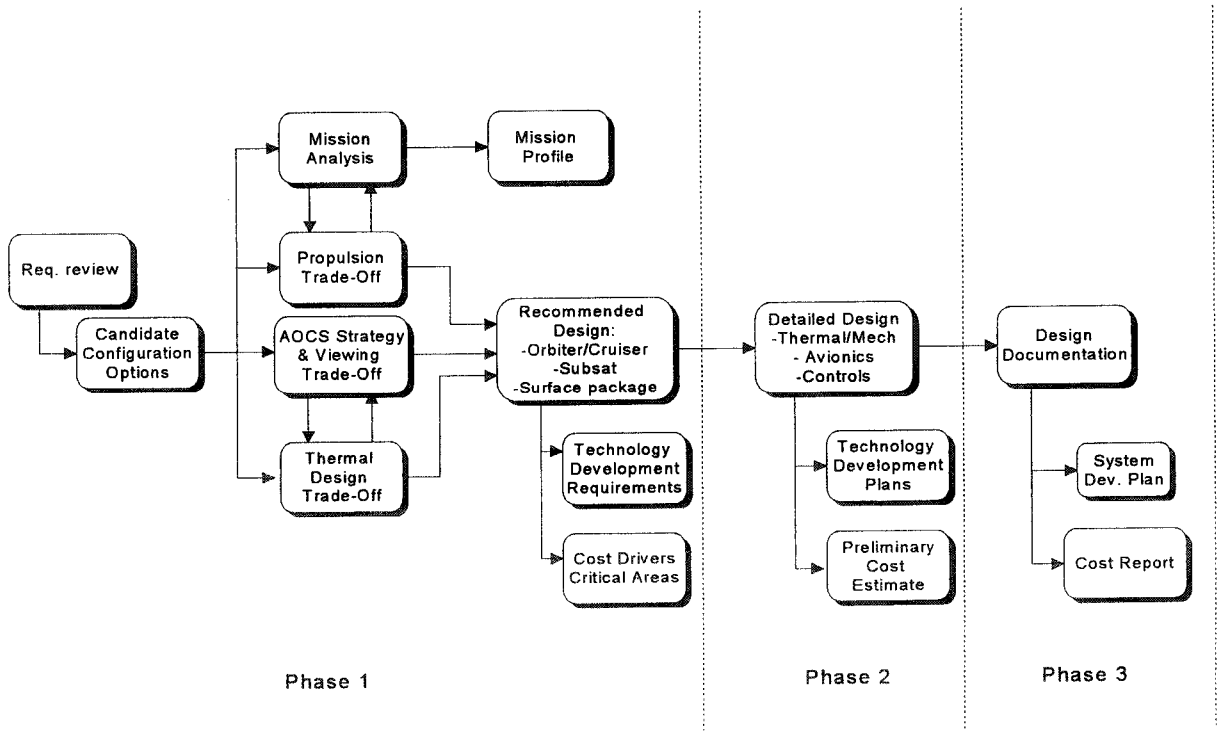

Figure 1.3-2 Overall Study Logic

	March	April	May	June	July	August	Sept.	Oct.	Nov.	Dec.	Jan.	Feb.	March	April
Meetings & Reviews	∇ KO 12.3	∇ PM1 30.4	∇ WM1 28-29.5	∇ SAG 8.6	∇ PM2 1-2.7		∇ PM3 & SAG 8-10.9	∇ Phase 1 Review 15.10	∇ Phase 2 ATP 2.11	∇ PM4 17.12	∇ PM5 28.01	∇ PM6 26.02	∇ Phase 2 Review 30.03	∇ EOC 30.04
PHASE 1														
Payload Assessment														
Mission Profile														
Cruiser/Orbiter Trades														
Subsat / Surface Package														
PHASE 2														
Cruiser/Orbiter Design														
Subsat / Surface Package														
System Analysis & Perf.														
Prel. Planning & Cost														
PHASE 3														
Design Consolidation														
Cost & Schedule Report														

Fig. 1.3-3 Study Schedule

2. PHASE 1 TRADE-OFF OVERVIEW

The principal trade-offs performed in Phase 1 are summarised below. Motivations are given in summary form, and further details can be found in the dedicated chapters. The main issues addressed were:

- Strategy for the interplanetary cruise and the approach to Mercury
- Characteristics of the planetary orbits
- Solar array designs and global satellite system configuration
- Orbiter attitude strategy
- Telecommunication frequency bands.

2.1 Interplanetary cruise and Approach to Mercury

Following Ref. 4, in the first part of the study a strategy was addressed in which the cruise and the Mercury approach would be entirely done by electric propulsion. The basic motivation for this strategy is to relax the launch window constraints: four weeks per year are available for this option. The mission analysis [Ref. 5] produced five reference cruise trajectory designs, which can be approximated, in terms of propellant mass versus specific impulse, by the rocket equation with $\Delta v = 18$ km/s as shown in Fig. 2.1-1. It is apparent from the figure that the huge Δv required would lead to a propellant mass fraction (even before accounting for the tankage factor, another 15 to 20%) of at least 50% for a specific impulse of at least Isp = 3000s. Indeed, significantly higher specific impulses were postulated to reach a reasonable mass fraction. This would produce a design dominated by the propulsion, and would exclude all electric thruster designs with a lower specific impulse, among them the SPT thrusters, a strong contender for development in the commercial market. Moreover, the thrusting times required [Ref. 5] would in all cases exceed the current lifetime limits of the thrusters (some 10,000 hours for ion thrusters with grids, and 6,000 hours for stationary plasma thrusters), leading to a configuration in which all thrusters would have to be doubled for reasons of degradation (deterministic failure), while more thrusters would have to be added for redundancy (random failure).

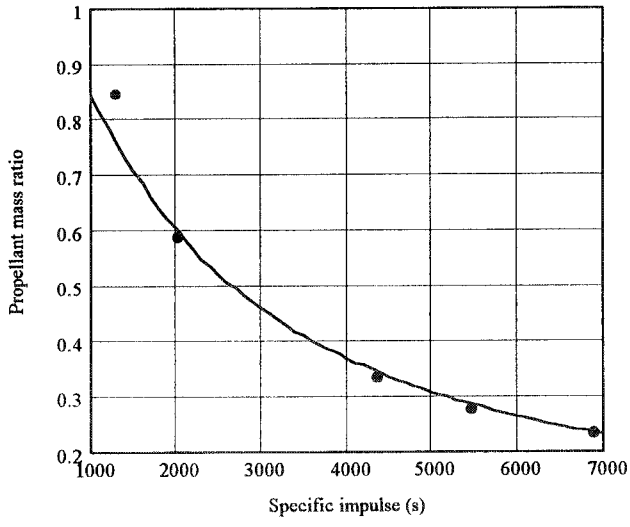

Fig. 2.1-1 All-electric propulsion reference cases

Given the forced selection of ion thrusters with grids, the power demand would be high, leading to the need for installing solar arrays delivering at least 20 kW at 1 AU. Such large solar arrays would be extremely difficult to design for environmental conditions encompassing extremes ranging from deep space at 1 AU to the vicinity of the planet at Mercury perihelion (0.3 AU). This argument is developed in section 2.3 below.

The cost to the ESA scientific programme of an all-electric propulsion option was estimated to be very large, since both the thrusters and the solar array would be special designs for the Mercury mission.

A much more realistic design option emerged when solutions for the interplanetary cruise were found incorporating gravity assists by Venus and Mercury [Ref. 6]. The price to pay is a narrower launch window (2 weeks per year), but (a) the propellant mass fraction is reduced to about 30%, (b) the mission is compatible with thrusters with specific impulse from 2000s upwards, and (c) the thrust time is in each case compatible with the thruster lifetimes. Note that in the case of the ion thrusters with grids, the specific impulse postulated was still very high (4700s).

The difficulty remained of having the cruise solar array function in the vicinity of Mercury, at least as long as it is needed to deliver the Subsatellite and Orbiter to their destination orbits. The low thrust characteristic of the electric thrusters makes the planetary manoeuvres extremely slow, particularly when the destination orbit is near-circular, as is the case of the Orbiter, so that the manoeuvre time would encompass at least a full Mercury year, with solar flux increasing from Mercury aphelion to Mercury perihelion. As the strategy for keeping the solar array temperature reasonably low is based on progressively increasing the solar aspect angle (see chapter 9.3), the Mercury perihelion case leads to impossibly steep solar aspect angles or, if a maximum SAA is postulated, does not permit the array to reach low planetary altitudes (Fig. 2.1-2).

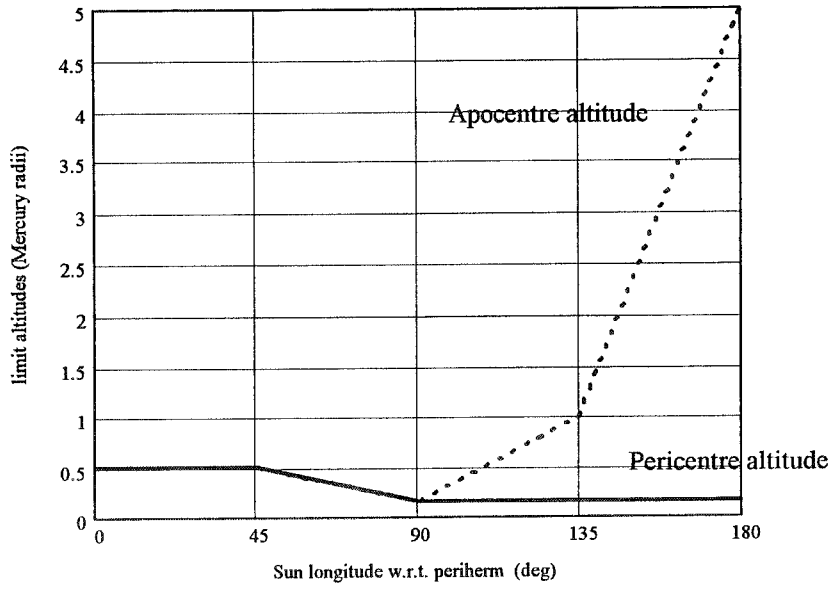

Fig. 2.1-2 Minimum permitted altitude of the Cruiser solar array. The spacecraft orbit around Mercury is in a plane perpendicular to Mercury's orbit plane, and the pericentre lies in the direction from planet to sun when Mercury is at aphelion. λ is the longitude of the sun in Mercury's orbit plane counted from the pericentre; when $\lambda = 0$ the subsolar point is directly under the pericentre and r = 0.467 AU; when $\lambda = \pi$ the subsolar point is under the apocentre and r = 0.308 AU (perihelion).

The above figure should be understood as follows. Assuming that:

- the Cruiser solar array has a limit temperature of 150°C with a tolerance of 10°C;
- temperature control is done by rotating the array away from the sun, and the solar aspect angle β cannot be greater than about 65°
- the solar array does not have any other degrees of freedom, therefore, depending on λ, β and the position on the orbit θ, the array can receive planetary radiation from the back (the most dangerous situation) as well as from the front;

then, at $\lambda = 0$ the planet is at the maximum distance from the sun and the spacecraft approaches Mercury at the maximum permitted temperature (T = 150°C) with $\beta < 65°$. The worst case for the planet irradiance is the periherm; the array is rotated up to $\beta = 65°$ (to lower the solar heat input) and the minimum altitude at which the planetary flux permits Tmax < 160°C is about 1200 km. About the same situation holds at $\lambda = 45°$ (subsolar point moves from below pericentre but distance to sun gets smaller). At $\lambda = 90°$ the planetary flux seen by the array is small throughout the orbit and a circular orbit at 400 km is possible. As $\lambda = 180°$ is approached, the pericentre gets cold (eventually in the shadow) but the apocentre gets hot; in addition, the array arrives at Mercury already at the maximum temperature with the maximum solar aspect ($\beta = 65°$). Therefore the planetary flux that can be withstood is very small and the limit temperature is reached already at 5 radii (with $\beta = 72°$).

The situation sketched above (slow manoeuvres in an extreme environment for a temperature-limited solar array) prompted yet another variation of the mission profile, in which the capture and insertion manoeuvres are performed by a dedicated, chemical (bi-propellant) propulsion stage [Ref. 7]. The advantages of this option are very significant:

- the propellant mass fraction becomes $\approx 25\%$
- the specific impulse is compatible with that of any commercial thrusters
- the thrust time is less than the thruster lifetime making possible a configuration with 3+1 (or 3+2) 200 mN thrusters
- the power demand ranges from 10 kW (ion thrusters with grids) to 6.5 kW (SPT thrusters), compatible with commercial (GEO) solar array designs
- the cruise solar array can be optimised for the interplanetary environment only.

This option was considered to be the less expensive of all, since all building blocks (electric propulsion, chemical propulsion, solar array) can be inherited from commercial designs with minor modification. The arguments on the solar array and the chemical propulsion stage naturally lead to a jettisonable Cruiser stage (see chapter 2.3 below).

Hence the solution with electric propulsion + gravity assists + chemical capture was recommended for the Phase 2 baseline.

2.2 *Characteristics of the planetary orbits*

The definition of the planetary orbits has important impacts on the propulsion, the telecommunications, and the environment. The thermal environment is the overriding concern, since the closer the orbit is to the planet, the larger the IR flux the thermal design has to contend with.

Generic scientific requirements on the orbit selection are as follows.

For the Subsatellite, a polar, highly eccentric orbit is demanded in order that the magnetosphere can be explored from an altitude of a few hundred kilometres up to several planet radii. Because of the sun's third-body attraction, such an orbit is not stable: at first order, the eccentricity will change secularly according to [Ref. 8]:

$$\Delta e = \frac{15}{8}\frac{\mu_S}{a_p^{\,3}} e \frac{\sqrt{1-e^2}}{n} \sin(2\omega)\sin^2(i)$$

where Δe is the eccentricity variation per orbit period, μ_S is the gravitational parameter of the sun, a is the semi-major axis of Mercury's orbit, e, i and ω are the eccentricity, inclination and argument of pericentre of the satellite's orbit and n its mean motion. An assumption of $\omega = 0$ (line of apsides in the equatorial plane), which makes the orbit stable, was considered acceptable for the science. The nominal altitude of periherm was taken as hp = 400 km, while for the apoherm several altitudes were considered. Table 2.2-1, column 2 shows the orbit parameters eventually adopted for the Subsatellite study.

For the 3-axis Orbiter, the original requirements called for a polar, circular orbit. Ideally, an ability to change the altitude during the mission would be desired, in order that the planet can be mapped first globally, at high altitude and low resolution, and then at low altitude and high resolution in areas selected from the first survey. This was the rationale for the mission profile with several orbit change manoeuvres originally proposed in Ref. 3. When it became clear that a capability for orbit changes could not be sustained, a number of options were explored:

Circular orbit at 1000 km altitude. This orbit was proposed for the relatively benign thermal environment, but it would not permit high-resolution observations. Moreover, a circular orbit with constant nadir pointing attitude (see chapter 2.4) was shown to require two-axis, wide-angle articulation of the high-gain antenna. In an attempt to simplify the antenna articulation, a high eccentricity orbit was proposed.

Eccentric orbit, 400 x 4200 km. With a high enough apoherm, the IR flux is sufficiently reduced by the $1/r^2$ effect that the satellite can be safely turned into an attitude with one axis perpendicular to the ecliptic. Then, 1 rotational degree of freedom is sufficient to point the HGA at the Earth in any situation.

This orbit would permit both high-resolution observations (from periherm) and global mapping (from apoherm). However, since the rotation of the periherm is not permitted (natural J2 effects are too small, and propellant cost of an active rotation are too high), high-resolution mapping would not be possible for the polar regions (as in the case of the Subsatellite, the line of apsides has to be close to the equator for stability reasons). Moreover, this orbit was shown to be incompatible with the gravity field experiment. Therefore, this option was dropped.

Eccentric orbit, 400 x 1500 km. This orbit was eventually adopted as a compromise between the conflicting requirements of global mapping, high resolution mapping, and gravity field determination. This choice does mean that two-axis articulation of the high-gain antenna has to be implemented.

Table 2-1, column 3 shows the orbit parameters eventually adopted for the Orbiter.

	Subsatellite	Orbiter
Apoherm altitude	12, 200 km (= 5 R_M)	1500 km
Periherm altitude	400 km	400 km
Semi-major axis	8737 km	3389 km
Eccentricity	0.675	0.162
Inclination	90°	90°
Argument of pericentre	0°	0°
Period	9.6 hours	2.32 hours
Maximum duration of eclipse	118 minutes	42 minutes
Inertial direction of pericentre	Pericentre at local noon when Mercury at aphelion	Pericentre at local noon when Mercury at aphelion

Table 2-1 Elements and characteristics of the selected satellite orbits [R_M = 2439 km]

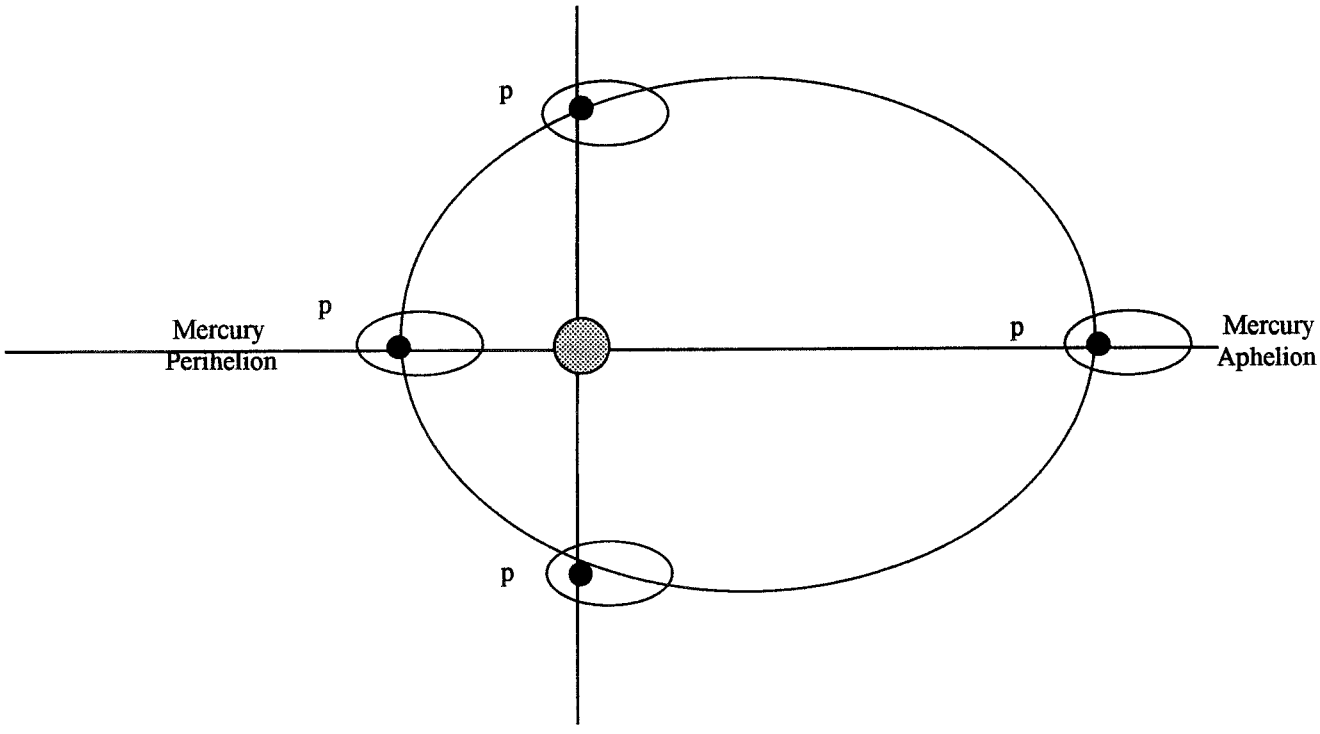

Fig. 2.2-1 Pericentre at local noon when Mercury at aphelion. For clarity, the satellite orbit plane has been rotated into Mercury's orbit plane

An important consideration concerns the direction of pericentre in a sun-centred inertial frame.

Natural perturbations will not change the direction of pericentre appreciably for a time span of about 1 year. For eccentric orbits with the line of apsides in Mercury's orbit plane, the most benign situation from the point of view of the heat fluxes is that in which the pericentre is at the subsolar point (local noon) when Mercury is at aphelion (Fig. 2.2-1). In that way, the worst cases (worst case for IR flux, when the satellite is at periherm; worst case for solar flux, when Mercury is at perihelion) do not sum up. This solution imposes a constraint on the arrival conditions at Mercury, which was shown compatible with the mission design [Ref. 7]. Thus, it was adopted as a boundary condition for both the Orbiter and the Subsatellite.

2.3 Solar array and global satellite system configuration

The original concept of the Mercury spacecraft was that of a large satellite with integral electric propulsion module, functioning all the way from Earth orbit to Mercury orbit, plus an ejectable Spinner [Ref. 3]. The motivation for such an approach was the flexibility a large propulsion module would give to orbit manoeuvres around the planet. However, it was recognised early that the huge range of variation of the environmental parameters, from near-Earth space to deep space to near-Mercury space with its extreme thermal environment, would make an all-encompassing design extremely demanding, if possible at all (with the corresponding cost impact).

The main element whose design must be radically different in deep space and in the vicinity of Mercury is the solar array. A complete discussion is in Chapter 9; here a brief summary is given. The main reasons are:

1. The required array size in the two mission phases ranges from several tens of m^2 in the cruise, to order of 1 m^2 in Mercury orbit
2. The solar array for the cruise - until capture by Mercury - can be standard technology; hence the design can be derived from commercial GEO designs with minor modification and a small cost impact. On the contrary, the array for the Mercury orbit needs special provisions (large OSR fraction, metallic substrate, HT cells), whose application on the large cruise array is not possible. Hence, an array for all seasons is not feasible.
3. The Orbiter array can be made in multiple fixed array sections, while the cruise solar array needs 1 rotational degree of freedom.

Further areas where requirement conflicts arise, because of the different environments and satellite design requirements, include the thermal design and the AOCS.

Attitude control :

4. Very large cruise array wings would interfere with the instruments FOV in Mercury orbit
5. Very large cruise array wings have very low normal modes (< 0.1 Hz) and produce large solar radiation pressure torques. In Mercury orbit, where high accuracy attitude control is required, special provisions would be needed (frequency notching) leading to high computational burden and robustness concerns; moreover, the low disturbing acceleration requirements of the payload accelerometer would not be guaranteed.

Thermal control :

6. The thermal design in Mercury orbit needs special provisions (HT insulation all over the spacecraft except radiator and instrument apertures, IR shield) that would be difficult to reconcile with the demands of the large propulsion stage (heat leaks from thruster nozzles, and their thermal protection; view factors of large array to the IR shield and radiator).

The above consideration led to a new concept, in which the electric propulsion is accommodated in a dedicated module (Electric Propulsion Stage, or Cruise Module) that is jettisoned on arrival at Mercury.

In that way, both the Cruise Module (thrusters and solar array) and the Orbiter designs can be optimised, in terms of power demand, viewing, attitude and attitude control, for coping with, respectively, the deep space environment and the planetary environment. Furthermore, the design developed for the Orbiter array is applicable in the Subsatellite too. The price to pay is the duplication of power equipment in the Cruiser and Orbiter, the appearance of an additional separation interface, and the giving up of the ability to perform large orbital manoeuvres around Mercury.

The arguments in favour of another, chemical propulsion module specialised for planetary insertion and orbit acquisition have been summarised in Chapter 2.1. Again, a trade-off arises: chemical propulsion module integral with the Orbiter versus an expendable module. The reasons favouring an expendable module are again related to the Orbiter thermal control, that demands a special design without extraneous sources of heat, and to the concerns about the durability of the bi-propellant under high heat fluxes.

The final choice was thus that of a modular design of the Satellite with:

- Electric propulsion stage for the cruise, jettisoned before Mercury capture
- Chemical propulsion stage, jettisoned after capture and acquisition of the Subsatellite orbit (one burn) and Orbiter orbit (second burn)
- 3-axis Orbiter, performing remote sensing and acting as communications relay for the other science elements
- spinning Subsatellite, performing particle-and-field experiments
- Surface Package, accommodated on the Orbiter and deployed to an impact trajectory targeted for an area close to one of the poles.

2.4 *Orbiter attitude strategy*

The 3-axis Orbiter attitude is intimately related to the thermal control: the attitude strategy in Mercury orbit must be that making the task of the thermal control as easy as possible. There are two sources of heat, the sun and the planet IR radiation, whose magnitudes are comparable in the worst cases (the equivalent of about 10 solar constants, in the visible and IR bands, at the perihelion and at the subsolar point). To manage this enormous heat load, the attitude strategy must provide at least one surface free from sun and planet IR radiation, where a large radiator can be located. Another important consideration is simplicity of the implementation: we want an attitude law that is simple and robust, avoiding, if possible, complex rotations of the satellite as a whole and/or of parts of it, in order that the safety of the satellite is not put in danger by small deviations from the correct attitude.

A number of strategies were proposed, prior to and during Phase 1 of the study:

1. Nadir pointing with yaw steering
2. Dual spinner
3. Time sharing of Nadir pointing and inertial pointing
4. Nadir pointing all the time.

1. Nadir pointing with yaw steering (Fig. 2.4-1a)

This attitude law was proposed in Ref. 3. The idea is to make one side of the satellite (+Z) point at the Nadir all the time, while another rotation is executed around the Z axis (yaw steering) to keep the unit vector of the +Y side always parallel to the direction of the sun. In this way (and if an additional rotation – by π radians about Z - is executed twice per Mercury year) there is one side always in the shadow of the sun (-Y) and two sides ($\pm$X) with the sun at zero incidence. This proposal solves the sun problem (but not the planet problem) and permits to implement a solar array in two wings with 1 rotational degree of freedom (around $\pm$ X). The disadvantages, however, are numerous:

- the Nadir view rotates in the experiments' field of view (not compatible with a line-scan camera)
- the high gain antenna needs two axis articulation
- the rotation rates of both the array and the antenna are continuously variable and they become very large as the sun (the earth) approaches the orbit plane: indeed the law becomes singular when the sun (earth) is in the orbit plane
- the yaw rotation affects any concept for an IR shield, whose view to the planet would change continuously too
- the attitude law is definitely not simple.

The above mentioned disadvantages prompted consideration of another strategy, put forward in the Contractor's proposal:

2. Dual Spinner (Fig. 2.4-1b)

In this concept, the satellite would be made up of two modules: a despun platform, orientated nearly-inertially, with two sides always parallel to Mercury's orbit plane, and platform rotating at the orbit rate. The high gain antenna and solar array would be placed on the despun platform and they would require 1 rotational degree of freedom only; the instruments would be placed on the other platform on the side facing the Nadir.

This solution has one side always in the shadow of the sun (-Y on the rotating platform) and the nadir pointing side could carry an IR shield much as is proposed in solution 4 below. A significant advantage is that the rotation rates required (despin; solar array pointing mechanism; antenna pointing mechanism) are small and near-constant. However, signals, power and heat (since the despun body has no side where a radiator can be placed) would have to be transferred across the contactless despun interface; in particular, no simple and efficient solution was found for the heat transfer problem. This problem kills, for practical purposes, an otherwise attractive solution.

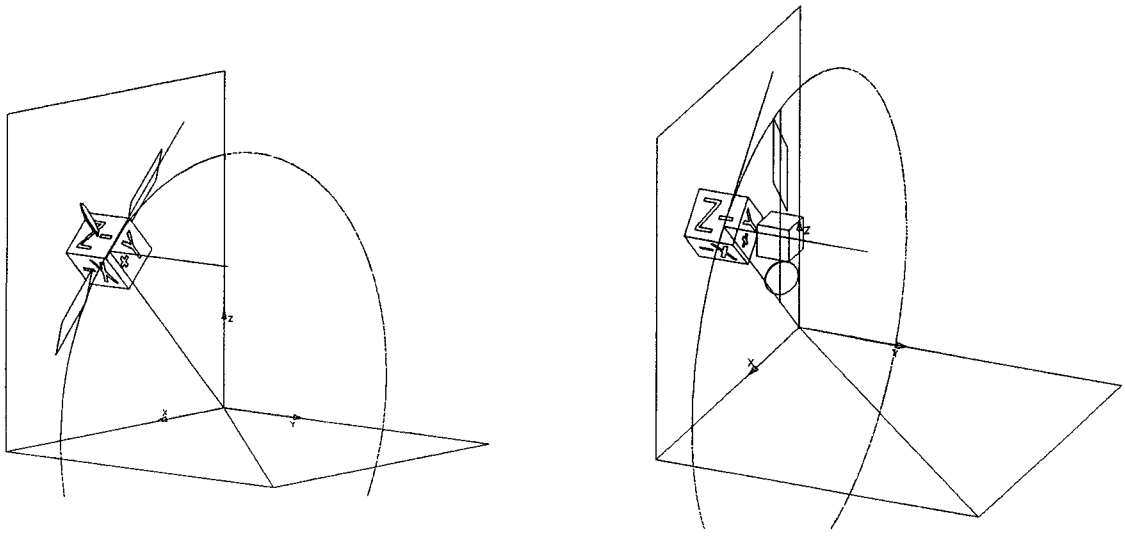

(a) Nadir pointing with yaw steering

(b) Dual Spinner

Fig. 2.4-1a/b Attitude strategies

3. Time sharing of Nadir pointing and inertial pointing

A simplification of the antenna pointing mechanism is possible if the nadir rotation can be halted for the time required for the communications. However, to safely turn the spacecraft away from its safe attitude (w.r.t. planet heat fluxes), the distance to the planet must be sufficiently high that the IR flux is made relatively harmless. Hence, solution 3 can only be proposed if a highly eccentric orbit is accepted; then, the periherm portion of the orbit would be used for observations and the apoherm portion for telecommunications. Two large slew manoeuvres per orbit would be required. This solution was discarded for incompatibility with some experiment requirements, as discussed in section 2.2.

4. Nadir pointing all the time (Fig. 2.4-1c)

The solution eventually proposed for detailed study in Phase 2 is the simplest of all, i.e., Nadir pointing throughout the orbit. This solution allows to accommodate a large IR shield on one side of the spacecraft, realising one radiator side free from sun and planet illumination (with a whole-body rotation about the radial direction twice per Mercury year). The solution:

- was demonstrated compatible with the thermal control requirements (Chapter 10)
- is compatible with a fixed solar array, on three sides of the spacecraft
- does not introduce any motions disturbing the experiments viewing
- on the minus side, it does require two axis antenna articulation, at near constant rate: despin + a low (Earth orbital motion) frequency rotation by up to π radians.

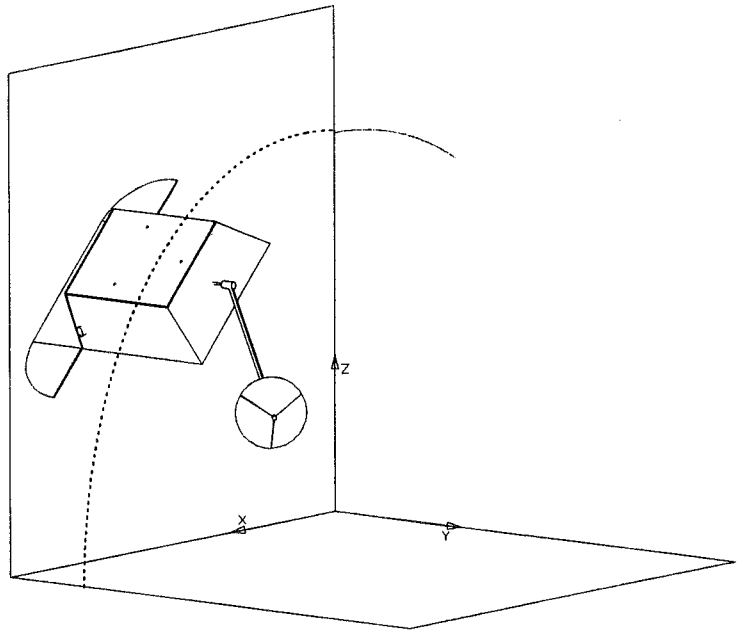

Fig. 2.4-1c Attitude strategies: pure Nadir pointing

2.5 *Telecommunication frequency bands*

Efficient telecommunications with the Earth at Mercury distance require either X band or Ka band. The trade-off depends on programmatic aspects but it has important design aspects, too.

X-band transmit and receive equipment will be implemented in (at least one) ESA ground station by the time of the first Horizon 2000+ Cornerstone mission. Thus, in the X-band option the cost of the ground station upgrading does not have to be borne by the programme. Similar plans do not exists yet for Ka band, hence the costs will impact on the programme budget. According to ESOC [Ref. 9], the cost of upgrading the Perth station to X/Ka band is about 5.5 MAU, half of it needed for X band.

An important factor in the trade-off is that Ka band is needed anyway (carrier recovery and ranging) for the Radio Science experiment. Hence, if Ka band is not part of the platform telecommunications system, the corresponding equipment costs are on the payload budget. Notice that, because of the Radio Science, the high gain antenna reflector must be Ka-band class in any event.

On the spacecraft design side, Ka band telemetry would permit to multiply by at least 3 times the data rate, at constant reflector size, or it would permit to reduce the size of the reflector, at constant data rate, which could help solve the antenna accommodation and articulation problems. In the event that Ka band is selected, the on board telecom system would be dual-frequency anyway (X up, Ka down, X up/down for low gain emergency and low-rate communications). Development of an X/Ka transponder is already under way in the ESA technology programme.

The trade-off was not closed in Phase 1, and the question will be re-addressed in Phase 2 following the evolution of the design and the programmatic scenario.

3. PAYLOAD DEFINITION AND ASSESSMENT

3.1 Orbiter Payload

The Orbiter payload is devoted to experiments in remote sensing and radio science. Table 3.1-1 provides a summary of the instrument types, broad objectives of the investigations, and measurement band.

All Orbiter instruments share a requirement for a polar orbit (for complete coverage of the planet), with reasonably short orbital period, 2 to 3 hours (for proper ground track shifting). The orbit with pericentre ~ 400 km and apocentre ~1500 km, selected partly as a compromise with engineering constraints, is compliant with these requirements. Low resolution observations from apocentre will identify areas of interest, while observations around the periapsis will serve for the higher resolution studies. All viewing instruments share a requirement for Nadir pointing.

3.1.1 Remote Sensing Experiments

The **Camera** (CAM) instrument will map the planet's surface and support the geochemistry package. The proposed optics is a Ritchey - Chrétien line scanner with correcting lens, 38 mm aperture and 330 mm focal length for a FOV of 27.3 mrad. A spectral resolution ~ $\lambda/\Delta\lambda = 10$ is obtained. The optics focuses the incoming radiation onto a linear CCD array (7 pixel lines with 1000 pixels per line, 9μm pixel pitch), realising a swath width of ~10.5 km and a spatial resolution ranging from 10.5 m at 400 km to 39.4 km at 1500 km. During mapping, the boresight is pointed at Nadir, with the swath width along the cross track direction. Off-nadir pointing by up to 5° is required. The camera requires relative pointing error ≤10 μrad/s and attitude determination better than 3 μrad (post-flight). The CAM can generate very large data volumes: with a compression factor of 7, each "snapshot" generates about 14 kbits with no binning; as images can be generated at msec rate, the data volume can reach Gbits/orbit. The CAM data output can be reduced by timelining and/or more aggressive data compression. Filters or mirrors (and shutters for the worst cases) are being considered for thermal protection from the planet's heat input. Though no cooling system is mentioned, some form of active cooling may have to be adopted.

Exp.	Name	Instrument type	Objectives	Band
REMOTE SENSING PAYLOAD				
CAM	CAMERA	Line-scan camera, optics and CCD	Surface Imaging in VIS and Near-IR	350-1000 nm
IMS	INFRARED SPECTROMETER	Imaging Spectrometer optics , CCD	Mineralogy- Observation of absorption bands	0.8-2.8 μm
ALI	UV SPECTROMETER	UV Spectrograph optics and MCP	Exospheric composition and morphology- UV photometry	70-330 nm
MXS	X-RAY SPECTROMETER	Solid state (ss) or Proportional counter (pc)	Elemental mapping /composition of upper 1μm surface layer	0.5-10 KeV (ss) 1-10 keV (pc)
MGS	γ-RAY SPECTROMETER	High Purity Ge detector	Determination of the chemical composition of the surface, including volatiles	0.1 – 8 MeV
MNS	NEUTRON SPECTROMETER	2 ^{3}He Proportional counters, 1 plastic scintillator counter	Observation of n moderating materials Search for water ice deposits	0.01 – 5 MeV
RADIO SCIENCE PAYLOAD				
RS-F	RF SYSTEM	2 Transponders, 2 exciters, 2 HP amplifiers [1]	Tests of general relativity	X + Ka
RS-C	CAMERA		Measurement of planet's rotational state	450 – 850 nm
RS-A	ACCELEROMETER	Electrostatic spring-driven 3-axis accelerometer	Global mapping of Mercury gravity field	10^{-4} Hz - 10^{-2} Hz

Table 3.1-1 3-axis Orbiter payload complement. Note [1] : 1 Transponder + 1 HPA provided by the spacecraft

The **IR Spectrometer** (IMS) will investigate the 0.8-2.8 μm range, where the absorption bands of most major rock-forming minerals are found. It is complementary to the γ- and X-ray spectrometers in that it provides information on both elemental composition and element bonding (i.e. mineralogy) at high spatial resolution (0.1 mrad) and moderate spectral resolution. IMS consists of a detector and its electronics. The detector has 256 mrad FOV, with 8 mm aperture for a focal length of 32 mm, 128 observation channels and a spectral resolution of 15.6 nm. The optics feeds the incoming radiation onto a grating (TBR) and from there onto a square 512 x 512 CCD array, with 0.5 mrad pixel IFOV. The detector focal plane requires an operational temperature of -153°C to -73°C , hence an active cryo cooling system is needed. As the observation band is precisely that where most of the radiative heat load occurs, some way of reducing the thermal input into the sensor at all times outside exposure has to be found. The IMS requires relative pointing error <1°/s and attitude determination better than 0.2 arcmin. The data volume generated per orbit is highly variable, depending on the spectrum collection repeat rate. At maximum repeat rate and high resolution values around 1.5 Gbit/orbit are reached.

The **UV spectrometer** (ALI) performs UV photometry of the surface and detects the abundance of several elements such as Al, S, Na. The optics include an entrance slit, focusing the light to a grating which disperses the radiation onto the focal plane, where a UV-sensitive microchannel plate detector records the spectrum. A tiltable mirror may be present upstream of the entrance slit to allow sideways pointing; the mirror diameter would be about 10 cm, with 2 degrees of freedom. The instrument has 0.1° x 1.8° FOV and operates in the 70–330 nm band; spectral resolution varies from 0.98 nm to 1.25 nm ($\lambda/\Delta\lambda$ = 55–200). Each spectrum consists of ~1.04 Mbits. The instrument has a protection cover closing when the Sun transits within an 11° halfwidth cone about the FOV axis. The detector has to be windowless, otherwise a crucial part of the spectrum below 120 nm would be absorbed: this may be critical due to the thermal load in orbit. Alignment relative to the CAM is to be known within 0.03°.

The **X-ray spectrometer** (MXS) will determine composition for elements with Z>11. A solid state detector could consist of a matrix of X-ray sensitive CCD preceded by a filter plate (to avoid optical contamination) and a mechanical collimator with 5° full FOV to stop secondary X-ray emission. The spectrum range covers 0.5-10 KeV. A companion experiment, the Solar Monitor (SOM) will monitor continuously the solar X-ray flux, for calibration of the flux returning from Mercury's surface. MXS nominally works in a 180° arc on the sun-illuminated side of Mercury. The data volume is low, about 0.6 Mbit per orbit. The working temperature is from –50°C to +50°C; a Peltier cooler will be implemented. The detector is covered by a 4÷7.5 μm Be window located behind the collimator; any additional material in the field of view would reduce the detector efficiency due to X-ray attenuation.

The **γ-ray Spectrometer** (MGS) will carry a solid state detector such as High Purity-Ge crystal to develop elemental composition maps of the near surface of Mercury (the upper 30 cm), including volatiles, by detecting the characteristic γ-ray fluxes, in the 0.1–8 MeV range, of cosmic-ray excited elements such as O, Si, Fe, H and naturally radioactive elements K, Th, U. Long integration times are needed to collect enough data to estimate the abundances. The detector has omnidirectional FOV and energy resolution from 2.5 KeV @1.3 MeV to 7.5 KeV @ 7.5 MeV. It can operate continuously with moderate data volume, ~ 1.5 Mbit. The MGS needs cooling to ~ -190°C, both when measuring and when in stand by (a Stirling cooler is envisaged), and annealing of the crystal after radiation damage.

The **Neutron Spectrometer** (MNS) will determine the abundance of hydrogen in the form of buried water ice (to depths > a few 10 cm) in permanently shadowed crater floors and walls in the polar regions, and in the form of solar wind implanted H in mature regolith. Neutrons are produced by cosmic rays interacting with surface regolith; determination of the H content requires knowledge of the elemental composition, that is obtained by operating together with the MGS. Three separate fluxes of thermal (0.01<E<0.4 eV), epithermal (1<E<2 keV) and fast (0.01<E<3MeV) neutrons are measured for maximum specificity to H, and minimum sensitivity to variations in regolith chemistry, by normalizing both the thermal and epithermal fluxes to the fast neutron flux. A typical set up consists of 2 ^{3}He gas proportional counters, for thermal and epithermal neutrons, plus a plastic scintillation counter coupled with a photomultiplier for fast neutrons. The gas-filled proportional counter has omnidirectional response and the cross sectional area determines the n efficiency. The n flux emitted by the Mercury surface is very low, hence the bit rate is very low (0.03 kbps). The working temperature range is - 50°C to +50°C and a cooling device may have to be used; MLI can be used for thermal protection, since neutrons are very penetrating.

3.1.2 Radio Science Experiments

The radio science experiments include:

1) Measurement of Mercury's rotational state (libration experiment)
2) Global mapping of Mercury's gravity field
3) Tests of Gravitation Theory, including:

- the Sun's quadrupole moment J_2 to a precision of 10^{-7},
- the time derivative of the gravitational constant, (dG/dt)/G, which is relevant to cosmology and galaxy formation
- parameters γ, related to the curvature of space per unit mass, and β, related to the nonlinearity in gravity superposition.

The basic observables are the range (spacecraft antenna position relative to Earth antenna position), and the Doppler tracking (spacecraft antenna relative velocity vs. Earth antenna relative velocity). An order of magnitude of the positional accuracy (post facto) is obtained from the requirement on (two-way) phase stability versus integration time:

$$\sigma_y = 10^{-14},\ 1000\ \text{s} < \tau < 10{,}000\ \text{s}$$

$$\sigma_y = \frac{\Delta\nu}{\nu} = 2 \cdot \frac{1}{c} \cdot \frac{\Delta l}{\tau} \rightarrow \Delta l = \sigma_y \cdot c \cdot \frac{\tau}{2} \rightarrow 1.5\ \text{cm}\ @\ 10{,}000\ \text{s},\ 1.5\ \text{mm}\ @\ 1000\ \text{s}$$

Note that this very challenging accuracy must take into account several error sources, including RF noise and antenna phase centre shifts (in the measurement bandwidth). A multiple frequency, two-way link (two-frequency up / four-frequency down) is needed for calibrating the propagation noise sources (non-diffusive, interplanetary plasma, coronal plasma), and is realised by means of two ranging transponders + frequency translators as shown in Fig. 3.1-1. Relative timing at milli-second accuracy is needed as well.

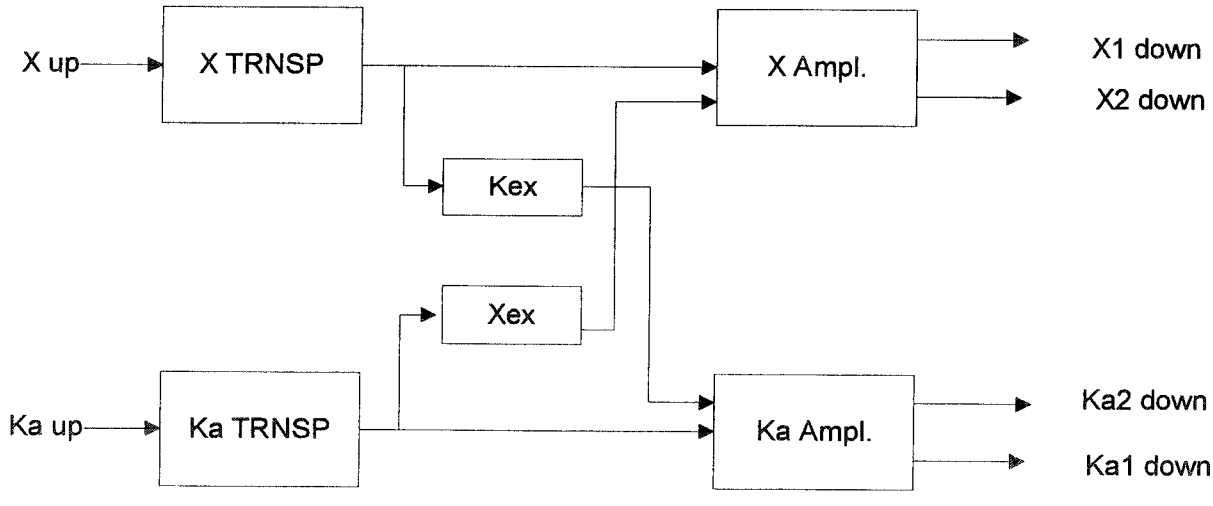

Fig. 3.1-1 Schematics of the Radio Science RF subsystem

The libration and gravity experiments are system experiments, in that they involve, besides the RF tracking, many satellite functions and subsystems. In the libration experiment, the vector position of a landmark (or pattern) on the surface of the planet must be reduced to an inertial frame. Thus, the measurement involves a camera (tracking the landmark), star trackers (measuring the attitude with respect to the distant stars), as well as the range, determined by the two way RF link. The requirements are:

- $\approx$ 1.5 m position accuracy in a planetocentric frame
- $\leq$ 2 arcsec absolute attitude measurement error, distributed among (1) attitude error as determined by the star trackers, (2) attitude stability of camera w.r.t. star tracker, and (3) camera pointing error (or pattern matching error).

In the gravity experiment, the trajectory as determined by gravity alone must be reconstructed, and this means that all non-gravitational accelerations must be measured, modelled and subtracted with great accuracy. The accelerometer makes the experiment possible by measuring the non-gravitational accelerations acting on the centre of mass. Radiation pressure is the dominating perturbation in Mercury orbit; solar radiation pressure is the main contributor with 10^{-5} m/s^2, while the most dangerous disturbance is the planetary radiation (albedo plus infrared emission), which produces an effect modulated at the orbital frequency and its harmonics.

The accelerometer's resolution is specified as $3 \cdot 10^{-8}$ m$\cdot$s$^{-2}\cdot$Hz$^{-1/2}$ in a band between 10^{-4} Hz and 10^{-2} Hz (TBC). Ranging and Doppler tracking, simultaneous with the accelerometer measurements, are needed for a cumulative time of about 18 (Earth) days, with the tracking arcs distributed homogeneously on the surface of the planet. Such tracking arcs must therefore be selected at times when different areas of the planet are being flown upon, while the two-band, two-way RF tracking is on (that is, the satellite is not under occultation by the planet, and the Earth tracking station is in view).

The above requirements, as well as engineering constraints from ground station availability, data rate limits, thermal load limits, viewing requirements of the different experiments, all require timelining of the operation of the Orbiter payload. A preliminary exercise at operation scheduling is planned for Phase 2.

3.1.3 Orbiter Payload Budgets

A number of issues related to the definition of the payload must be resolved in Phase 2, including:

- finalisation of configuration and layouts (optics and coolers)
- active cooling needs and thermal input reduction
- data downlink: observation strategy and operations scheduling
- need for mechanisms (particularly ALI, MGS)
- shielding from radiation, choice of materials (particularly MXS), radiation hardening (all)
- detector technology (particularly MXS, MGS).

A summary of the accommodation and performance requirements placed on the Orbiter, compiled on the basis of the information available in Phase 1, reads as follows:

- Mass: ~ 100 kg, excluding harness and margin
- Electrical Power: ~ 124 W average continuous, ~ 175 W peak
- Data volume per orbit (unrealistic, assuming simultaneous operation): ~ 7.9 Gbit compressed (CAM, IMS) i.e. ~ 950 kbps average continuous to Earth
- Data Storage: some 10 Gbits
- Attitude: absolute pointing accuracy: ~ arcmin level (driven by remote sensing instruments); pointing stability: ~ 10 arcsec/s (driven by CAM); pointing knowledge: ~ arcsec (driven by CAM), Alignment knowledge and stability: ~ arcsec; Attitude reconstruction in inertial frame: ~ 2 arcsec (driven by libration experiment).

3.2 *Subsatellite Payload*

3.2.1 Payload environment

The Subsatellite payload is intended to cover those aspects of science concerned with fields and particles science. The ideal orbit for these goals is a highly elliptical polar one, with the angle of the line of apsides 60 to 70° from the spin axis of Mercury, with the pericentre as low as possible. It should be noted that the orbit is effectively inertial, and thus covers all the magnetospheric bow shock during 1 Mercury year. The orbit is not fully stable however if the line of apsides is not in the equatorial plane.

Consequently a provisional orbit has been recently chosen for the Subsatellite starting at pericentre/apocentre altitude of 400/12200 ($5R_M$) km, and with the periherm in the equatorial plane, giving a stable orbit without significant loss of science.

Payload requirements also called for a spinning satellite as best suited to the experiments envisaged, with a spin rate approximately 15rpm.

3.2.2 Payload at start of study

The original payload at the start of the study for the Subsatellite was defined as below in Table 3.2-1.

Instrument	Acronym	Mass (kg)	Power (av) (W)	Data rate (av) (kb/s)
Magnetometer	MAG	2.5	2.5	1
Plasma Ion Spectrometer	IMS	7.0	5.0	1
Electron Electrostatic Analyser	EEA	2.2	2.5	1
Radio & Plasma Wave Detector	RPW	6.6	6.0	1
Positive Ion Emitter	PIE	2.7	3.8	0.02
Total		21.0	19.8	4.02

Magnetometer boom length = at least 3.5m (to meet 0.3nT DC field)
RPWH boom length =2.5m nom.
RPWE wire boom length = 35m per boom
PIE forms part of payload

Table 3.2-1 Original Subsatellite Payload Definition

3.2.3 Revised baseline payload

It soon became clear that the mass limitations of the mission demanded that the Subsatellite and its payload be made lighter while still achieving its main goals.

On the payload side the instrumentation was reviewed, particularly from the point of view of using advanced build techniques, and with a view to reducing the number of elements and interfaces to the Subsatellite systems.

In the course of this review the instrumentation basis was slightly altered to add a CPD and an EPD for further plasma and particle assessment, while allocating the PIE to the satellite functions as it only served a support function.

The key change was the decision to have only the front end electronics as part of each core instrument, and to combine all the main instrument electronics into a central unit. The end effect was almost to halve the payload mass while retaining and expanding the science covered. The payload is summarised in table 3.2-2.

Notes: Instrument	Acronym (provisional)	Mass (kg)	Power (W)	Notes
Magnetometer	MAG	0.5	1	plus boom harness
Ion Spectrometer	IMS	3.0	2.2	todays technology
Ion/Electron Analyser	EEA	0.9	1.8	
Wave Analyser (E)	RPWE	1.12	4	including wire boom
Wave Analyser (H)	RPWH	1.0		to be confirmed
Cold Plasma Detector	CPD	0.7	1	
Energetic Particle Detector	EPD	0.2	1	
Integrated Electronics:				
Magnetometer		0.5		
Wave Analyser		0.5		
Wave Preamp		0.15		
Converter		1.0		
DPU				
Power switches				
Housing		0.3		
Total Integrated Electronics		2.45	3	
Total		9.87	14	

Notes:
Magnetometer boom length = at least 2x satellite diameter
RPWH boom length = 1m
RPWE wire boom length = 30m per boom
PIE forms part of bus
Basis of mass/power: 24 June meeting + Carr fax 7/8/98

Table 3.2-2 Revised Subsatellite Payload Definition

The resulting key fields of view combined on a nominal satellite body are shown in Fig 3.2-3.

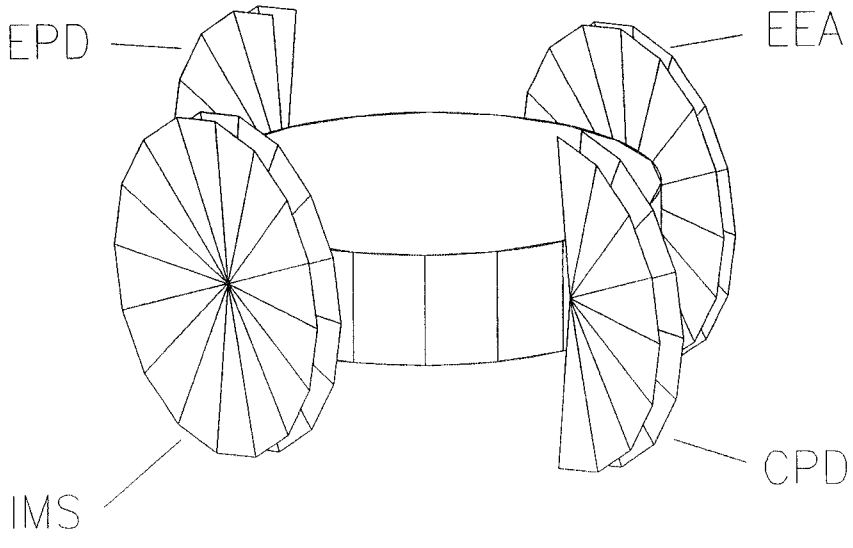

Fig 3.2-3 Nominal Fields of View of Particle/Plasma detectors

4. MISSION PROFILE

4.1 Reference Missions

After the mission trade-offs documented in Chapter 2.1 and 2.2, the reference mission profile comprises the phases summarised in Table 4.1-1.

As the first part of the mission depends on a Venus flyby, mission opportunities recur approximately with the synodic period of Venus, 1.6 years. Two opportunities were studied, with launch on September 2010 and March 2012. The launch window is about two weeks long.

The satellite is injected into an escape trajectory directly by Ariane 5, with a large excess velocity. The maximum launch mass is about 2200 kg in 2010, much larger (3000 kg) in 2012. In the first part of the cruise, until Venus flyby, no electric thrust is applied. Hence, the electric engines are turned on for the first time 4 to 6 months after launch. According to the analysis of (temperature-limited) solar array power versus distance to the sun, the power delivered by the array is approximately constant below 0.6 AU; hence, constant electric thrust can be assumed and no throttling capability of the thrusters is required. In the Phase 1 mission analysis, 600 mN thrust was assumed for all thruster types, which produces a power requirement (including the spacecraft subsystems power demand) of 10 kW for the mission with ion engines, and 6.5 kW for the mission with stationary plasma thrusters.

The Venus flyby is followed by two Mercury flybys, the second of which is thrust-assisted and produces a low arrival velocity (0.4 km/s). After the second Mercury flyby, the electric propulsion mission is terminated and the electric propulsion stage is jettisoned. The whole electric mission thus lasts about two years, with total Δv = 4.8 km/s (6.4 km/s in the 2012 opportunity) and total thruster operation time of 4150 hours (5670 hours in the 2012 opportunity).

Capture into Mercury orbit is executed by chemical propulsion (400N bipropellant engine). The insertion Δv is 375 m/s and it brings the spacecraft directly into the Subsatellite destination orbit (400 km x 12200 km). The Subsatellite is then released some time after the insertion manoeuvre. There follows another manoeuvre of the bipropellant engine (600 m/s), in a single thrust arc around the pericentre, to lower the apocentre to 1500 km, the design apocentre altitude for the Orbiter. Shortly thereafter, the bipropellant stage is jettisoned.

The total cruise time is 2 years and four months in the 2010 opportunity, 2 months shorter in the 2012 opportunity.

With the assumptions in Table 4.1-1 (launch mass and dry mass of the various stages), the total mass delivered into the destination orbits (Orbiter + Subsatellite + Lander) is 710 kg, i.e., about 30% of the launch mass. Should the dry mass values vary, the mission profile remains valid so long as the electric propulsion accelerations do not change, which means that a mass increase must be compensated by a proportional thrust force increase (hence a power increase). The mission profile may need some adjusting in Phase 2, when the mass budgets are firmed-up.

The Hard Lander is attached to the Orbiter, and it is delivered into an impact trajectory at some convenient time after the end of the injection sequence. A preliminary discussion of the initial conditions for Hard Lander delivery is in the next chapter.

		2010 Mission Opportunity		2012 Mission Opportunity	
		Ion thrusters	SPT thrusters	Ion thrusters	SPT thrusters
0	*Launch epoch (T0)*	*Sept. 2010*		*March 2012*	
	Escape velocity	3.4 km/s		3.47 km/s	
	Asymptote declination	34° South		4° North	
	Max launch performance (incl. Adapter)	2200 kg		3000 kg	
	Assumed launch mass	2000 kg	2100 kg	2100 kg	2270 kg
1	*Venus flyby*	*February 2011*		*June 2012*	
2	*1st Mercury flyby*	*September 2012*		*January 2014*	
3	*2nd Mercury flyby*	*October 2012*		*February 2014*	
4	*Electric propulsion stage jettisoning*				
	Electric propulsion stage dry mass	635 kg	565 kg	635 kg	565 kg
	Total electric thrust operation	4150 hours		5670 hours	
	Electric propulsion Δv	4.84 km/s		6.44 km/s	
	Xenon propellant mass	285 kg	455 kg	385 kg	625 kg
	Mass after EP stage ejection	1080 kg		1080 kg	
5	*Capture & insertion into Subsat orbit*	*January 2013*		*May 2014*	
	Arrival velocity	0.44 km/s		0.4 km/s	
	Insertion manoeuvre Δv	375 m/s		375 m/s	
	Insertion orbit	400 x 12,200 km		400 x 12,200 km	
6	*Subsatellite separation*	*T5 + 1 day*		*T5 + 1 day*	
7	*Insertion into Orbiter orbit*	*T6 + 1 day*		*T6 + 1 day*	
	Orbit transfer Δv	600 m/s		600 m/s	
	Final orbit	400 x 1500 km		400 x 1500 km	
8	*Bipropellant stage jettisoning*	*T7 + hours*		*T7 + hours*	
	Bipropellant fuel mass	280 kg		280 kg	
	Bipropellant stage dry mass	90 kg		90 kg	
9	*Hard Lander delivery (by Orbiter)*	*T8 + days*		*T8 + days*	
	Payload delivered into Mercury orbit (Subsatellite + Orbiter + Hard Lander + interfaces)	710 kg		710 kg	

Assumptions:

Electric thrust = 600 mN; specific impulse (EOL) = 3200s (ion thrusters), 2000s (SPT)

Installed electrical power @ 1 AU = 10 kW (ion thrusters), 6.5 kW (SPT); 0.5 kW for s/c subsystems

Chemical thrust = 400 N; bipropellant specific impulse = 320s

Table 4.1-1 Example mission opportunities [adapted from Ref. 7, 10]

4.2 *Hard Lander delivery*

For a preliminary analysis, the following assumptions were made.

1. The Hard Lander (penetrator) is to be deployed in a polar region
2. the impact velocity must not exceed 200 m/s, with impact angle (to the vertical) <25° and angle of attack (to the vertical) <12°
3. the penetrator dry mass consists of:
   - penetrator and payload, including communications and power: 2 kg
   - AOCS/cold gas RCS to orient the Probe: 2 kg
   - Motor casing: 25% of fuel mass

The above masses are estimated by similarity with Lunar-A or DS2, assuming typical casing mass for the retrorockets. The propellant is assumed to be HTPB solid or CTBP (Carboxyl Terminated Poly-Butadiene), with an exhaust velocity just under 3000 m/s. The deployment strategy is as follows:

a) a small Δv is imparted to de-orbit the Lander

b) when the Lander is a small distance above the desired impact point, another, large Δv, equal and opposite to the orbital velocity at that point is imparted. Then, the Lander drops like a stone along the vertical. The condition that the impact velocity must not exceed 200 m/s fixes the altitude at which the second Δv is applied, about 5 km.

Hence the penetrator must be two-stage and it must posses an attitude re-orientation capability.

The Δv required is minimum when the second burn occurs 180° from the point of release; however, the penalty for a shorter arc is not large and an impact trajectory from apocentre to pole as sketched in Fig. 4.2-1 can be assumed. The Δv turns out to be about 3.7 km/s, which produces a propellant mass fraction of about 71%. Hence, the penetrator needs to weigh at least 35 kg to deliver 2 kg equipment (that includes the payload) to the surface. Note that this result holds for the optimistic exhaust velocity of 3 km/s; the wet mass would rapidly grow for smaller exhaust velocities (48 kg for v_{ex} = 2.8 km/s, 78 kg for v_{ex} = 2.6 km/s).

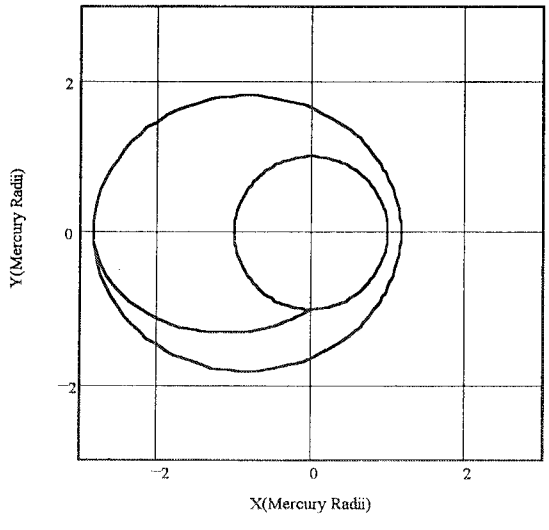

Fig. 4.2-1 Example penetrator impact trajectory

5. CRUISER/ORBITER CONFIGURATION CONCEPTS

5.1 *Satellite Configuration Overview*

The satellite design concept is thoroughly modular, in order to accommodate without conflict the requirements arising from the various environments and missions. At payload level ,

- the dedicated **Subsatellite** hosts the particle-and-field experiments
- the 3-axis stabilised **Orbiter** hosts the remote sensing and radio science experiments
- simple, short-lived in-situ experiments are accommodated in the **Hard Lander**.

The propulsion equipment is also made modular:

- **Electric Propulsion Stage** (EPS, or Cruise Module) for the interplanetary transfer
- **Chemical Propulsion Stage** (CPS, bi-propellant) for quick and accurate capture / orbit acquisition
- limited propulsion capability, for attitude control tasks, is provided in the Subsatellite and Orbiter.

The command and control tasks, on the other hand, are centralised in the Orbiter, providing central processing for overall monitoring and control tasks, and managing telecommunications, through all mission phases. This drives the Orbiter design through the requirements for high gain antenna (HGA), low gain antennas (LGA), and star trackers to operate throughout the mission (free viewing & articulation of HGA).

The **mechanical and thermal configuration** is driven by the accommodation in Ariane-5, single launch, short fairing. Simple load paths are to be provided from launcher interface through the stacked modules, with clear separation interfaces. The modules are stacked to be deployed in the following order, and with the following separation interfaces:

1. jettison Electric Propulsion Stage before capture (separation interface between EPS and CPS)
2. deploy Subsatellite, after 1st Chemical Propulsion Stage manoeuvre (spin-eject device, mounted to CPS)
3. jettison CPS, after 2nd manoeuvre (separation interface between CPS and Orbiter)
4. deploy Hard Lander, after acquisition of Orbiter orbit (spin-eject device, mounted to Orbiter).

The thermal control is passive (with heaters), and adapted to the needs of each module. The configuration concept so defined has yet to be validated by a proper mechanical design exercise (Phase 2).

The propulsion and power functions lead to different configurations of the Electric Propulsion Stage, depending on whether ion thrusters (RITA-XT, UK-T6) or stationary plasma thrusters are implemented (see Chapter 8).

The **Propulsion** subsystems include:

- In the Electric Propulsion Stage, 3+1 (or 3+2, depending on the redundancy concept adopted) 200 mN thrusters to realise 600 mN nominal thrust; in the current configuration exercise three (ion thrusters option) or four (SPT thrusters option) Xenon propellant tanks are included
- In the Chemical Propulsion Stage, one 400N bi-propellant thruster + 8 10N thrusters for attitude control (both in the Cruise phase and the approach phase)
- In the Orbiter, 8 cold-gas thrusters.

Electrical power / energy is provided:

- In the Electric Propulsion Stage, by a 10 kW, 65 m² GaAs cell solar array, in two 4-panel wings (3 panels, 6.5 kW in the SPT option)
- In the Orbiter, by 3 fixed panels, with special high-intensity, high temperature GaAs cells, with 70% OSR fraction
- by one Li-ion battery, residing in the Orbiter, also providing energy storage, if needed, in the cruise phase.

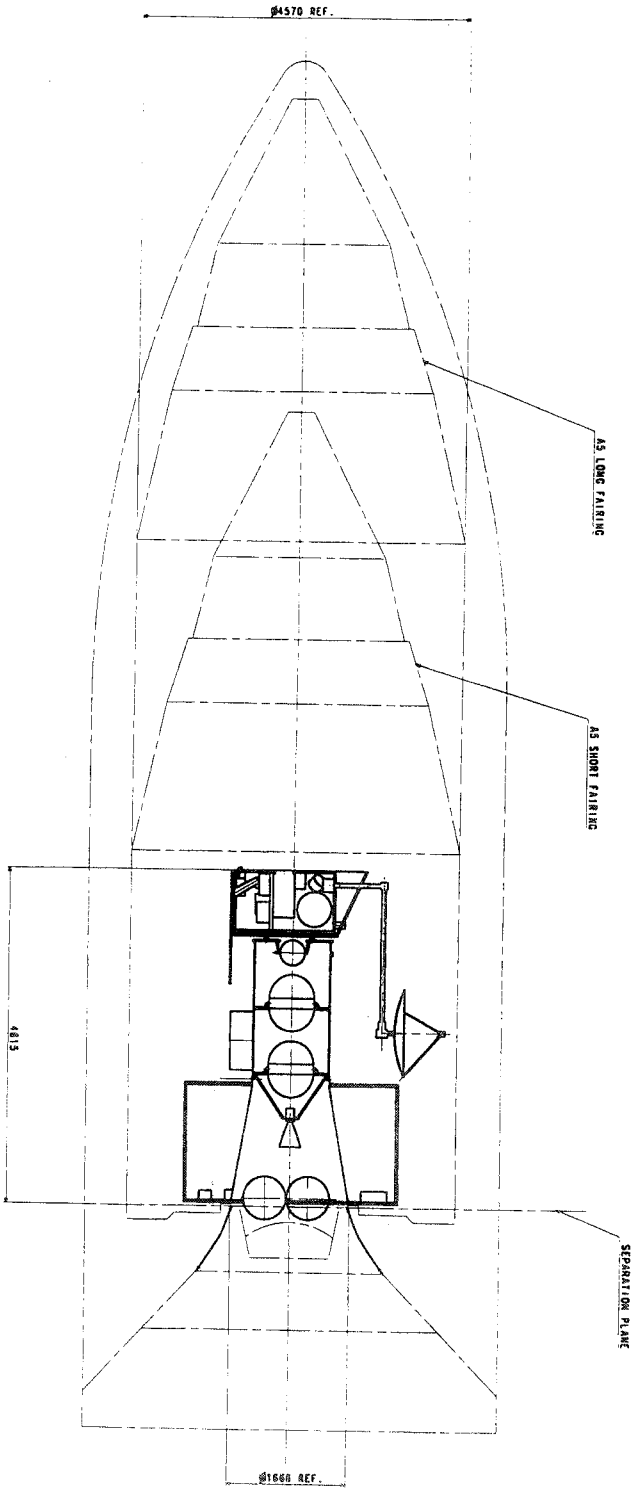

Fig. 5.1-1 Configuration under the Ariane 5 fairing

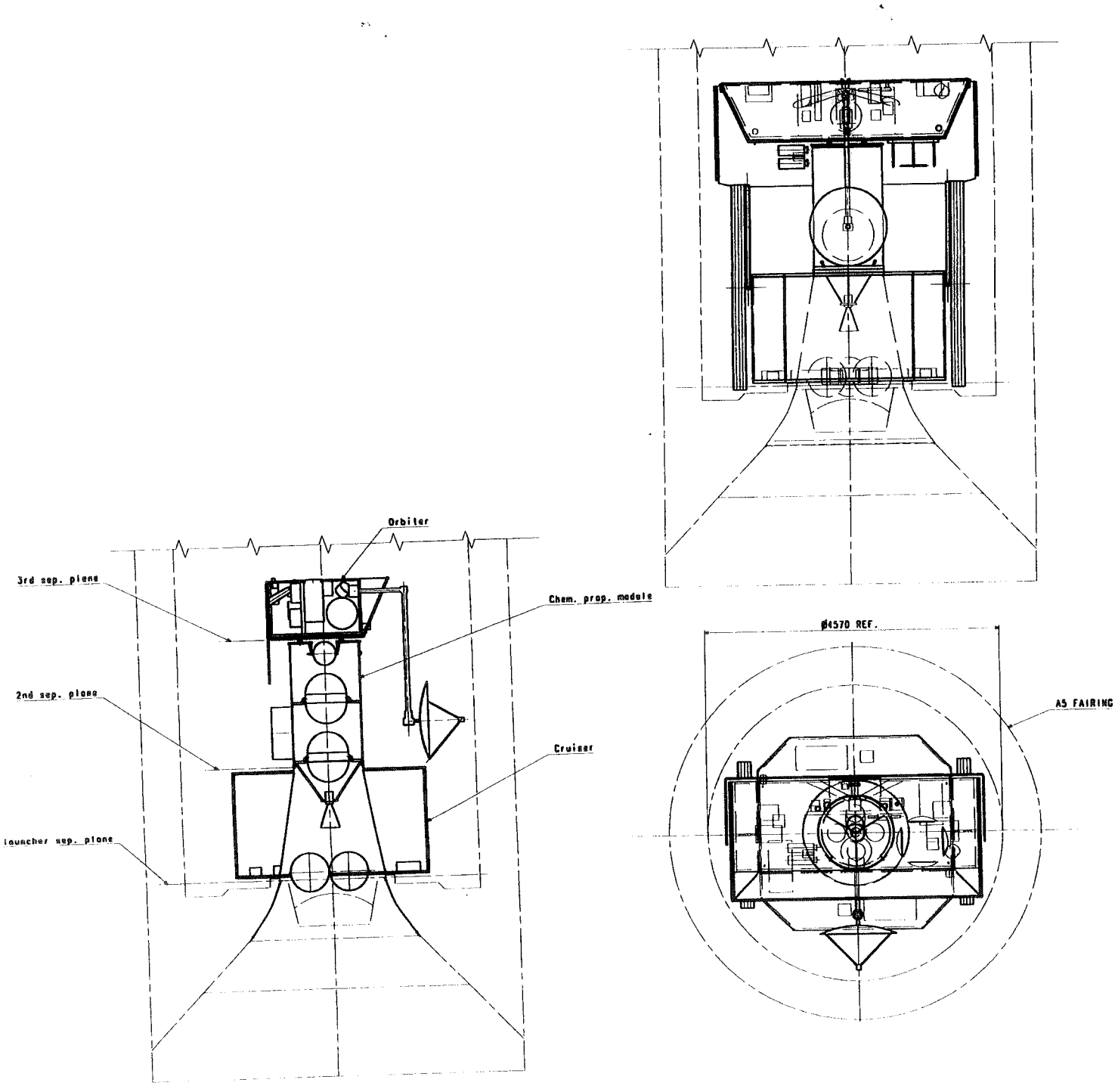

Fig. 5.1-2 Details of the configuration under the Ariane 5 fairing, showing main equipment accommodation

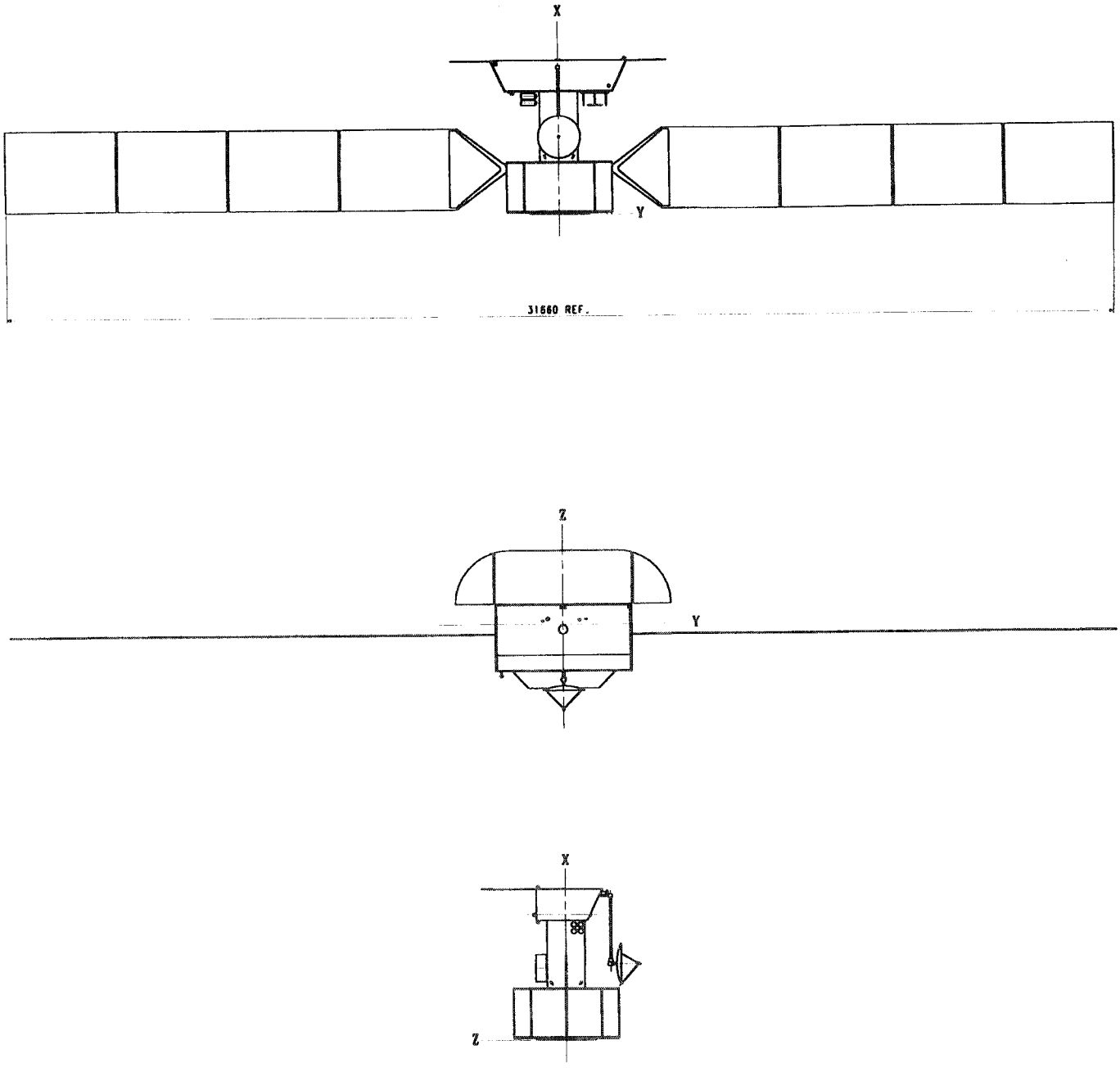

Fig. 5.1-3 In-orbit (cruise) configuration

Attitude measurement equipment include:

- three wide-field, autonomous star cameras for operational attitude measurement, in all phases
- sun sensor and Inertial Measurement Unit (IMU) for the acquisition phases
- Mercury Horizon sensor + IMU for Mercury safe mode (in the Orbiter).

Telecommunications are handled by:

- One 2-axis articulated high-gain antenna, X/X or X/Ka band, for high data rate telecommunications, all phases
- two low-gain antennas (X-band horns) for emergency and back-up
- directive UHF antennas (2 on Subsatellite, 1 on Orbiter) for the operational data relay in Mercury orbit.

Figures 5.1-1 to 5.1-3 show views of the configuration under the Ariane 5 fairing, and the orbital configuration during the cruise.

5.2 Propulsion Modules Configuration

5.2.1 Electric propulsion Stage

The electric propulsion stage configuration depends on the thruster type adopted (see chapter 8) and the launch opportunity. There is no significant difference in the accommodation of either the RITA-XT thruster system or the UK-T6 IPS (same specific impulse, hence same propellant mass, Δ dry mass = -1 kg). Major variations apply instead in the event the SPT thruster system is implemented. Table 5.2-1 shows the major differences in the four options. The options range from

- ion thrusters , 2010 option: smallest propellant load and largest solar array, to
- SPT thrusters, 2012 option: largest propellant load and smallest solar array.

For the purposes of the Phase 1 configuration exercise, an all-encompassing approach was taken, in that the module was designed to show how both the largest propellant load, and the largest array can be accommodated. This means that, in particular, the estimated structural mass is oversized for the lighter 2010 option.

The module is a simple octagonal prism shape, sized for maximum volume (four large tanks needed in the 2012 SPT launch). A central thrust cone is the main structural element, to transmit loads to launcher interface, and houses the propellant tanks. The tank volumes have been selected to suit the configuration constraints, by choosing from existing high pressure tanks (assumed Xenon storage pressure 125 bar @50°C); Xenon tanks of large volume are not available today.

Four 200 mN thrusters are installed at the level of the launcher separation plane, at the corner of a square. An additional thruster may have to be installed at the centre, to realise a fully one-failure-tolerant configuration (see Chapter 12). The thrusters are clustered near the centre to minimise misalignment torques.

Two solar array wings, with four panels each (total surface $\cong$ 65 m^2), provide the required 10 kW power (ion thruster option). On each wing, a solar array drive mechanism (SADM) provides one rotational degree of freedom, around the yoke axis, sufficient for the array orientation needs during the cruise. The propulsion drive and power conditioning electronics equipment are mounted to internal side of the wider lateral panels.

Table 5.2-2 shows the EPS mass budget estimate, made according to the criteria outlined above.

	Ion thrusters (RITA-XT, T6 IPS)		Stationary Plasma Thrusters (SPT)	
	2010	2012	2010	2012
Thruster system dry mass [1]	116 kg	116 kg	94 kg	94 kg
Xenon propellant mass	285 kg	455 kg	385 kg	625 kg
Xenon tank volume	200 l 3 spherical tanks ∅ = 640 mm	320 l 3 spherical tanks ∅ = 640 mm	270 l 3 spherical tanks ∅ = 640 mm	430 l 4 spherical tanks ∅ = 640 mm
Solar array size	65 m² 2 x 4 panels	65 m² 2 x 4 panels	42 m² 2 x 3 panels	42 m² 2 x 3 panels
Solar array mass	200 kg	200 kg	130 kg	130 kg

[1] Excludes propellant tanks, 15 to 10% of propellant mass

Table 5.2-1 Electric Propulsion Stage configuration drivers [assumed Xenon density = 1.45 kg/l]

Electric Propulsion Stage Mass Budget Summary [1]	Total Mass [kg] Ion Thrusters	Total Mass [kg] SPT thrusters
Thrusters & Equipment	140	113
Propellant Tanks	63	97
Solar Array & SADM	240	156
Power & Harness	58	58
Thermal Control	18	13
Structure & Mechanisms [2]	134	134
Total incl. equipment margins	***652***	***571***

[1] Each item includes 20% mass margin [2] The structural mass is sized for the maximum mass option

Table 5.2-2 Electric Propulsion Stage dry mass budget

5.2.2 Chemical propulsion Stage

The 400N bi-propellant engine used for planetary capture and Mercury orbit acquisition, together with a system of 8 10N thrusters used for cruise and manoeuvre attitude control, are accommodated in a separate module, rather than made an integral part of the Orbiter. The rationale is avoidance of adverse effects on the Orbiter thermal design (thermal leak through thruster nozzle), and because of the unknown behaviour of bi-propellant in a high-T environment. An additional reason is that the 10N attitude thrusters are too powerful for Orbiter attitude control, as they would disturb the gravity experiment; hence, another thruster system would have to be implemented in the Orbiter anyway. Incorporation of the bi-propellant stage in the Orbiter, on the other hand, would have mass advantages (lighter structure, one less separation interface) and might allow supplementary orbit change manoeuvres to be introduced in the Orbiter mission profile. The trade-off may thus be reconsidered in Phase 2.

The Chemical Propulsion Stage is shaped as a cylinder, continuing the EPS thrust cone, for structural reasons and because of diameter constrains due to articulation of the high gain antenna during the cruise. The separation interface to the Orbiter is made discrete, on three points, to minimise thermal leaks into the Orbiter after separation. Table 5.2-3 shows the mass estimate.

Chemical Propulsion Stage Mass Budget Summary [1]	Total Mass [kg]
400N engine	3
Thrusters & Equipment	19
Propellant & Pressurant Tanks	33
Structure & Mechanisms	36
Total incl. equipment margins	91

[1] Mass margins 5% (first two items), 20% (last two items)

Table 5.2-3 Chemical Propulsion Module mass budget

5.3 Three-Axis Orbiter Configuration

5.3.1 Configuration Design Description

The configuration of the Orbiter (Fig. 5.3-1) is driven by the thermal design, the purpose of which is to reject as much as possible the very large heat inputs from the sun and the planet, by means of highly efficient insulation all over the body, and a large radiator protected from direct illumination.

The external shape is a flat prism with slanting sides, tilted by 25° to reduce the view factor to the planet. Three sides (±X, +Y) are partially covered with solar cells, mounted on an Al substrate, with 30% cell filling factor; the remaining 70% of the surface is covered with Optical Solar Reflectors. The cells are a special HIHT design, and the upper limit panel temperature is +250°C. Enough power is generated at any permitted solar incidence thanks to the 25° slant.

The –Y side is taken up by a large (2.6 m²) radiator, the size of which is driven by the internal power dissipation (500W assumed); a reduction of the dissipated power would allow a reduction of the overall size of the spacecraft. The radiator is protected

- from the sun, by the attitude law (nadir pointing + 180° rotation every half Mercury year)
- from the planetary IR radiation, by a deployable shield, placed at right angles to the radiator, and large enough as to block IR radiation at any permitted view factor to the planet. The IR shield is composed of a fixed part and two lateral wings, stowed at launch (because of launcher fairing constraints). The size is about 6.5 m² for 400 km minimum altitude. The radiator is tilted by up 30° when the sun moves within 30°of the orbit plane, on the side of the apocentre (once per Mercury year).

The payload instruments are mounted to the +Z (nadir) side, protected by the sun by baffles (small FOV instruments) and MLI sheets (large FOV instruments). Preliminary scientific instrument and equipment layout have been developed, to be addressed in detail in Phase 2 (driven by the low temperature requirements of many instruments). High-temperature MLI covers every surface but the radiator, the instrument apertures and the solar cells.

The major element mounted externally is a deployable, 2-axis articulated, 1.5m high gain antenna (HGA), mounted on a boom protruding from the +Y (anti-radiator) side. A suitable latch mechanism restrains the boom at launch. Two low-gain antennas are mounted to the ±Y sides, and they ensure up to ±50° RF coverage. The data relay antenna (UHF dipole array) is mounted to the zenith (-Z) side. Three star sensors are accommodated on radiator side, and are mounted to a stable bench-like structure, in solid with payload cameras.

The separation interface is on three points (to reduce the heat input into the Orbiter after separation), on the -Z (zenith) side. This configuration permits, in principle, observations by the scientific instruments during the cruise (Venus fly-by); attitude, thermal & communications constraints to such observations will be addressed in Phase 2. Table 5.3-1 shows the Orbiter mass budget.

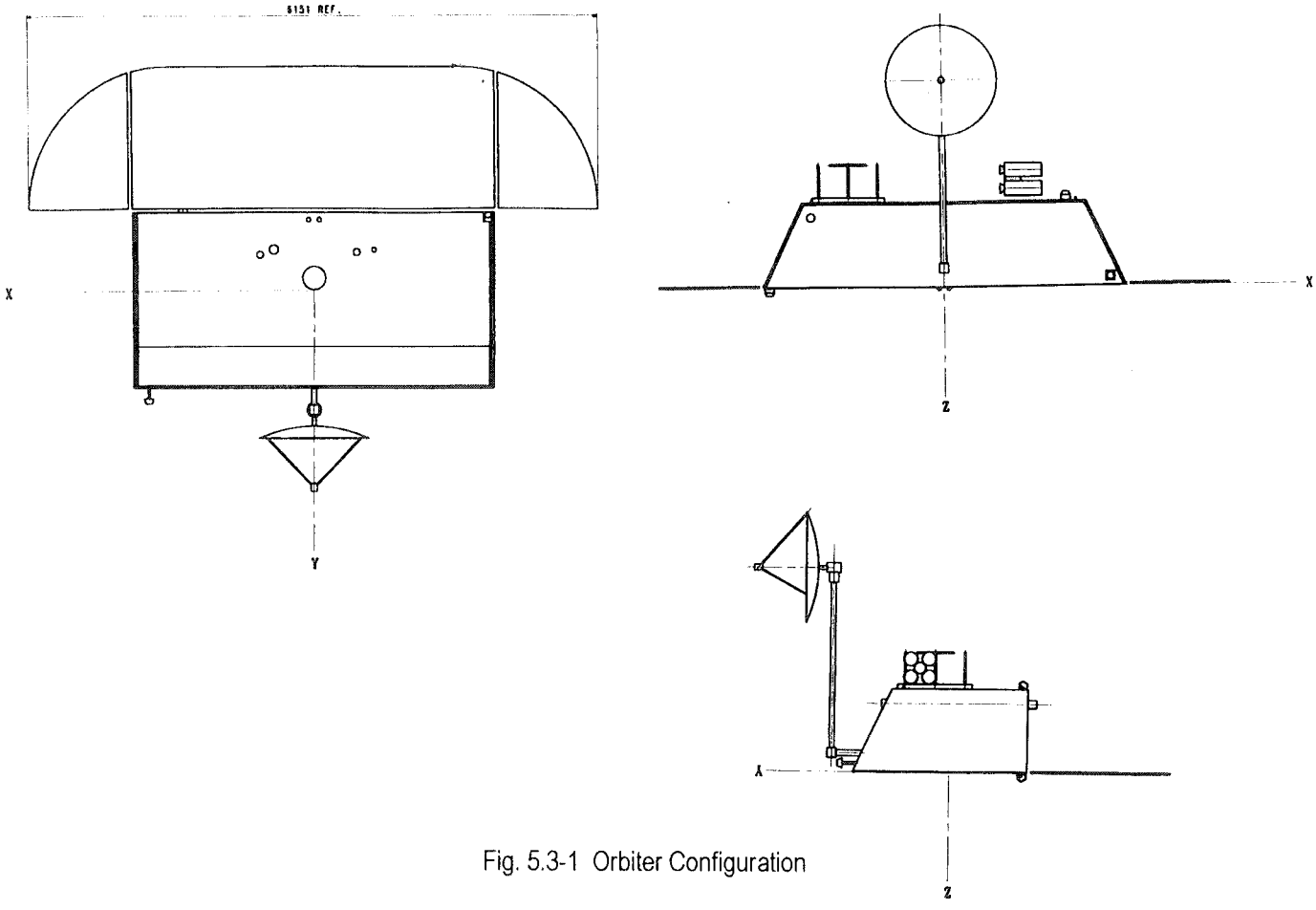

Fig. 5.3-1 Orbiter Configuration

Orbiter Mass Budget Summary [1]	Total Mass [kg]
Payload [2]	120
Data Handling	35
RF	29
Power & Harness	76
Solar array	30
GNC/AOCS	19
RCS incl. Propellant	29
Thermal Control	89
Structure & Mechanisms	121
Total incl. equipment margins	***548***

[1] 20% mass margins on all items [2] Allocation, 100 kg + 20%

Table 5.3-1 Orbiter mass budget

5.3.2 Orbiter solar array configuration trade-off

A preliminary estimate of the Orbiter power demand is in Table 5.3-2. In principle, the solar cell area needed to provide 500W power in Mercury orbit is small, even at high temperature; a rough estimate gives

- 0.3 m² cell area @ 200 °C @ normal incidence @ Mercury perihelion
- 0.7 m² cell area @ 200 °C @ normal incidence @ Mercury aphelion.

The large seasonal excursion due to the varying distance of the planet to the sun is apparent. To cope with the seasonal excursion, and to limit the temperature, the solar array could be wing-mounted; however, (a) design without mechanisms would in principle be preferred in the harsh Mercury environment, and (b) cooling by back radiation is negated by the large IR flux from the planet. Three options were traded-off:

- two-axis articulation
- single-axis articulation
- a fixed, body mounted array in several sections.

The arguments pro and con the three options are summarised in Table 5.3-2.

Equipment	Power [W]	Margin [W]	Total Power [W]
Remote sensing payload, average	128.	19.2	147.2
X band transponder	12.	1.8	13.8
X band TWTA	48.	7.2	55.2
UHF transceiver	6.	0.9	6.9
CDMU	25.	3.75	28.8
RTU	7.	1.05	8.1
AIU	5.	0.75	5.8
PCDU	15.	2.25	17.3
Star sensor + electronics	15	2.25	17.3
Thermal Control heaters	0.	0.	0.
Harness loss	13.1	0.	13.1
System margin (10%)			31.3
Total power demand	**261.**	**39.2**	**300.2**
Battery recharge			175.4
Power budget			**475.6**

Table 5.3-2 Orbiter power budget (sunlight)

1. *Two-axis articulated* *(a) 1st rotation about out-of-plane axis* *(b) 1st rotation about in-plane axis*	Pros:	constant power output temperature control by offset sun-pointing
	Cons:	high turning rates & blackouts when sun close to orbit plane (b) mechanism complexity (2 d.o.f.) configuration conflicts : interference with HGA (a)
2. *1-axis articulated* *(a) rotation about out-of-plane axis* *(b) rotation about in-plane axis*	Pros:	some degree of temperature control by offset sun-pointing simpler mechanism (1 d.o.f.) low steady rotation rate : orbit frequency (a)
	Cons:	variable power output (b) variable rotation rate : orbit frequency and seasonal (b) blackouts when sun close to orbit plane (b) or orbit normal (a) configuration conflicts : interference with HGA (a)
3. *Fixed*	Pros:	no mechanisms sides allow large OSR fraction for temperature control
	Cons:	power output varies with true anomaly large power excursion between perihelion and aphelion

Table 5.3-3 Orbiter solar array configuration trade-off

Articulation of the array in two axes (option 1) would permit to rotate the array to any given angle to the sun, realising constant power output and some degree of temperature control by off-set sun pointing (but for the planet radiation).

If the first rotation axis is parallel to the Y axis (out-of-plane, parallel to the normal to the orbit) the two rotations are decoupled (orbit rate about X, sun rate about the second axis) and low-frequency. However, the accommodation on the –Y side is prohibited (view factor to radiator), and the accommodation on the +Y side would lead to conflict with the HGA (that has to be there, see section 5.3.3 below); moreover, this configuration produces no power when the sun is orthogonal to the orbit plane. If the first rotation is about an in-plane axis, the turning rates about the two axes both depend on the orbit frequency, and they become the larger, the closer the sun is to the orbit plane (up to infinite rates when the sun is in the orbit plane).

Since the array does not have to be pointed at a given direction, but only within a given cone angle to the sun line, a simpler configuration, with articulation about one axis is possible. Again, if the rotation axis is out of plane (option 2a), the turning rate is slow and near constant (=orbit rate), but conflicts with the radiator and HGA arise, and no power is produced when the sun is orthogonal to the orbit plane; if the rotation axis is in-plane (option 2b), the turning rate is variable with the orbit frequency and the season, and it becomes singular when the sun is in the orbit plane. Thus, both 2a and 2b have seasonal blackouts.

The simplest solution is with solar panels distributed on three sides of the spacecraft; no mechanism is needed and the sides are large enough to allow a very large reflecting fraction (OSR) to lower the temperature. On the minus side, the power output is continuously variable with the orbital position and with the season; if the panels are sized for the low intensity case (aphelion), a large power excess arises at high intensity (perihelion). This is the preferred solution; methods for shedding the excess power without raising the panel and cell temperature above their safety limits will be studied in Phase 2.

5.3.3 High-Gain Antenna Accommodation Trade-off

The high-gain antenna must be pointed at the Earth with accuracy such that the pointing loss is negligible (e.g. 4 arcminutes at 32 GHz for 0.2 dB loss). As a guideline, the antenna configuration must not preclude the communications with the Earth at any time the link is possible (Earth station in view, no planet occultations), both during the cruise and during the orbit around Mercury, although short-term interruptions may be tolerated.

During the cruise, the direction of the Earth is within a few degrees of the trajectory plane; with the orbital configuration in Fig. 5.3-2, the axis of rotation must be parallel to the axis of rotation of the solar array. During Mercury orbit, so long as the spacecraft attitude is Nadir pointing, articulation in two axes is required. An option where the attitude of the spacecraft was changed for communications purposes was rejected on scientific grounds, as it required an eccentric orbit (see Chapter 2.2).

Similarly to the discussion made for the solar array, two options exist for 2-axis articulation in Mercury orbit, depending on whether the first rotation axis is in plane or out of plane (Table 5.3-4). In the first case, the antenna does not need to execute a full turn (despin) but high rotation amplitudes and rates and blackouts occur. In the second case, the rotation rates are regular and low-amplitude, but a full 2π turn is required and a long boom must be implemented for the antenna to 'see' across the spacecraft body, when the Earth is on the half-plane opposite to the side where the boom root is placed. The second option was preferred because of the detrimental effects of high rotation rates to the pointing. The solution requires (a) high-T mechanism and / or transmission of motion from spacecraft body, (b) a long boom to view across spacecraft body, subject to distortion, (c) large (albeit slow and regular) amplitude turns in both axes : 2π (despin) + π, and (d) contactless RF joints.

The combination of such characteristics makes the implementation difficult, and the whole subject of HGA accommodation is set aside for a new assessment in Phase 2. An alternative option to reduce the boom length could consist in two smaller antennas placed on two opposite sides (+Y, -Y), with a cost impact but a redundancy benefit. Smaller antenna dishes would require Ka band to realise sufficient telemetry data rates.

1. *Two-axis articulated* *1st rotation about in-plane axis*	Pros:	reduced interference by spacecraft body limited amplitude motion (no despin)
	Cons:	coupled rotations : N x orbit rate on both axes high rates when sun close to orbit plane blackouts when sun close to orbit plane
2. *Two-axis articulated* *1st rotation about out-of-plane axis*	Pros:	uncoupled rotations: orbit rate (Y) and earth rate (X') no blackouts because of rotation rate
	Cons:	large interference by spacecraft body long boom length despin

Table 5.3-4 Orbiter high gain antenna articulation trade-off

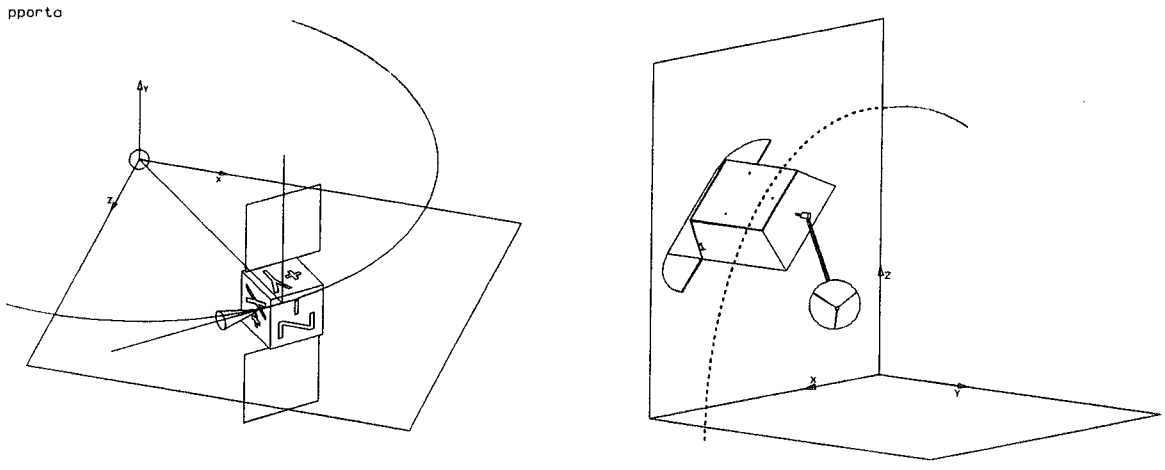

Cruise Phase : Main antenna rotation axis ≈ parallel to solar array rotation axis

Orbit phase : 2 degree-of-freedom antenna articulation

Fig. 5.3-2 HGA articulation during the cruise and Mercury orbit

5.4 *Open Points of Satellite Configuration*

The following aspects are identified for continued study in Phase 2:

- Mass budget, with regard to the 2010 launch option (see Chapter 14)
- HGA configuration, with regard to the articulation and pointing
- Design of the many mechanisms, with particular regard to the environmental requirements. A list of mechanisms appearing in the configuration is in Table 5.4-1.

Cruiser solar array deployment & SADM	HGA hold-down & release device
2 separation systems (1) - Cruise Stage to Chemical Propulsion Stage - Chemical Propulsion Stage to Orbiter	HGA articulation & pointing device (2)
2 spin-eject devices (1) - Subsatellite - Hard Lander	IR shield deployment & tilt device (2)
Subsat cover eject device (1)	Payload instrument aperture shutters, two-way

(1) delayed operation, 2+ years into mission
(2) continued operation in HT environment

Table 5.4-1 Mechanisms list

6. SUBSATELLITE CONFIGURATION AND DESIGN CONCEPTS

6.1 *Basis for the Subsatellite Design*

The Subsatellite of the Mercury mission can be regarded as a small component of the total mission, not in science return, but as physically small in comparison to the main Orbiter satellite. This aspect has driven the design of the Subsatellite to be miniaturised, in conjunction with the condition that no operational orbit manoeuvres should be undertaken by the Subsatellite.

The Subsatellite is intended to cover those aspects of science concerned with fields and particles science. The ideal orbit for these goals is a highly elliptical polar one, with the angle of the line of apsides 60 to 70° from the spin axis of Mercury, with the pericentre as low as possible. It should be noted that the orbit is effectively inertial, and thus covers all the magnetospheric bow shock during 1 Mercury year. The orbit is not fully stable however if the line of apsides is not in the equatorial plane.

Consequently a provisional orbit has been recently chosen for the Subsatellite starting at pericentre/apocentre altitudes of 400/12200 ($5R_M$) km, and with the periherm in the equatorial plane, giving a stable orbit without significant loss of science.

The payload for the Subsatellite is currently defined as in Table 3.2-2 of the Subsatellite payload description section. Part of the Subsatellite requirements also called for a spinning satellite as best suited to the experiments envisaged, with a spin rate approximately 15rpm.

6.2 *Satellite flight attitude*

Before the basic configuration concepts for the Subsatellite can be addressed, the key design driver far outweighing all others has to be taken into account. This is the thermal environment in the neighbourhood of Mercury, and its contrast with the conditions in near-Earth and transfer to Mercury.

The radiation from the Sun is between 4.5 and 10.5 times as great as that for Earth conditions. Worse, when on the sun side of Mercury, about 80% of this is re-emitted in IR onto the side of the satellite not exposed to the Sun. In addition when the satellite is in eclipse, the Mercury albedo is practically nil, so the satellite is effectively in cold deep space for a significant period in the apoherm case.

At the same time solar energy must be collected to power the satellite.

Fig 6-1 shows the possible flight attitude scenarios of the Subsatellite during a Mercury year.

The satellite is assumed spin stabilised, thus requiring no fuel for attitude correction other than through disturbing forces of the Sun and Mercury gravity, and the radiation pressures.

If the spin axis is in Mercury's orbit plane, then depending on season, different parts of the satellite see the sun, sometimes the rim, sometimes the top or bottom of the cylinder, or a mix of both. This makes the thermal design extremely difficult for a spinning satellite. Only by correcting the orbit continuously to make it sun-synchronous is it possible to have e.g. only the rim or only the top face illuminated.

If the spin axis is perpendicular to Mercury's orbit plane the illumination problem and thus the thermal problem is minimised in that only the rim is illuminated irrespective of season.

It should be further noted that if the orbit is held sun-synchronous, then not all of the bow shock is investigated, but only one plane within it, thus contradicting the science requirements.

The conclusion is that there is only one attitude for the spinning satellite that is valid, and that is with the spin axis perpendicular to Mercury's orbit plane (about 7° tilted with respect to the ecliptic).

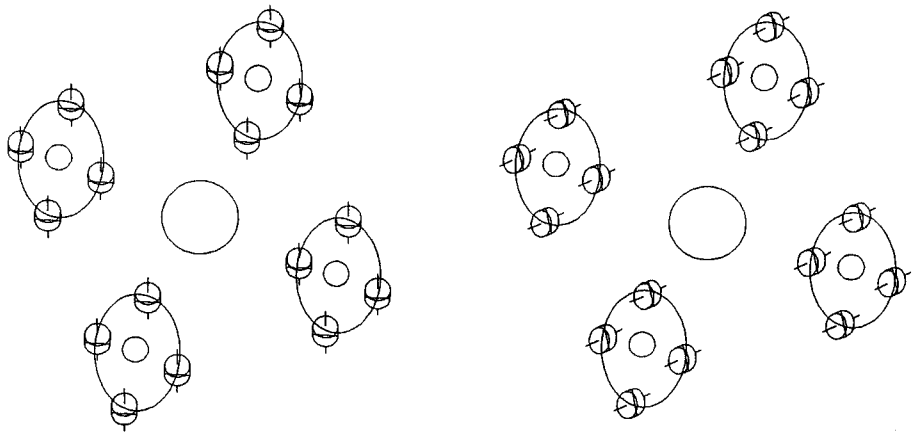

Spin axis perpendicular to Mercury orbit plane Spin axis in Mercury orbit plane

Fig 6-1 Sun illumination for 2 alternative stabilised flight attitudes

6.3 *Satellite configuration alternatives*

With the above requirements framework and conclusions from the orbit assessment, several configuration spinning body concepts were reviewed from the point of view of the solar array. These are shown in pictorial form in Fig 6-2.

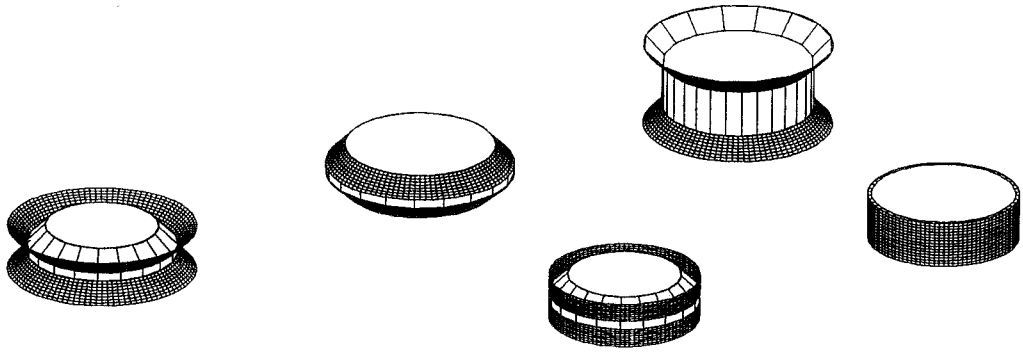

Fig 6-2 Initial Subsatellite configuration concepts

It is clear that whichever configuration is chosen, all have a solar array ring around the circumference, and radiator surfaces at the top and bottom of the body cylinder.

It is at this point in the selection procedure that thermal design and concepts play a key role, together with solar cell thermal capabilities.

Driving the choice of layout was a short analysis of the internal temperature of the satellite body. It was clear from the outset that the body temperature (and also the solar cells) would rise to over 110°C if the body was uninsulated thermally, and this for the case of a simple drum with radiators top and bottom, and only heated by the Sun. Heating of the "backside" by the planet would raise this temperature significantly further.

Two measures can then be taken to reduce this problem.

The first directly affects the configuration, and that is to reduce the body rim directly exposed to the Sun. The second is to adopt a Helios type of solar array or similar, so that the cells backface radiation does not impinge significantly upon the body.

This second measure also reduces the temperature of the solar cells to reasonable values. The first measure however on its own reduces the height of the body such that not enough internal volume remains.

With the revision of the payload described in section 3 including the addition of 2 extra instruments came also a change in the fields of view demanded, and this is shown in Fig 6-3.

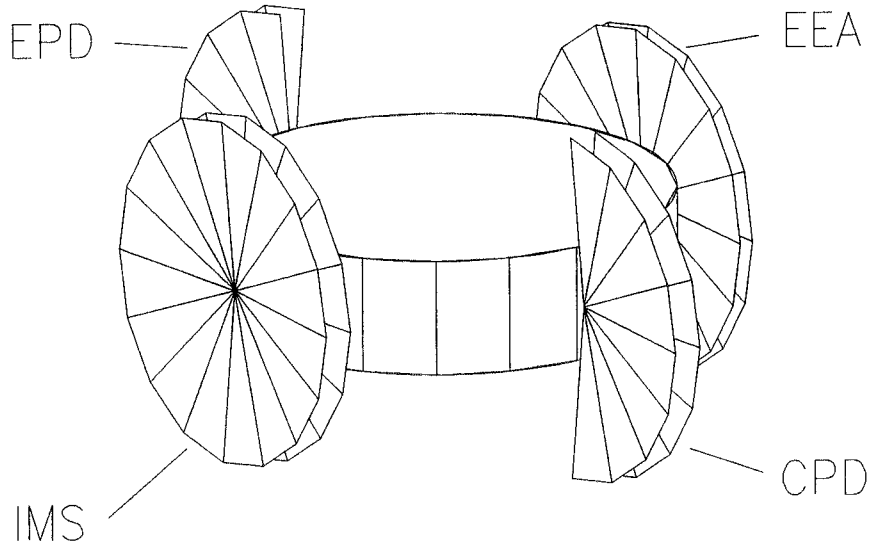

Fig 6-3 Instrument Fields of View

The orbiter solar array studies were far enough advanced to offer a new high temperature variety of solar array, capable of surviving temperatures up to possibly 250°C. Because the solar array rotates with the spinning body, such temperatures are not reached by a simple cylinder of cells with open back faces. This allowed a configuration concept as shown in Option 5 of the same figure. This solved the fields of view problem and the severest thermal restrictions simultaneously.

All of this review and initial analysis was conducted assuming a body diameter of approx 0.8m, and a cylinder body height of greater than 0.2m.

Using this concept a configuration incorporating the revised payload was developed as provisional baseline with a body height of 0.3m, and a revised diameter of 0.9m, caused mainly by the addition of the 2 new instruments, and is illustrated in Fig 6-4.

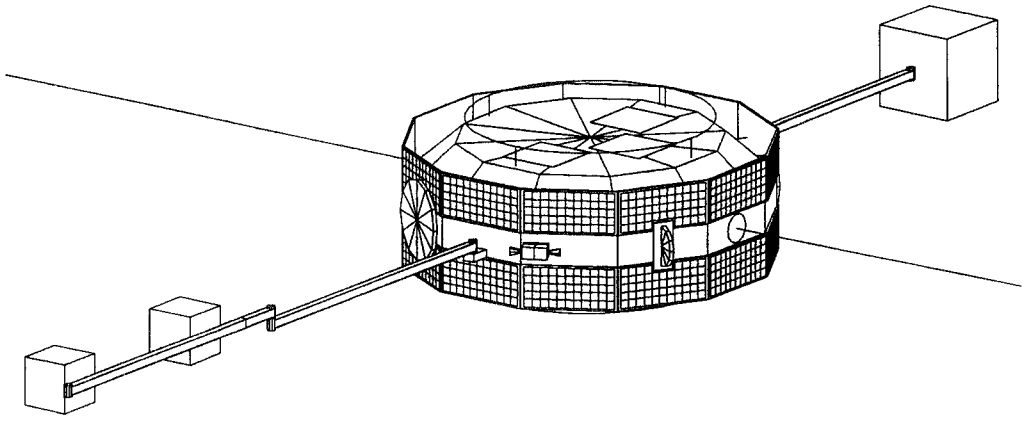

Fig 6-4 Provisional Phase 1 Baseline Configuration of the Subsatellite.

The main features are:

- Solar array segments form a cylinder of flat panels
- Straight and shorter rigid booms (revised payload)
- 4 instruments on the body periphery with large fields of view (revised payload)
- Shorter wire booms (revised payload)

An initial assessment of the internal configuration has been undertaken. In terms of volume and shape the electronics units have not been optimised as yet, and this leads with the additional 2 instruments to a satellite configuration with the diameter of 0.9m, as stated above. This is illustrated in Fig 6-5.

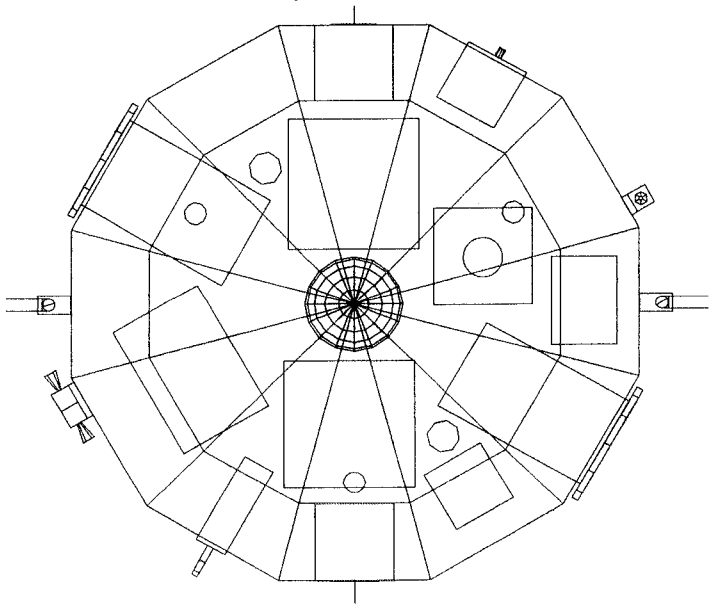

Fig 6-5 Internal Subsatellite configuration

Further refinement of this internal layout will not be made at this juncture here, but it is expected that with rearrangement of the overall unit shapes the unused volume available within the satellite body can be utilised better than at present. This may allow a reduction of the 0.9m overall diameter to a lower value if this is critical to the Orbiter/Cruiser design.

6.4 *Thermal design and Constraints on Orbits*

The primary aim of the satellite thermal design is to attempt to create conventional near-Earth temperature conditions for the electronics mounted in the interior of the satellite body. This is to reduce or eliminate development costs for high temperature electronics. To that end the main body of the satellite has been designed to form a thermally insulated chamber, with radiators top and bottom, as shown in Fig 6-6.

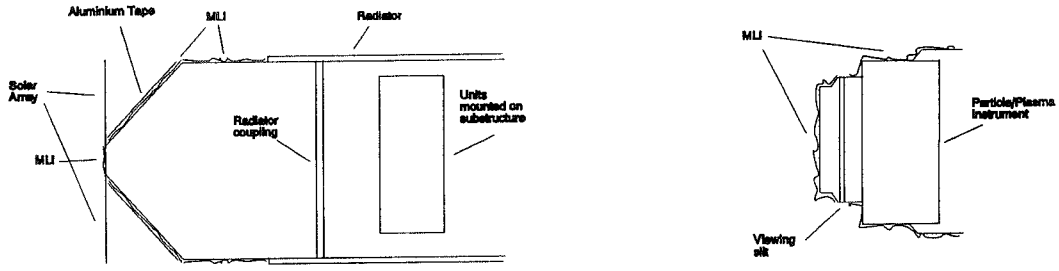

Satellite body

Particle/plasma instruments

Fig 6-6 Basic Thermal Concepts

Inside this chamber are all the electronic units, excluding any pre-amps needed for the detectors mounted on rigid booms. This means that only the detector heads for the 4 particle/plasma instruments with large fields of view protrude. Fig 6-6 also illustrates this, and shows that the protruding heads are also covered in MLI, except where the viewing slits are located.

The wire boom dispensers are contained in the main body, and only small holes in the structure are provided to allow the wire to deploy.

Fig 6-6 also shows that the top and bottom radiators are thermally connected with e.g. CFRP rods. The electronic units are mounted on substructures, and not directly attached to the radiators.

It is assumed that the radiators can be of fixed exposed area for steady state conditions in sunlight, and that the heat loss without covering the radiators during eclipse is tolerable.

A major factor for thermal loading is the position of the orbit w.r.t. the sun and Mercury. The design assumption is that the Subsatellite pericentre is between the sun and Mercury at Mercury aphelion (see Chapter 2.2).

The second major factor in thermal loading is the altitude of the pericentre for the Subsatellite orbit. The higher the pericentre, the lower the thermal loading from the planet surface.

The third major factor in thermal design is the reverse problem of the satellite becoming too cold. When the satellite is in eclipse, the Mercury albedo is practically nil, so the satellite is effectively in cold deep space for over 2 hours at apoherm. This will also occur only seasonally and not near dawn/dusk orbits as the orbit is not sun-synchronous. The thermal inertia of a satellite of 50kg is not large and cannot be used as a sufficient aid in resolving this aspect.

These 3 factors:

- relation of satellite pericentre to Mercury aphelion
- height of pericentre
- eclipse

can only be resolved by analysis of a simplified satellite thermal model in various operational scenarios. Then it should become clear what restrictions on the orbit choice result from the assumption of electronics operating at near-Earth temperatures. Also clearer will be the extent to which the radiator surface must be varied, either mechanically with louvres or with variable emittance panels (e.g. ESTHER).

An initial analysis for the case of Mercury at aphelion and the Subsatellite with periherm above the Mercury dayside (Fig 6-8) indicates the following.

The worst case internal temperature range is relatively stable and between about 0 and 80°C. This is the environment for the electronics, and is within the range of present technology capability.

The rigid boom and boom harness temperatures can be above 200°C and a detailed thermal analysis is needed of the units mounted on the booms, requiring as start point a detailed instrument mechanical description, because the internal temperatures of these units can also be very high. The wire booms reach 400°C in sunlight.

The effects of the transfer from Earth to Mercury must also be taken into account. In this case the Subsatellite is attached to the Cruiser/Orbiter. There is therefore no control over the illumination conditions on the Subsatellite, it is driven by the operational requirements on the Cruiser of the transfer orbits. Further, the heat input near Earth is very much smaller than for the Mercury design case.

It must therefore be assumed that the additional thermal measures needed to protect the Subsatellite from large temperature excursions are undertaken by the Cruiser. This means heating power from the Cruiser, and/or a cover over the Subsatellite during the cruise phase.

6.5 AOCE/OBDH/Memory

The concepts chosen for AOCS electrical part (named the AOCE here and excluding sensors) and OBDH dictate the signal/data exchange concept within the satellite and how the electrical system in the Subsatellite relates internally, and externally to other parts of the satellite.

The classical approach, particularly for larger satellites, is to have a data bus with RTUs or DBUs distributed to the various elements as interfaces. As the number of interfaces reduces with, e.g. less payload elements, the approach restricts itself to e.g. a CTU and an RTU. For the small Subsatellite this approach is not viable due to the mass and size constraints. A fully integrated system is required with the absolute minimum of internal and external interfaces between modules/elements.

Further the approach where each subsystem is separate and can be tested in isolation is not possible as this drives the mass up through the mechanical consequences of interconnections and separate unit box casings.

To this end the AOCE, OBDH and memory must be treated as a single mechanical unit, and the functions, e.g. processing, must be shared where possible.

This is also true of the TM/TC function, which should also be integrated where possible, excluding the transponder/antenna part.

In this way the number of individual chips is reduced and replaced by software where necessary. To assist this approach the revision of the payload now includes an "integrated" central payload electronics unit that serves all payload detectors and front ends, allowing one major electrical interface to the satellite "bus". Developments are under way or being investigated leading to a concept of a miniaturised central satellite control and data unit.

The nominal data rate for the Subsatellite payload is 6kb/s. It must be initially assumed that all the data is required to be sent to the Orbiter, and that none is filtered out. With present memory technology (e.g. PALASIM) capacities of up to 800Gbit are possible, so this aspect has no problems whatsoever.

Recent assessments of the link scenarios to the Orbiter indicate that contact periods of about 30mins per orbit. To transfer all the data thus requires a transmission rate of 110kbit/sec. This rate must be assessed together with the link capabilities, the ability to compress the data on board the Subsatellite before transmission, and the potential for reduction of the sampling to reduce the total of raw data generated.

6.6 AOCS Mechanical and Sensor Parts

The sensors for a spin stabilised satellite also do not require any conceptual change. The major factor here will be to develop sensors that are capable of tolerating the external temperature extremes, since they will be externally mounted.

It is envisaged that fine a Sun sensor and Mercury horizon sensors would be required. The horizon sensor should also be designed to work with the dark side of Mercury, where the IR return is significantly weaker than in the case of Earth.

The RCS has therefore the task of maintaining the spin as elements are deployed, and maintaining the operational attitude during the mission. No orbit correction manoeuvres are foreseen.

Cold gas is the obvious answer for the mission. An initial assessment of the gas volume required to achieve spin-up at release from the Orbiter/Cruiser results in a tank size of 0.1m diameter. This clearly indicates that enough margin is available for increasing the tank above this size for the small attitude corrections necessary during the operational life.

6.7 Communications/TT&C

The Subsatellite has only to communicate with the Orbiter. The payload data rates envisaged for transmission to the Orbiter are 6kb/s real time, plus as a maximum of 200Mbit that stored from the worst case out of contact scenario. This must be downloaded in the following contact period. An approach using higher gain antennas with beam directionality on both satellites is the only practical one.

The resulting contact period is of the order of 30mins each orbit of the Subsatellite. The download of the data collected of 200Mbit must occur in this period, so a total of 110kb/s is required to be transmitted by the Subsatellite with the target of using less than average 15W power. A UHF system with a loop antenna on each of the top and bottom of the satellite provide maximum gain along the spin axis of the Subsatellite. Initial analysis indicates this is the preferred maximum gain direction for the link. The antennas can be easily mounted as a rail onto the edge of the solar array.

6.8 Power and Solar Array

The total power that the power subsystem should provide is estimated to be less than 50w average. Battery charging must also be allowed for (eclipse/sun ratio is 1:6 worst case) so the solar array should provide around 60W, allowing for power subsystem losses.

The power subsystem could be based on the approach suggested in the LISA report of JPL, 27 January 1997. Here the power electronics is assumed capable of being built at 100W/kg. The technology suggested is integrated chip module to VME boards for power control, management and distribution.

Because the solar array cannot be a simple unbroken cylinder (see configuration illustration Fig 3-6), the output will have a significant ripple. The best way to deal with this is to have a so-called battery bus, where the battery is used as a capacitor to smooth the ripple.

The battery itself is also based in the JPL LISA approach, using Li-Ion technology, giving a favourable 80Whr/kg energy density. Given that the longest eclipse is about 2 hours, the battery sizing leads to a mass of 2kg.

Using the technology proposed for the Orbiter for a solar array capable of operating at up to about 250°C, the simple cylindrical solar array concept is possible provided the back of the solar array is open. The area provided by the chosen satellite configuration allows sufficient solar array area to be available.

6.9 Structure

The intention was to choose a simple Aluminium construction since it is cheap and alignment for the Subsatellite elements is not a problem.

A factor affecting the structure design directly is radiation. The radiation environment near Mercury is severe, but this severity is almost entirely due to direct radiation from the Sun (note that radiation does not necessarily follow direct paths). Circumferential walls may be needed to provide radiation protection for the internal electronic units.

A number of materials can be used, but the effort required to establish what is effective and how such material is to be incorporated would be the subject of a technology development programme. The material (probably a form of ceramic) can possibly be used as a structural material.

6.10 Mechanisms

Some mechanisms are integral with the instrument. An example of this are the wire boom deployment units. Others are not. The most obvious are the rigid boom hinges and driving elements. These must expect to function in the full external thermal environment. Development effort is needed here as the level of heat soak has to be established, and thus for individual components, the resulting temperature ranges. It is assumed here that conventional approaches may be made to the design at this stage.

The release mechanism for the Subsatellite, which mechanism remains attached to the Cruiser is at present envisaged to provide a minimum spin rate commensurate with a stabilised Subsatellite and a separation velocity to be estimated taking into account the stability and residual rotation rates of the Cruiser.

6.11 Autonomy

The satellite design concept proposed assumes the typical single point failure protection for the "bus" subsystems but not for the instruments. In the same way the safe mode would be conventionally defined. For the spinning satellite this is only of significance if the thrusters or thruster command system malfunctions to produce a thruster "jammed" on. This case can be removed at the design level by careful consideration of single point failure types.

This situation is fortunate for 2 reasons. First the Subsatellite can only talk to the Earth via the Orbiter. This link is not transparent in real time but only via internal Orbiter procedures, partly due to the fact that the link to the Subsatellite is probably only around 30mins per orbit. Secondly the Orbiter, if in its proposed eccentric orbit, only communicates with the Earth near its orbital apocentre. The time of contact for the Subsatellite in any case is thus severely restricted. The question is then whether the Subsatellite should incorporate a degree of "self-repair". As stated, this is not the present assumed baseline.

6.12 Mass Budget

A provisional mass budget based on the approaches already discussed is presented in Table 6-8. It should be noted that the masses are raw, and contain no maturity or margin. It would be expected at this stage to add up to 20% to arrive at the real mass when the satellite is eventually built. Note the protection cover for use during the cruise phase is not included, nor is the release mechanism for the Subsatellite.

Item	Mass Kg
Magnetometer	1.0
Ion Spectrometer	3.0
Ion/Electron Analyser	0.9
Wave Analyser	2.75
Cold Plasma Detector	0.7
Energetic Particle Detector	0.2
Central Electronics	1.3
Structure (incl rad shield)	7.5
Thermal	2.5
Nutation dampers	1.0
Power	1.0
Battery	2.0
Solar Array	1.0
AOCS/OBDH Electronics	4.0
AOCS sensors	1.5
RCS	5.5
Memory	0.5
Comms/TT&C	5.0TBC
Harness	2.0
PIE	2.7
Mechanisms/booms	2.0
Balance	1.0
Raw Dry Mass	49.05

Table 6-8 Mass Budget

6.13 Power budget

The power budget is shown in Table 6-9. The payload power is based on that given in Section 3.

Item	Power (W)
Payload	15
AOCS/OBDH	15
Comms/TT&C (av)	15
Other	5
Total at output	50
Total at Solar array	60

Table 6.9 Power Budget

7. SURFACE PACKAGE

7.1 Introduction

The definition of the surface package at the start of the study was open. It was not clear whether the package should be a penetrator or a soft lander, but the opinion was that a penetrator was the most likely approach. Initial discussions with the scientific group resulted in an revised approach to this part of the Mercury mission, where the mass of the surface package payload would be defined after some analysis had been carried out to indicate the maximum mass permitted due to other mission constraints. To achieve this some guidelines as to the maximum mass of the total surface package that could be carried by the cruiser/orbiter was necessary.

A short review of typical penetrator probes for other planets was undertaken, and as a typical example the DS2 Mars penetrator was chosen as representing the characteristics of such an element. At this point the concept of a soft lander was not considered, as all soft landers reviewed were large relative to the mission parameters for Mercury.

7.2 Description of DS2

A simplified description of DS2 is given below, together with an illustration of the package after landing (Fig 7-1).

Total probe mass = 2kg
Diameter = 12.6cm
Height = 8.5cm (stowed)
Lifetime = 48hrs
DS2 Instruments:
Accelerometers
Drill and soil sampler
Temperature sensor
Pressure sensor
Sun sensor
Impact velocity < 200m/s
Impact angle < 25°
Angle of attack < 12° to vertical

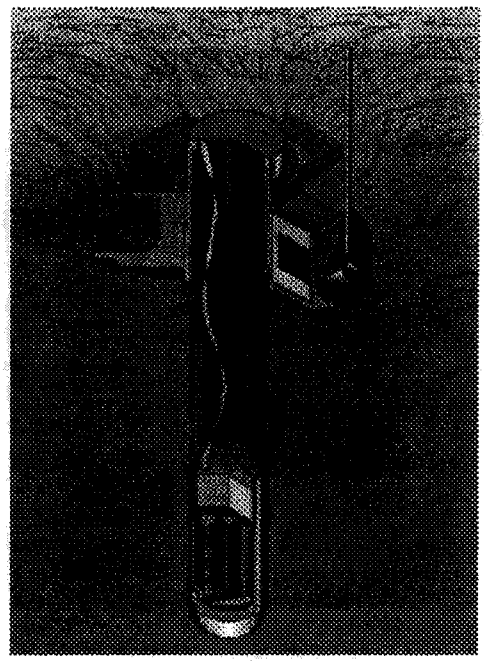

Fig 7-1 DS2 after impact

As is easily seen, the mass of the payload is only a small proportion of the 2kg total, as batteries form a significant part of this. This means that the instruments are miniaturised, but must be capable of withstanding at least 30,000g deceleration at impact.

7.3 *Mercury surface package*

The impact itself is restricted to a near vertical approach by the penetrator. This is reasonable to enhance the chances of mission success in achieving a good impact without tumbling on an unpredictable surface (slope, presence of rocks). The requirement to approach vertically is for Mercury a major restriction not seen in other missions using penetrators. Nearly all others use the appropriate planetary atmosphere to reduce the orbital velocity to that of the impact, and allow a near-vertical approach to the surface without additional energy expenditure.

Mercury has no atmosphere, so this approach cannot be used. Instead de-orbiting and landing motors would be required to reduce the velocity from orbital values to those acceptable to the penetrator at impact. In itself this provides a large mass increase for the orbiter/cruiser to carry, but the absence of atmosphere also removes the ability to orient the penetrator using atmospheric drag forces. This must now be done by a suitable miniaturised AOCS and thrusters.

The initial orbit assumptions for the surface package are those for the sub-satellite, i.e. apoherm at 12,200km altitude, periherm at 400km altitude, and a resulting periherm velocity of approx. 2600m/s. However the de-orbiting is conducted, it must be in 2 burns if solid propellant is used, one to de-orbit, and the second to directly reduce the impact velocity after de-orbiting. Analysis indicates the propellant required is essentially independent of method.

The result is that, for a 2kg penetrator, with additionally 2kg for AOCS/thrusters/guidance sensors, the total mass of the surface package as attached to the orbiter/cruiser, is 35kg.

Using solid propellants, the approximate size of such an assembly is 450mm long and 450mm nominal diameter, based on the illustration of Fig 7-2

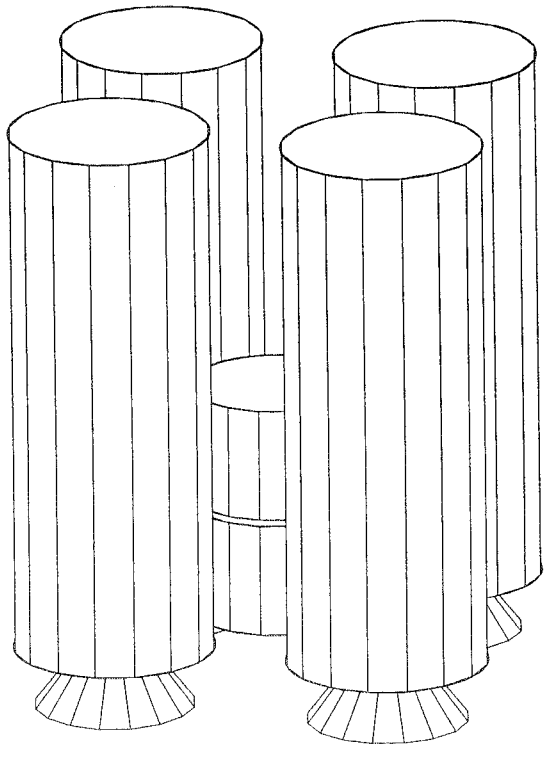

Fig 7-2 Conceptual volume model of Surface Package

7.4 *Design aspects of the penetrator*

In principle the design approach for DS2 can be used for the Mercury mission, but with some significant changes. These relate to the provision of power to the payload after landing. In DS2 the power is provided by batteries, which give a life of about 48hrs. Given that the Mercury Subsatellite and the orbiter are not always going to be in line of sight or within range for reception of signals from the penetrator, then this tight restriction cannot be allowed.

The alternative is to have a small substructure on top of the penetrator carrying solar cells, and these would provide continuous power.

Related to this topic is that of temperature at the planet surface. It is not envisaged that the lander should be capable of surviving the temperatures seen on the planet near the equator, but rather that the lander be located near the poles. This would also allow longer term observations. To permit this longer term it is not acceptable to use batteries only, and this means the lander must land in sunlight and be positioned on the planet to maximise the remaining time in sunlight (land near Mercury dawn).

Because of the shallow angle of sunlight to the surface, there is a greatly increased risk of shadow if the penetrator lands in a crater, or simply behind a boulder. Only use of batteries resolves this by permitting landing on the dark side as well, and being independent of sun illumination. The price is the short lifetime limit, and this is not viewed as acceptable at present.

No estimate has been made, but it must significantly reduce the chances of success if not only possible tumbling on impact due to collision with a rough surface or boulders are accounted for, but also the chances of shadowing.

7.5 *Alternative approaches*

Given the limitations on the penetrator approach to the surface package, this approach was critically reviewed. It was realised that, if so much energy was required to de-orbit and land a penetrator, the extra required to reduce the landing velocity to zero for a soft landing formed an insignificant increase in the fuel budget.

With this in mind the second part of the study will concentrate on the possibilities of a miniaturised soft lander for this mission, to allow comparison with the penetrator approach.

The exception to this is Lunar A, which carries probes with a de-orbiting motor, each probe weighing 13kg and carrying a very small payload.

How small this payload would be can be seen from our analysis of the penetrator, i.e.700gm for the whole penetrator!

8. ELECTRIC PROPULSION

8.1 *Electric Propulsion for Interplanetary Missions*

Electric Propulsion Systems generate the thrust by acceleration of a propellant by electric energy. The exhaust velocity is in general higher than for chemical propulsion systems and therefore the specific impulse is higher. The propellant necessary for a dedicated mission decreases accordingly.

The saving of propellant mass will be counteracted by a relatively high dry mass of the electric propulsion system, which is mainly caused by the thruster mass and by the mass of the power conditioning unit, which converts the power from the satellite main bus into the different voltages and currents necessary to operate the thruster.

In addition a power source will be necessary to supply the power for the thrusters, which will also increase the dry mass of the system.

The advantages of electric propulsion versus chemical propulsion can only be investigated by a comparison of the masses on satellite system level. A break-even point in favour of electric propulsion normally is achieved at satellite masses above 1000 kg and delta-v's above 500 m/s, which certainly is the case for an interplanetary mission like this one.

8.2 *Electric Propulsion Systems for the Reference Mission*

For the Mercury Orbiter Mission requiring a $\Delta v > 4$ km/s (considering a Venus gravity assist manoeuvre) the following criteria for the selection of a thruster system are applicable:

- Thrust level above 100 mN
- Specific Impulse above 1500 s
- European supplier preferred

Three thruster types meet the above mentioned criteria:

- SPT-type thruster, 140 mm discharge chamber diameter, manufactured by SEP, France, or by MMS, England (SPT 140 or similar)
- Electronbombardment Ion Thruster, 220 mm beam diameter, manufactured by MMS and DERA, England (T6 IPS)
- Radiofrequency Ion Thruster, 220 mm discharge chamber diameter, manufactured by Dasa, Germany, (RIT-XT)

8.3 *SPT-Type Thrusters*

8.3.1 Development Background

SPT (Stationary Plasma Thrusters) have emerged from a Russian propulsion technology, a few years ago, with the background of frequent space flight experience on Russian spacecraft. At present the SPT 100 (100 mm ionizer diameter, 80 mN thrust, 1500 s Isp) is the workhorse that many of the satellite Prime contractors are considering for an application to North/South Station Keeping of geostationary satellites.

A formal qualification, required by telecom spacecraft, to western standards and performances has been done by ISTI, a joint venture between SS/L, FAKEL, ARC, RIAME and SEP.

In addition some work is going on in USA, Russia and in Europe (MMS and SEP) to develop the higher thrust SPT 140 engine (140 mm ionizer diameter) to be used for orbit transfer to GEO and for interplanetary missions.

8.3.2 SPT Operation Principle

The thruster operation is based on the control of the electrons migration in a discharge by a transverse magnetic field. A discharge is established between the anode located upstream of an annular insulating channel and a cathode outside. The anode acts also generally as a Xenon distributor.

The magnetic field is provided by polar pieces located near the exit of the channel in order to provide a field maximum in the exit section. Due to low transverse (or perpendicular) plasma electrical conductivity in a magnetic field, the magnetic field lines translate into equipotentials. As a result, the electrostatic field is perpendicular to the magnetic field. Ions are accelerated by the electrostatic field while electrons obey essentially to the magnetic field. In the exit plane the electron current is only 20 % to 25 % of the total discharge current.

The steep radial magnetic field gradient is a key in the efficient operation of the SPT. This is obtained by either magnetic screens or multipolar layout (patent designs). The walls play an important role in the electrodeless transverse conductivity. It is very important to master the ceramic composition in order to get the proper secondary electron emission coefficient for a given electron energy.

The SPT family feature a centre coil and four outer coils and a magnetic circuit including two polar pieces, rods, magnetic breech and magnetic screens.

The accelerating channel is a single block of ceramics with the anode located upstream. Two cathodes are provided, one main and one in cold redundancy.

The Xenon flow is controlled by a set of valves and a thermocapillary enabling to adjust the Xenon flow rate and consequently the discharge current and the thrust. This is very useful for differential throttling and also to adjust the thrust to the available power and thermal dissipation.

Fig. 8.3-1 shows a partial cross-section of an SPT thruster.

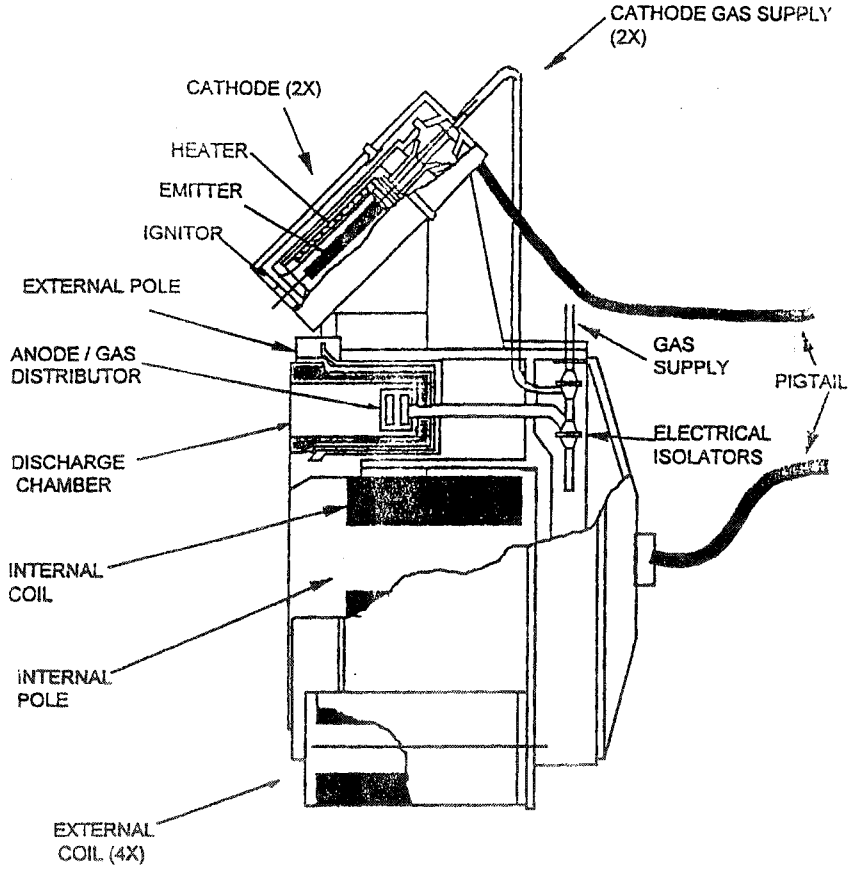

Fig. 8.3-1: SPT Partial Cross Section

8.4 *Electron Bombardment Thrusters*

8.4.1 Development Background

Development Activities over many years in the UK have culminated in the development of a 10 cm beam diameter gridded ion thruster (UK 10, also referred to as T5) which has been developed for tasks requiring moderate thrust below about 30 mN.

The UK 10 will be flown on ESA's geostationary communication satellite Artemis, alongside the German RIT-10 thruster, and used for north-south station keeping.

A collaboration agreement, covering further development and marketing of bigger diameter gridded ion thrusters for use on future large communication satellites was signed between MMS and DERA in 1997 as a response to the market assessments. Development of a 22 cm beam diameter ion engine T6 IPS with a nominal thrust of 150 mN is now in progress.

This thruster will be the basis for application to the reference mission.

8.4.2 Operation Principle

The gridded ion systems developed in the UK are based on Kaufman-type ion thrusters. Each thruster must be supplied with propellant gas at accurately regulated flow rates from a propellant supply and monitoring equipment (PSME), and with appropriately controlled voltages and currents by a power conditioning and control equipment (PCCE).

The thruster, shown in schematic form in Figure 8.4-1, follow the general principles laid down by Kaufman. Propellant gas – originally mercury, now Xenon – is fed from the PSME into the cylindrical discharge chamber via an axial hollow cathode and a by-pass distributor mounted on the soft iron backplate.

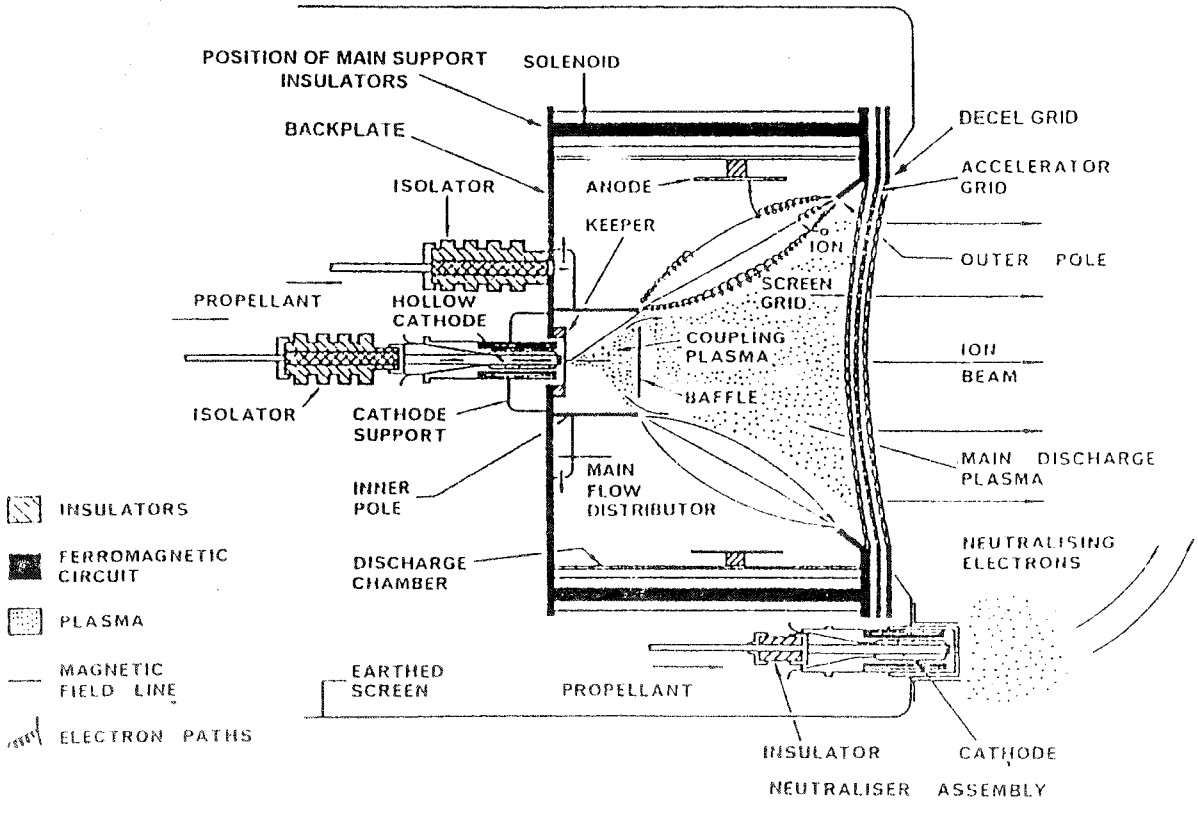

Fig. 8.4-1: Schematic View of the UK Kaufman-Type Ion Thruster

This gas is ionised in a DC discharge between the cathode and a concentric cylindrical anode. The efficiency of this discharge process is enhanced considerably by the application of an azimuthally symmetrical magnetic field to the discharge chamber. This field is generated by solenoids equispaced around the outside of the discharge chamber. Six solenoids are used in the T5 and UK-25 designs, whereas the T6 incorporates 12 to ensure complete azimuthal field uniformity.

The magnetic field links two cylindrical pole pieces, the one bolted to the back plate being of much smaller diameter than that at the exit from the discharge chamber. The tip of the inner pole piece surrounds a non-magnetic baffle disc, which effectively separates the hollow cathode region (the coupling plasma) from the main discharge plasma.

The design of these critical components is such that the primary electrons from the cathode gain the correct amount of energy in passing through the annular gap between this disc and the pole piece to achieve optimum ionisation in the discharge chamber.

The resulting highly ionised plasma drifts toward a set of closely spaced, perforated grids at the downstream end of the discharge chamber. The positive ions are extracted and accelerated to a high velocity by electric fields applied to these grids. This velocity is determined totally by the applied potentials, and is typically 30 to 50 km/s.

The positive space charge of the emerging ion beam is neutralised by electrons emitted from an external cathode, which is essentially identical to that in the discharge chamber. The neutraliser is fed with Xenon at a very low flow rate, and a plasma is created adjacent to its tip by a discharge between it and a nearby keeper electrode. Electrons are extracted automatically from this plasma to maintain the spacecraft at close to space potential.

8.5 Radiofrequency (RF) Ion Thruster

8.5.1 Development Background

The RF ion thruster (RIT) principle has been developed at the university Giessen by Prof. Loeb. At Dasa (Daimler-Benz Aerospace AG) RIT thrusters are under development since many years. Discharge chamber diameters from 10 to 35 cm have been investigated.

The most advanced thruster system is based on a 10 cm discharge chamber diameter (RIT 10). A thruster of this type has been flown on the retrievable carrier EURECA in 1992/93. Two thruster system are currently installed on the European telecommunication satellite Artemis, where they will perform north-south station-keeping together with the UK-10 thruster produced by MMS in Portsmouth after the launch into space, which is currently scheduled for the year 2000.

In addition function tests have been performed with the RIT 35 (35 cm discharge chamber diameter), which was able to produce a thrust level of 200 mN at specific impulses above 4000 s.

The ESA-XX has been developed in Cupertino with AEA Technology in Culham (England) and Laben/PROEL in Florence (Italy), using the RF-ionisation principle of the RIT, the grid system design from UK-25 and the neutraliser as developed from Laben. The function tests of this thruster using a discharge chamber diameter of 26 cm have been successfully completed in September 1998.

Dasa has now started the development of a RIT ion thruster for commercial application for a nominal thrust level of 150 mN, which is expected to be qualified in 2001. The data used during this study are based on this thruster system.

8.5.2 RIT Operation Principle

The RF-ion thrusters achieve ionisation of the propellant gas by inducing energy by means of a high frequency generator coil positioned around a discharge chamber. The operational priciple is illustrated in Fig. 8.5-1.

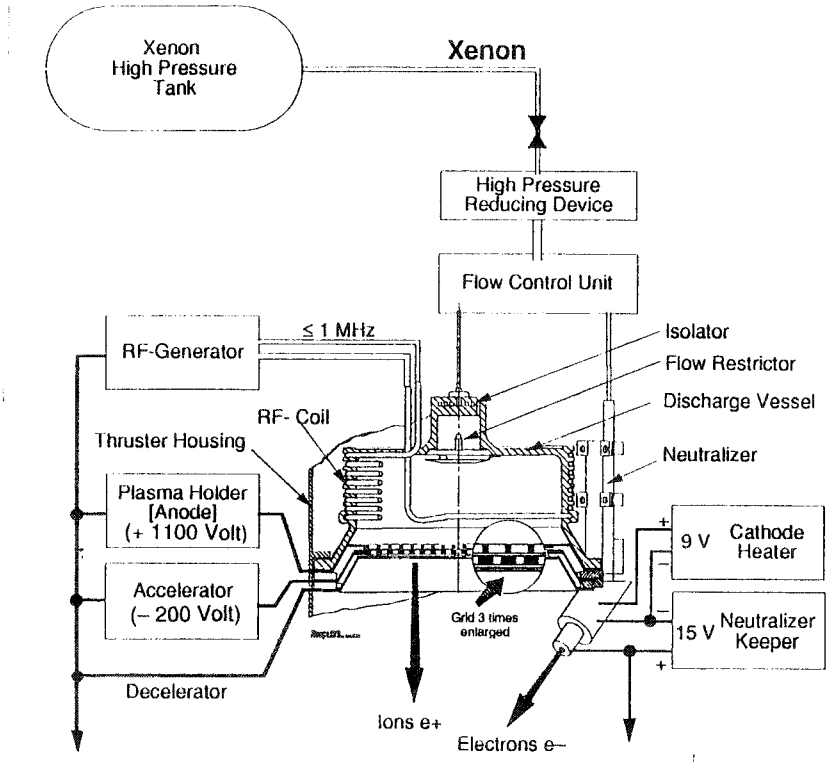

Fig. 8.5-1: RF-Ion Thruster Operating Principle

The propellant Xenon enters the discharge chamber of the thruster through the isolator and a gas distributor.

To start the ionisation of the Xenon the neutraliser is activated first. Electrons generated in the discharge at the neutraliser tip are drawn into the discharge chamber by application of positive potentials to the electrodes of the extraction system. The electrons in the discharge chamber accumulate energy from the RF-field of the induction coil and ionise the neutral propellant by inelastic collisions with the propellant atoms.

Once the discharge has started it is self sustaining and the voltages on the grids can be switched off. The thruster is now in a state of Stand-by condition, ready for thrusting.

To generate thrust, a positive high voltage (900 to 1200 V) is applied to the plasma holder and a negative high voltage (-200 to -600 V) is applied to the acceleration electrode. The decelerator is kept on thruster ground potential.

Under the influence of this electrostatic field positively charged propellant atoms (ions) are accelerated towards the thruster outlet at velocities in the range of 40 km/s.

The ion beam is neutralised by electrons from the discharge at the neutraliser tip, where the electrons are generated by ionisation of Xenon in a low voltage arc discharge between a cathode and the keeper of the neutraliser. The ion beam will act as potential wall for free electrons. The current drawn from the neutraliser thus match the needs for neutralising the ion beam automatically.

Thrust control can be realised easily and accurately by the control of the beam current via the density of the ions in the discharge chamber, which again is controlled by the energy of the RF-field via an automatic control loop.

8.6 *Thruster System Design and Interfaces*

8.6.1 Sources of the Data

The data presented in the following for the three types of electric thruster systems shall allow a comparison of the thruster systems and shall be used as inputs for trajectory calculations within the mission analyses and for the design of the spacecraft. The data have been collected from the following sources (see also Study Notes Ref. 8-9):

SPT thrusters:

SEP, Villaroche, Mr. E. Klinger, Fax ref. DI/P 13452/98, 11/08/98 and telephone conversations

Electron Bombardment Thrusters:

MMS Bristol, Mr. John Farrow, Fax ref. MERC/Fax/8, 29.6.98; Presentation MERC/JF/1, July 1998 at Dasa; Minutes of the Meeting, Doc. SD-MI-AI-0379, 3.7.1998.

RF-Ion Thrusters

Dasa - in house data, generated by the departments RIA 62 and RST 34

The data collected from the different sources have been simplified to fit to the requirements of the mission analyses and to be able to be used for the design of the spacecraft.

8.6.2 Electric Propulsion System Characteristic Data

The data in Table 8.6-1 give a survey on main data, on the heritage and on the next planned activities for the three electric propulsion systems.

	RITA-XT	SPT 140	UK-T6 IPS
Data source	Dasa	SEP	MMS
Thrust level	50 - 200 mN	150 – 250 mN	40 – 240 mN
Thruster Dimensions	300 ∅ x 200	220 x 200 x 175	300 ∅ x 200
Thruster Mass	6 - 7 kg	6,8 kg	5 kg
Flow Controller Mass	2.7 kg (for 2)	0.6 kg (for 2)	0.7 kg
PPU Mass	18 kg	13.7 kg	20 kg
PMA Mass	--	?	5 kg
Expected Lifetime	10,000 h	7,200 h	10,000 h
Heritage	RIT 10, 10 mN flown on EURECA RIT 10 15 mN qualified for Artemis ESA-XX tested at 200 mN	SPT-70 numerous flights in Russia SPT 100, 80 mN flown on Russian Satellites, qualified for western standards	UK-10, 18 mN qualified for Artemis UK-25, 200 mN tested
Planned activities	Start of commercial development of RITA-XT in 1998, qualification expected in 2001	Thruster and electronics under development, qualification expected in 1999	Thruster and electronics under development, qualification expected in 1999

TABLE 8.6-1: Electric Propulsion System Characteristic Data

8.6.3 Thruster System Operational Data

As an input to the mission analysis and trajectory calculations the data for total power input (from main bus) versus thrust level (Fig. 8.6-1) and total specific impulse (from the tank supply) versus thrust level for Begin of Life (Fig. 8.6-2) and End of Life (Fig. 8.6-3) have been generated.

The effect of lifetime on the thruster performance has been considered in a reduction of specific impulse, which could be caused by erosion in the grid system for the ion thrusters and by erosion of the discharge chamber for the SPT thrusters. The necessary power input has been kept constant.

During a progress meeting in June 1998 it has been agreed that the operational data of RIT-XT and UK T6 are so close that the effort for additional mission analysis using the specific UK T6 data is not necessary. Therefore the diagrams show equal data for RIT-XT and UK T6.

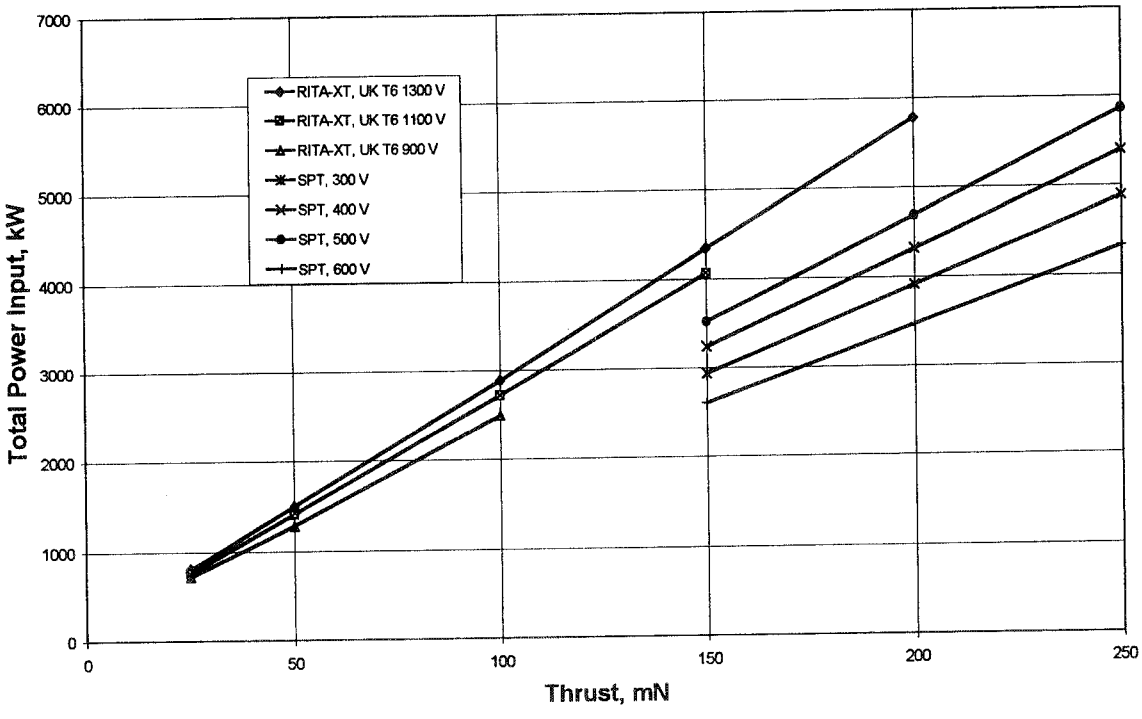

Fig. 8.6-1: Total Power Input versus Thrust level

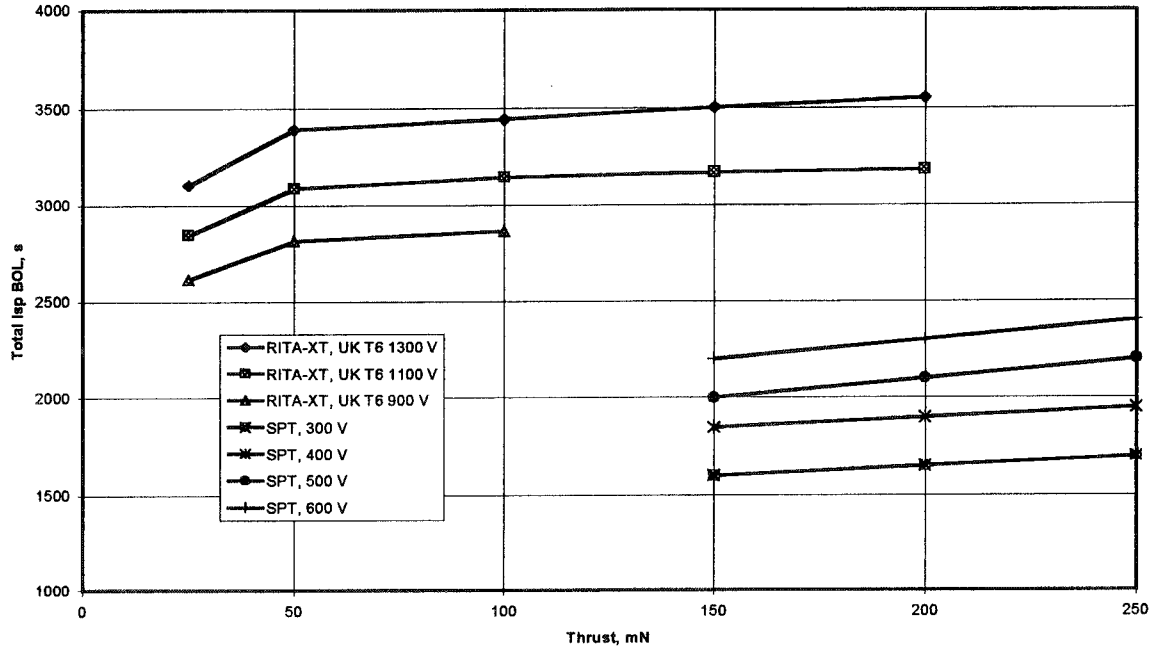

Fig. 8.6-2: Total Specific Impulse, BOL

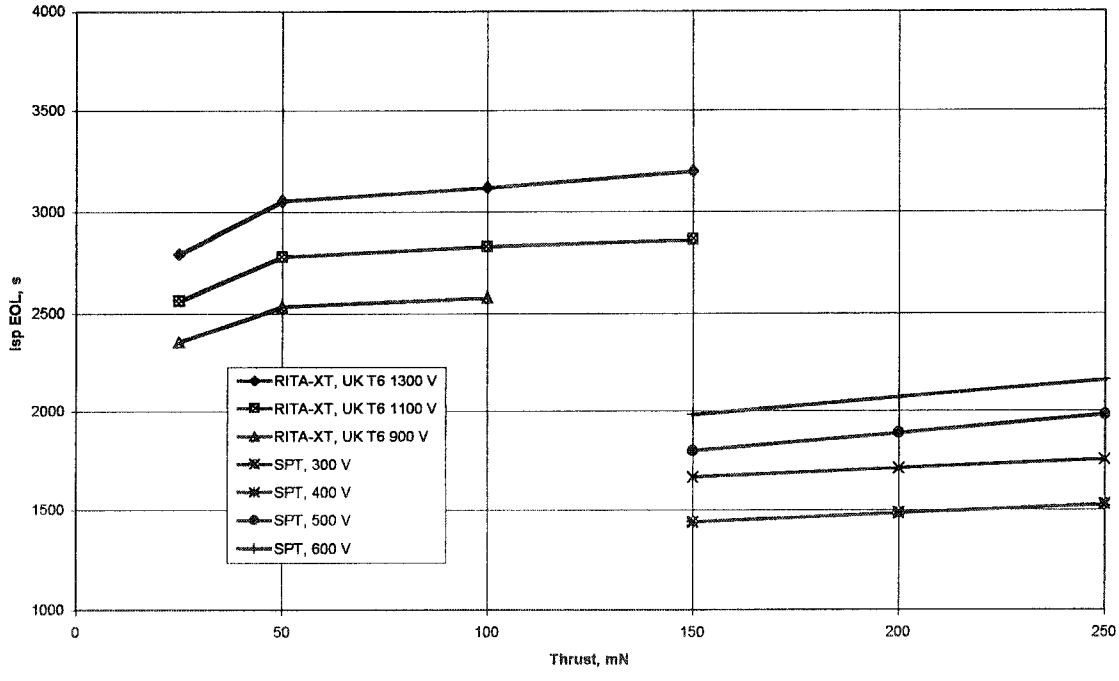

Fig. 8.6-3: Total Specific Impulse, EOL

8.6.4 System Block diagram

The mission – according to mission analysis – can be performed with 4 ion thrusters operating in parallel at 150 mN. In case of a thruster failure the mission can be continued with 3 thrusters at 200 mN. As an alternative, one more thruster could be added to reduce torques after 1 thruster failure (see Chapter 12.2).

The 4-thruster block diagram, which is valid more or less for all three thruster systems under consideration, is shown in Fig. 8.6-4

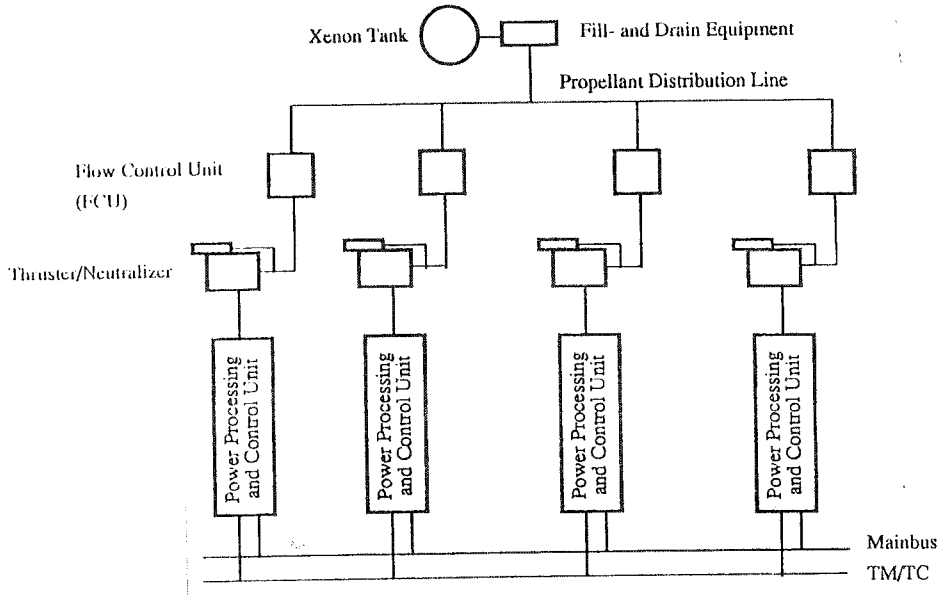

Fig. 8.6-4: Block diagram of the Electric Propulsion Subsystem

8.6.5 Thermal Interface of Electric Propulsion Units

For the layout of the spacecraft the following assumptions for the heat loss of each unit can be used:

- Thruster/Neutraliser

  The thruster will be mounted on the spacecraft thermally insulated. About 10 W will be conducted through this insulation into the spacecraft.

  The other heat loss in the thruster, which is in the range of 20 % of the thruster power, will be radiated into space by the thruster case at temperatures around 200° C.

- Flow Control Unit (FCU)

  The heat loss of the flow control unit is in the range of 15 W, which will be conducted into the S/C structure

- Power Processing Unit (PPU)

  The overall efficiency of the PPU is expected to be in the range of 92 %. That means that about 8 % of the total power input will be conducted into the S/C structure.

8.6.6 Mass Budget

Considering the installation of 4 thruster systems according to the blockdiagram in chapter 8.6.4 the following masses can be expected. The masses have been estimated by the thruster developers. Real hardware data are currently not available.

The tank mass will depend on the propellant mass necessary and will be between 15 and 20 %.

Unit	RITA-XT	SPT 140	UK T6
4 Thrusters	24 kg	27.2 kg	20 kg
4 Flow Controllers	10.8 kg	1.2 kg	1.2 kg
4 Pressure Reducers	0	1.2 kg	1.2 kg
4 Power Supplies	72 kg	54.8 kg	80 kg
Cabling/Tubing	10 kg	10 kg	10 kg
Total dry mass	**116.8 kg**	**94.4 kg**	**115.6 kg**

Table 8.6-1 Mass budget

8.7 Conclusion

According to the detailed investigations performed during the study all three thruster types will be able to fulfil the requirements on the relevant propulsion system.

The masses of the hardware are based on estimations. The rather small differences can change when actual hardware masses are available.

For final application a thruster system will be selected, which is developed for commercial application. Adaptation of technical parameters to the special requirements of the mission will be necessary and will have an impact on the costs.

The selection will mainly depend on the cost of the propulsion system, which will again depend on the number of commercially produced thrusters and the necessary changes.

9. SOLAR ARRAY

9.1 *HIHT-Solar Cell Parameters*

There exists no detailed knowledge on the behaviour of solar cells at high intensities and high temperatures. Therefore some assumptions with regard to the solar cell characteristics at high intensities and high temperatures have to be made.

For this study the solar cell IV-characteristic is described by the simplified formula

$$I = I_{sc} - I_0 \cdot \left(e^{(V+I\cdot R_s)/V_T^*} - 1\right) \qquad (9.1)$$

with $V_T^* = A \cdot V_T = A \cdot k \cdot T/q$ (see G. La Roche: „Solargeneratoren fuer die Raumfahrt", ISBN3-528-06945-7).

It is assumed that variation of the intensity at constant spectral conditions changes the short circuit current according to

$$I_{sc}(c) = c \cdot I_{sc}(1) \qquad (9.2)$$

(c = concentration factor = multiples of solar constant 1). That means, the current increases proportional to the intensity.

For the open circuit voltage applies:

$$V_{oc}(c) = V_T^* \cdot \ln(c) + V_{oc}(1) \qquad (9.3)$$

The open circuit voltage increases proportional to the logarithm of the intensity.

The above formulas apply for standard temperature conditions, e.g. 28°C. At different temperatures the initial values have to be corrected by application of the temperature coefficients. The following temperature dependent temperature coefficients have to be respected:

$$\left.\frac{dV}{dT}\right|_{I=const} = \frac{V - E_g(0)}{T} - \frac{3k}{q} - \frac{\alpha T}{(T+\beta)} - \frac{\alpha T^2}{(T+\beta)^2} \qquad (9.4)$$

with $3k/q = 2{,}59 \cdot 10^{-4}$ V/°K, E_g in eV and α in eV/°K

For Silicon is $E_g(0) = 1{,}153$eV, $\alpha = 2{,}30 \cdot 10^{-4}$ eV/°K and $\beta = 136$°K and for GaAs is $E_g(0) = 1{,}53$eV, $\alpha = 5{,}4 \cdot 10^{-4}$ eV/°K and $\beta = 204$°K.

For the temperature coefficient of the current applies

$$\left.\frac{dI_{sc}}{dT}\right|_{V=0} = \frac{dI_G}{dE_g} \cdot \frac{dE_g}{dT}$$

$$= \left(-0{,}0914 + 0{,}03328 \cdot E_g(T) + 0{,}00149 \cdot E_g(T)^2\right) \cdot \left(\frac{-2\alpha T}{(T+\beta)} + \frac{\alpha T^2}{(T+\beta)^2}\right) \qquad (9.5)$$

9.2 *Selection of Solar Cell Type*

9.2.1 Solar Cell electrical Characteristic

The solar cells selected for this study were Silicon Hi-eta and GaAs/Ge solar cells. The characteristic cell data are given in Table 9-1. With these data and the above intensity/temperature dependencies each a Silicon and a GaAs solar array have been defined providing 10kW electrical power under AM0 conditions. When approaching the sun both intensity and temperature increase. This has contrary effects on the solar cells. While increasing intensity increases also the solar cell power increasing temperature reduces the solar cell power. There exists a break-even point where the power gain by the intensity is compensated by the power loss due to the temperature. This point defines the maximum power coming out of the solar array. Further approach to the sun reduces the power until complete power loss due to a voltage break-down when a special temperature limit is reached.

	Si-Hi-eta	GaAs/Ge
I(sc) [A/cm^2]	0,04775	0,03063
I(mp) [A/cm^2]	0,04342	0,02888
U(mp) [V]	0,530	0,854
U(oc) [V]	0,630	0,998
AM0-Efficiency	16,83%	18,04%
dI(sc)/dT [A/cm^2·°C]	7,51E-05	1,71E-05
dI(mp)/dT [A/ cm^2·°C]	3,90E-05	2,88E-06
dV(mp)/dT [V/°C]	-2,10E-03	-1,96E-03
dV(oc)/dT [V/°C]	-2,15E-03	-1,94E-03
dP(mp)/dT [W/ cm^2·°C]	-5,96E-05	-5,40E-05
$C(I_{sc})$	0,148	0,317
$\Phi_0(I_{sc})$	6,06E+13	4,27E+14
$C(I_{mp})$	0,178	0,405
Φ_0 (I_{mp})	1,26E+14	6,21E+14
$C(V_{mp})$	0,059	0,087
Φ_0 (V_{mp})	4,85E+12	2,28E+14
$C(V_{oc})$	0,067	0,081
Φ_0 (V_{oc})	9,00E+12	9,84E+13
Coverloss	0,973	0,990
Absorptivity	0,760	0,730
Emissivity	0,805	0,805

Table 9-1. Characteristics of solar cells investigated

Keeping down solar cell temperature is possible by application of optical surface reflectors (OSR) so-called second surface mirrors (SSM) and/or by tilting the array away from the sun. Both effects have been investigated. 10kW solar arrays have been defined and equipped with Si-Hi-eta and GaAs/Ge solar cells respectively. These arrays were virtually sent to a mission to mercury under different solar aspect angles. Figure 9-1 gives the result for the Si solar array, Figure 9-2 for the GaAs solar array (both equipped with 20% SSM's).

The Si solar array has the maximum power at appr. 0.57AU but needs to be tilted by minimum 60° when approaching mercury at appr. 0.33AU. Otherwise the solar array power would break down completely. The maximum power is appr. 50% higher than the initial power near Earth.

The GaAs solar array has the maximum power at appr. 0.35AU close to the mercury perihelion. The solar array power never breaks down completely and the maximum power is appr. 250% higher than the initial power near Earth. Therefore, a GaAs solar array has been selected for further investigations.

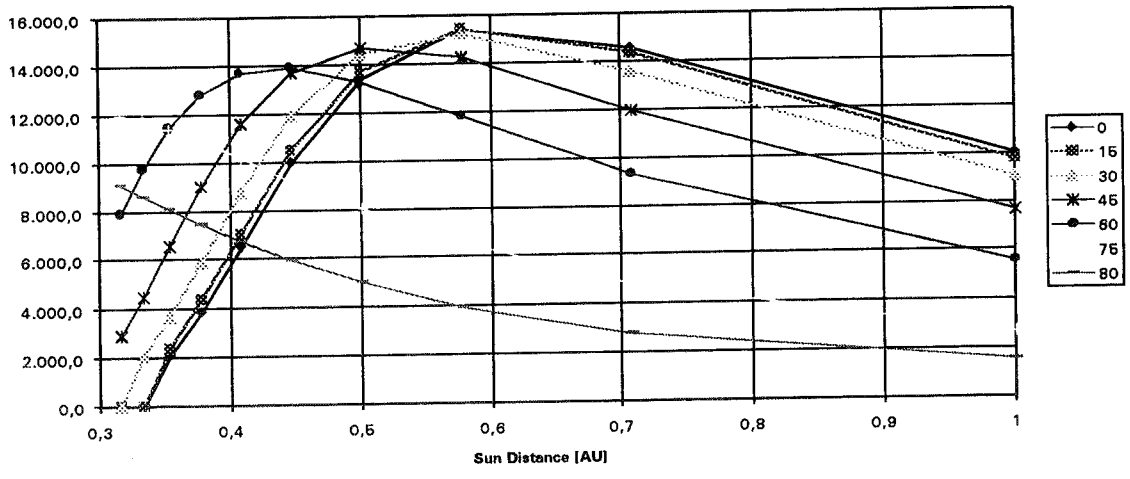

Figure 9-1. Si-Solar Array power as a function of sun distance and solar aspect angle

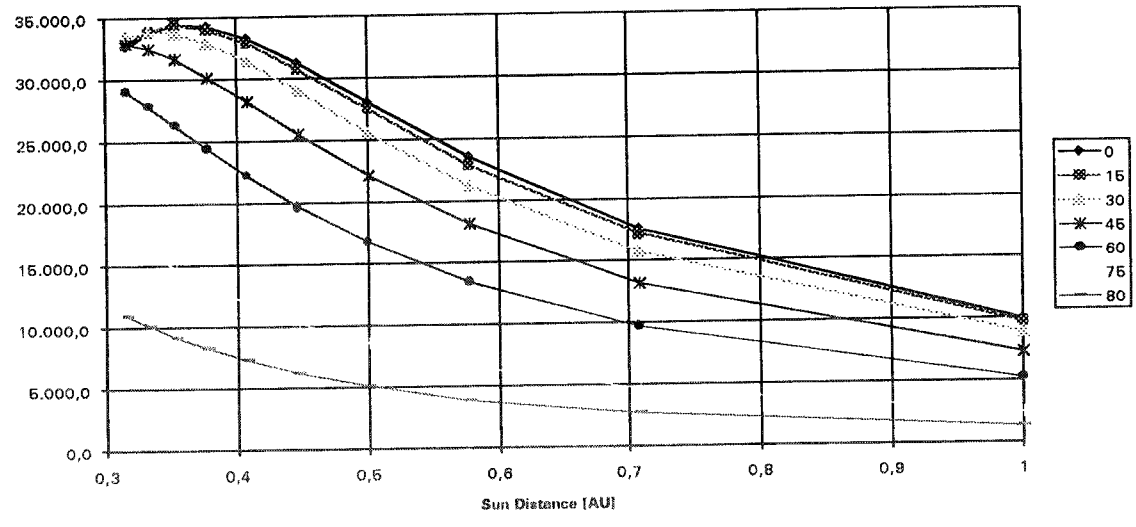

Figure 9-2. GaAs- Solar Array power as a function of sun distance and solar aspect angle

9.2.2 Verification of solar cell parameters

In order to verify the assumptions made for the description of the solar cells at high intensities and high temperatures competent solar cell manufacturers have been involved to provide DSS with experimental and theoretical data on their cells in the intensity and temperature range considered. Enel (formerly CISE, Italy) has provided DSS with a report (Enel SRI-PDM-LPI-98-3 of 24.9.98) evaluating test results on single junction and multi junction GaAs-based solar cells. For extreme temperatures and intensities a theoretical model developed by Enel has been used. The comparison of the Enel data with the data calculated from the DSS model is given in Figures 9-3 to 9-5. The data fit very good with a slightly better performance received with the Enel model. In consequence the DSS model was considered adequate to describe the solar cell performance under high intensity-high temperature conditions correctly.

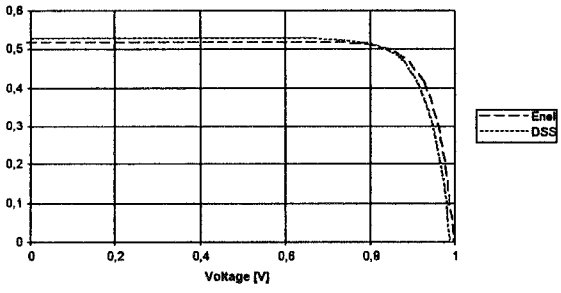

Figure 9-3. Basic Solar Cell Characteristics at 1SC; 32°C

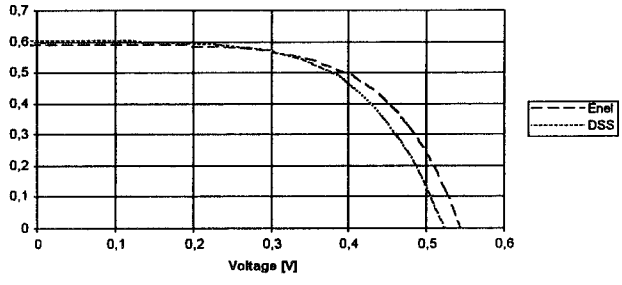

Figure 9-4. Basic Solar Cell Characteristics at 1SC; 260°C

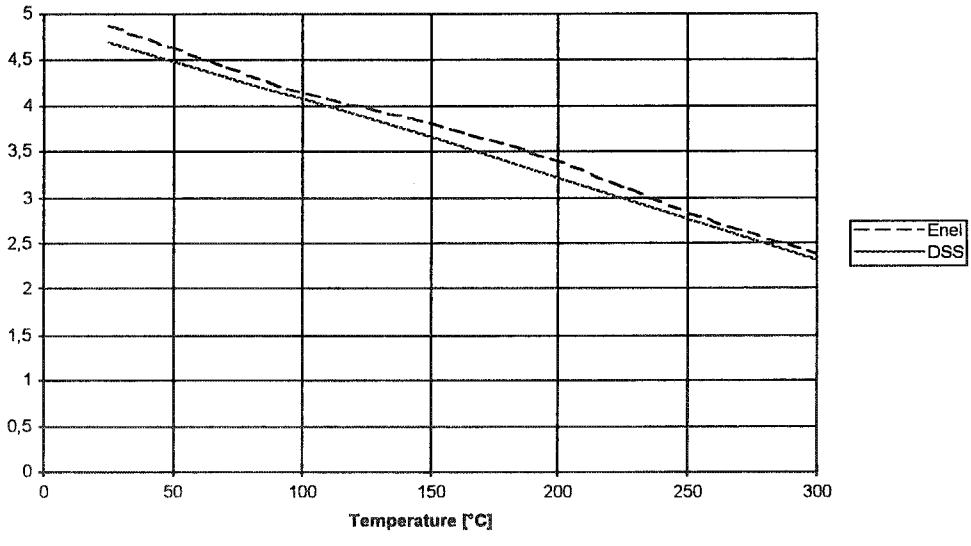

Figure 9-5. Comparison of maximum cell power calculated with DSS and Enel GaAs solar cell model

9.3 *Cruiser Solar Array*

9.3.1 Requirements

The cruiser solar array shall provide the electric power required for the cruise to mercury. The solar array needs to be rotated (±180°) around one axis perpendicular to the trajectory plane (~ ecliptic). No BAPTA is required. The power demand at 1AU shall be ≥10kW. Temperature limitation by tilting the solar array away from sun shall be utilised. The solar array shall be equipped with 20% second surface mirrors (SSM's).

9.3.2 Layout and materials

To meet the BOL requirements set forth the solar array must have an area of minimum 55m^2. An existing solar array meeting this requirement is a solar array out of Alcatel's Spacebus family. Figure 9-6 gives a possible layout.

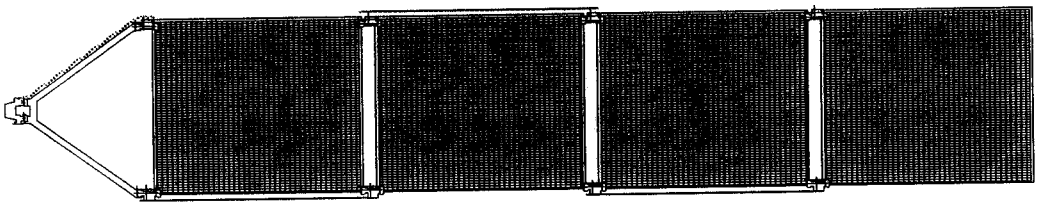

2 wings with 4 Panels per 2.16m x 3.25m. Total area: 56m^2; Mass: 192kg

Figure 9-6. Cruiser solar array based on Spacebus 3000

By keeping the solar array temperature below 150°C standard solar array technology is applicable. The standard panel substrate is an Al-honeycomb with a CFC-sheet on both sides. The maximum tolerable temperature is in the order of 150°C, short excursions up to 250°C should be tolerable (as already experienced by accident on a test coupon!). Portions of the structure which are exposed to direct insolation could be protected by thermal foils (superisolation multilayers).

The Yoke should be foreseen to be made of metal (Al, Ti or Mg) because it is exposed to full sun independent from the tilt angle.

If the temperature limit is increased to 200°C advanced materials shall be applied.

A list of applicable materials is given in Table 9-2.

Component	Technology available	Preferred for Mercury Mission
Substrates	CFC or Kevlar+Al-honeycomb Al and Al+Al- honeycomb Glassfibre on Kapton Kapton with printed circuits Milled Magnesium	CFC+Al-honeycomb; edges protected with Superinsulation foils
Yokes	CFC in winding technique	metallic structure (e.g. Ti or Mg) protected with Superinsulation foils
Hinges/Mechanisms	Al, Ti	Al protected with Superinsulation foils or sun shield
Solar Cells	Si, GaAs/GaAs, GaAs/Ge, CIS	GaAs/Ge with thickened contacts
Coverglasses	fused Silica, BRR microsheet CMX, CMZ, CMG, CMO	PST CMG-IRR/EAR
OSR	OCLI Corning 7940 Grade 6-G PST CMX-SSM	PST CMX-SSM
Adhesives	DC 93500, RTV-S 695, RTV-S 691	DC 93500, RTV-S 691
Insulation foils	Kapton Tedlar Superinsulation	Kapton plus Superinsulation
Cables	Axon Ag with Tefzel insulation Gore Cu with Kapton insulation	Axon Ag with Tefzel insulation
Interconnectors	Ag-foil, Ag-mesh Au-foil Mo-foil Al in-plane	Ag-foil (20µm)
Interconnection Techniques	Resistance/parallel gap welding US-welding, Soldering	Resistance welding
Connectors	Raychem MTC-wafers Deutsch, Cannon	Raychem MTC-wafers plus as required by BAPTA

Table 9-2. Materials list for the Cruiser solar array

9.3.3 Power versus sun distance

The power available at different tilt-angles is already shown in Figure 9-2. Figure 9-7 gives the solar cell temperatures under different sun aspect angles in dependence of the sun distance. For an untilted solar array the temperature would increase to nearly 300°C at the end of the cruise phase (mercury perihelion). Therefore a temperature limitation by tilting is required. Figure 9-8a gives the power as a function of sun distance if the array temperature is limited to 150°C and 200°C, respectively. Figure 9-8b gives the corresponding polynomial approximation curves.

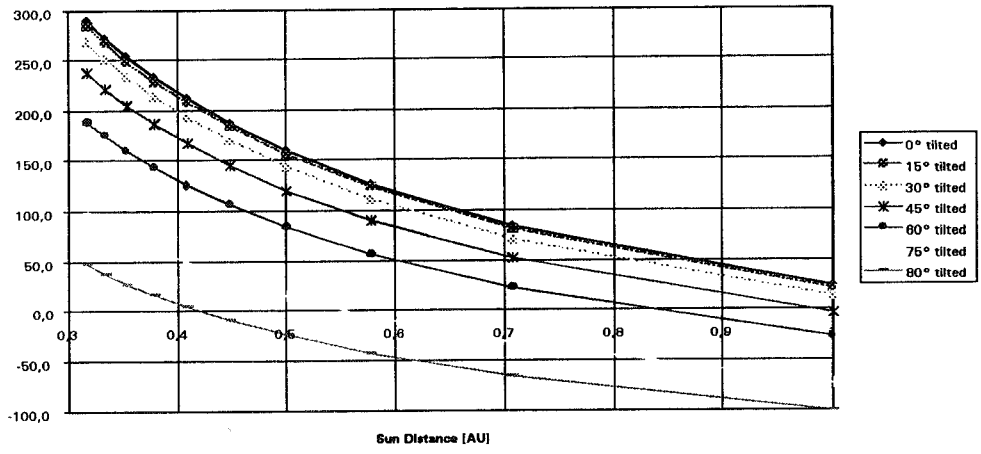

Figure 9-7. Solar cell temperatures versus sun distance at different tilt angles

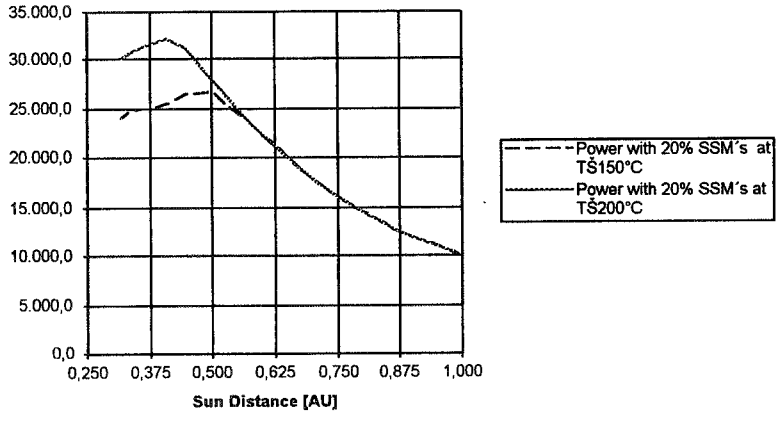

Figure 9-8a. Solar array power as a function of sun distance with temperature limited to 150°C and 200°C

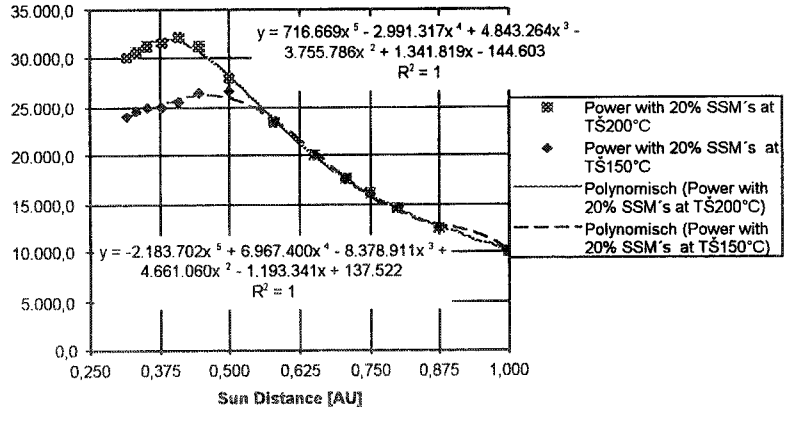

Figure 9-8b. Approximation curves for Figure 9-8a

The required tilting of the solar arrays is shown in Figure 9-9. The 150°C limit requires a maximum tilting of 68°, the 200°C limit requires 57.5°. Though tilting limits the temperature range power should be regulated by maximum power tracking in order to utilise always the maximum power generated by the solar array.

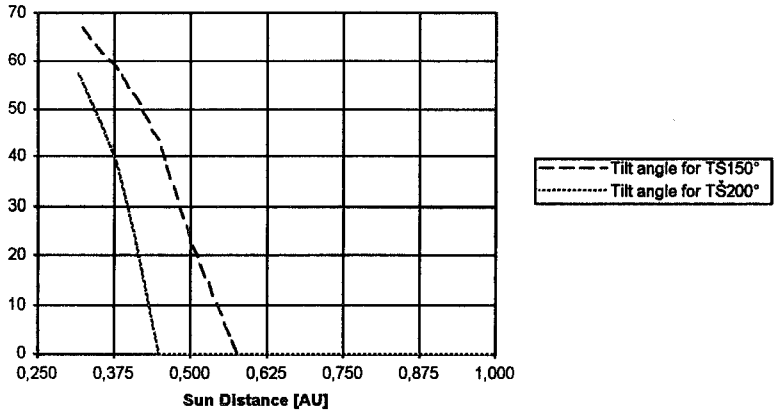

Figure 9-9. Required tilt angles to meet 150°C and 200°C temperature limits

9.4 Orbiter Solar Array

9.4.1 Requirements

The Orbiter solar array shall be body-mounted with 25° slant Kapton insulated Al-panels on ±X-side and +Y-side (Figure 9-10). The area of each panel is approximately $2m^2$. Temperature shall be passively controlled by the radiator (connected via heat pipes; heat conductivity 100 $W/m^2 \cdot K$) and 70% SSM's on the panels ($\alpha = 0.09$; $\varepsilon = 0.825$). The power requirement is ≤500W on a nominal 400x1500km polar orbit.

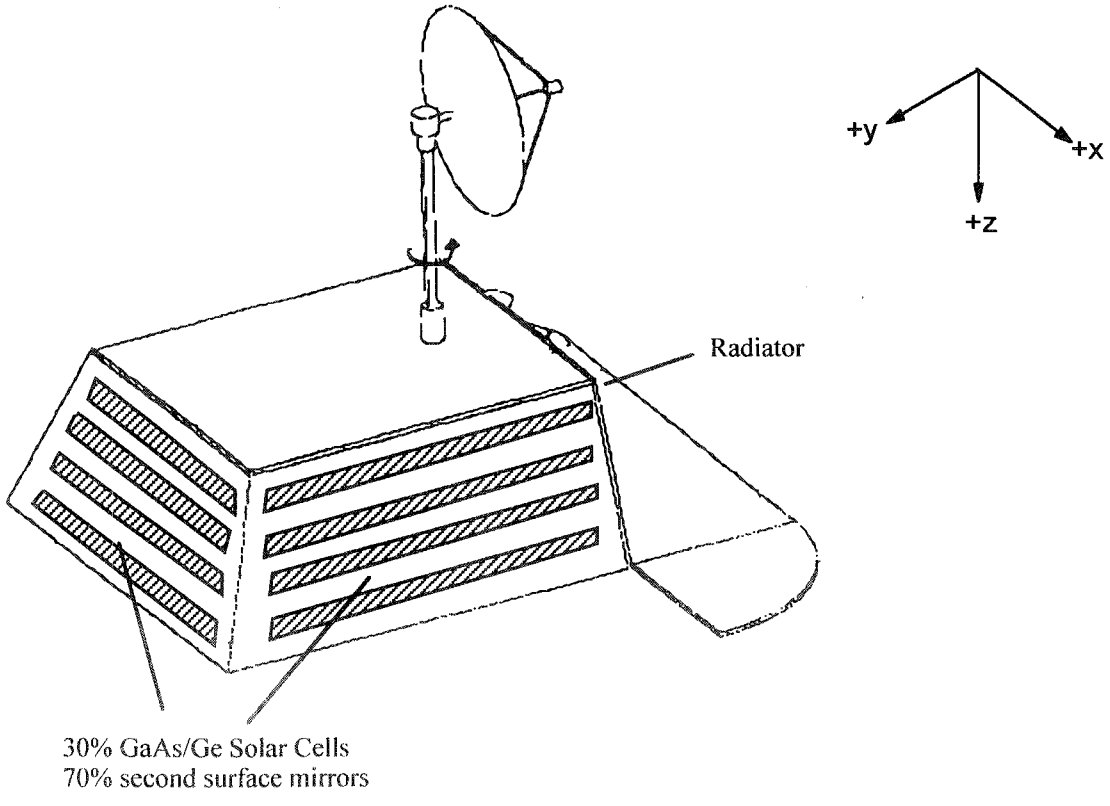

Figure 9-10. Orbiter Configuration

9.4.2 Layout and Power

Same materials are foreseen for the Cruiser solar array with the exception of the solar panel substrates, which shall be 2mm thick Al-plates with 25μm thick Kapton insulation foil, and the mechanisms, which are not required. The +z-axis of the orbiter is always nadir pointing. Therefore, depending on the ascending node, the solar aspect angle of the solar panels changes continuously. In Figures 9-11 and 9-12 the solar array power for two extreme orbits, a terminator orbit and a subsun orbit (for simplification reasons only a 400km circular orbit is considered) is calculated. The planet's position is in perihelion. Then the average power is 1022W for the terminator orbit and 875W for the subsun orbit. The calculated temperature extremes are 175°C and 195°C.

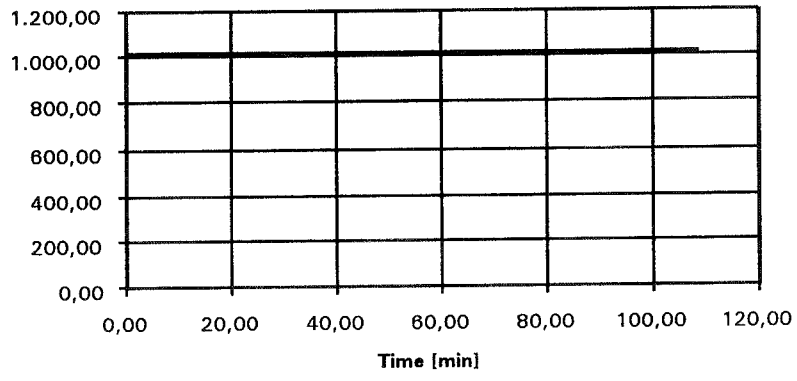

Figure 9-11. Solar array power in a terminator orbit (1022W in average)

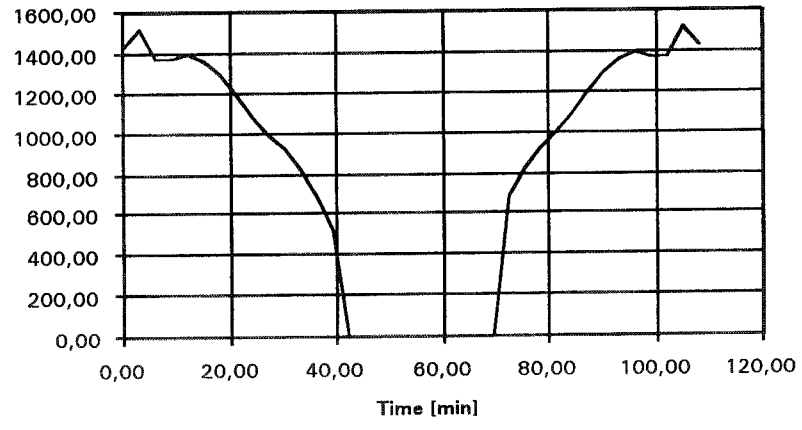

Figure 9-12. Solar array power in a subsun orbit (875W in average)

9.5 Subsatellite Solar Array

The solar array is a dodecagon with 12 panels 230mm x 110mm each (Figure 9-13). On each panel 26 (2cm x 4cm) GaAs/Ge Solar Cells plus 20% SSM's can be arranged providing for nominal 96W in spinning mode in a 200km-orbit at mercury perihelion and 211°C average temperature. Detailed analysis is required to assess the influence of shadowing by the booms. Solar cells with integrated by-pass diodes might be required. So far same technology as for the orbiter solar arrays is applicable.

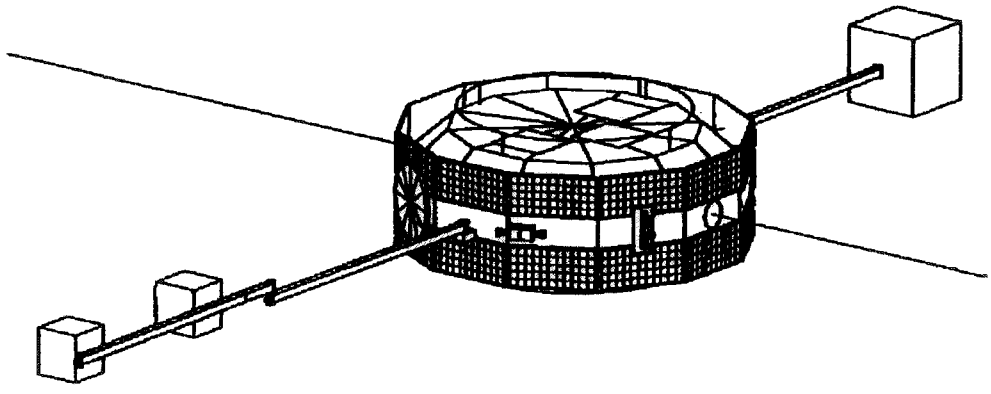

Figure 9-13. Subsatellite configuration

9.6 Conclusions

Solar arrays equipped with GaAs-based solar cells are required for the mission. Standard technology is applicable provided the solar arrays will be tilted to guarantee maximum temperature limits. Critical areas of the supporting structure and the mechanisms to be protected by superinsulation. Power control shall be by maximum power tracking. No BAPTA is required either for the cruiser solar array or for the body mounted Orbiter and Subsatellite solar arrays.

The following technologies have to be developed and further investigated:

a) HIHT cruiser solar array technology with emphasis on HIHT GaAs solar cell technology, HIHT solar cell assembly technology utilising blue/red reflecting coverglasses, HIHT module technology with 20% second surface mirrors, thermal control of yokes, mechanisms and panel edges.

b) HIHT lightweight body mounted Al-solar array technology. Special consideration of shadowing effects by extension booms.

c) Charging of solar arrays and preventive measures.

10. THERMAL CONTROL

10.1 Mercury Environment

Mercury is the closest planet to the Sun with a mean orbital distance from the Sun of 57.9 Million km. The slow rotation causes the surface temperature to be very high on the day side (about 700 K), while on the night side it remains very cold (about 100 K). The parameters influencing the thermal design of spacecraft orbiting around Mercury are summarised in Table 10.1-1.

	Perihelion	Aphelion
Solar constant	14490 W/m²	6290 W/m²
Planetary flux at subsolar point, sunlit side	13614 W/m²	7348 W/m²
Equivalent temperature	700 K	600 K
Planetary flux at subsolar point, dark side	6 W/m²	6 W/m²
Equivalent temperature	100 K	100 K

Table 10.1-1 Planet thermal parameters

The temperature of the surface as seen by a spacecraft varies significantly, both with the spacecraft position (orbit variation) and with the distance to the sun (seasonal variation), and proper modelling of these variations is important for the calculation of the IR fluxes.

Software packages that calculate IR fluxes (THERMICA or ESARAD) assume the planet at uniform temperature, hence the results have to be corrected to account for the actual planet temperature distribution. For the purposes of the study, the following approach was adopted:

- IR fluxes are calculated with THERMICA or ESARAD using a uniform planet temperature T_{ref}
- IR fluxes are modified by multiplying them by corrective factor $F_{k,j} = (T_{jk} / T_{ref})^4$, where T_{jk} is the equivalent radiative temperature of the planet as seen by face k of the spacecraft at orbital position j.

Step 2 is executed by means of a software routine developed specially for the purposes of this study, and documented in Study Note Ref. SN3. In the planet model, the optical properties are taken as $\alpha_{planet} = 0.89$, $\varepsilon_{planet} = 0.9$.

The seasonal variation is taken into account by assuming a variation of subsolar temperature T_{ref} with Mercury distance from the sun as shown in Fig. 10.1-1. The orientation of the orbital plane is taken such that the pericentre is at the subsolar point when Mercury is at aphelion (see Chapter 2.2).

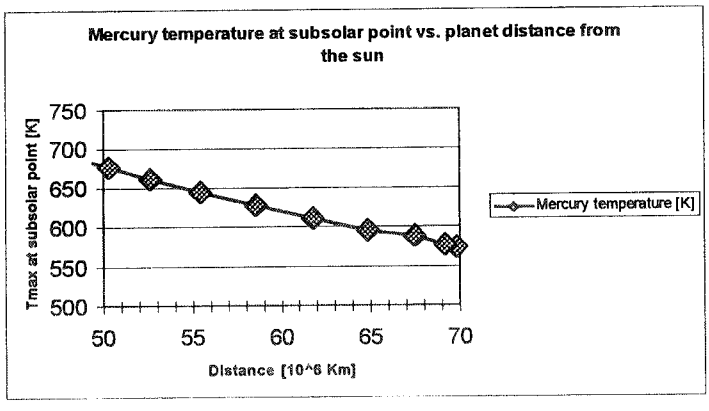

Fig. 10.1-1 Temperature at subsolar point as function of sun distance

10.2 Orbiter Thermal Control

10.2.1 Orbiter Thermal Configuration

Due to the extreme environment of the planet, the simplest possible thermal configuration of the spacecraft was sought. Fig. 10.2-1 shows the thermal configuration and the thermal model nodes.

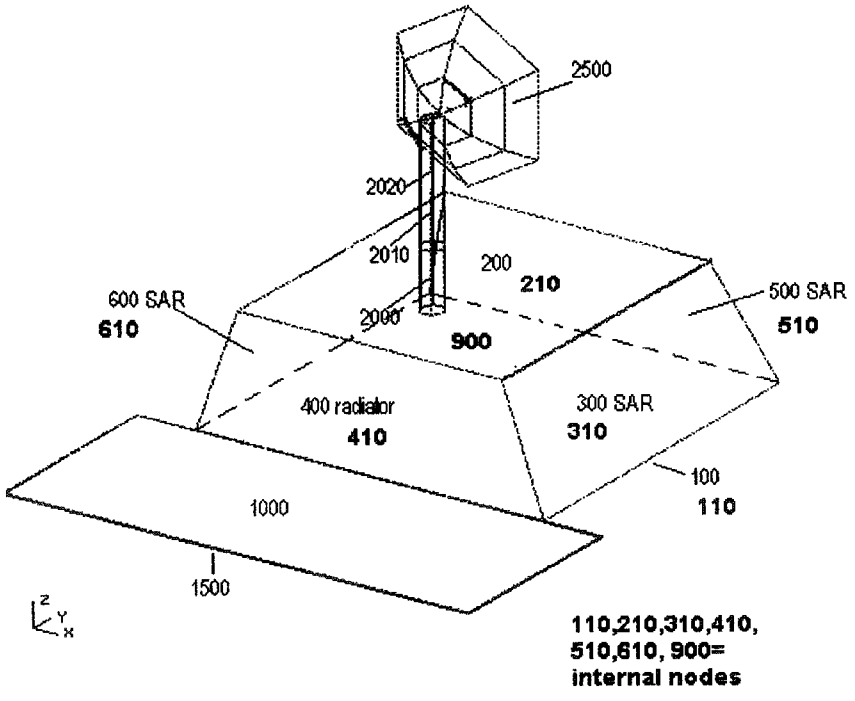

Node nomenclature:

300, 500, 600	solar arrays (cells + OSR)	2000, 2010, 2020	antenna boom (MLI)
400	Radiator (OSR)	100	Nadir side (MLI)
1000	IR shield +z side (OSR)	110,210,310,410, 510,610	S/C internal walls
1500	IR shield –z side (MLI)	900	internal node representing equipment
2500	antenna (metallic grid)		

Fig. 10.2-1 Thermal configuration (antenna position not representative of finally selected configuration)

The main features of the thermal configuration are as follows (Ref. SN3).

Radiator

The radiator is mounted on the side of the spacecraft protected from the sun by the attitude law (-Y side), and is covered with Optical Solar Reflectors (OSR, α=0.2, ε=0.8 at end of life). Its area depends on the internal dissipation and the selected orbit. For the nominal orbit, 2.65 m^2 are sufficient for the assumed 500 W internal dissipation and to maintain the internal temperature around 40°C.

Infrared Shield

The IR shield is necessary to protect the radiator from IR planetary fluxes. The dimensions of the shield depend on the orbit altitude and on the height of the spacecraft along Z. In order to make the shield size as small as possible, the spacecraft height was reduced to 1 m (the radiator cannot be tilted, otherwise it would be illuminated by the sun when the sun makes a small angle to the orbital plane). The resulting IR shield length is 1.7 m along axis Y, which makes the area = 6.8 m^2.

The shield is covered with OSR on the +Z side and MLI on the –Z side. The OSR should have maximum specular and minimum diffuse reflectivity, to limit diffuse reflection of solar radiation into the radiator. The parameters assumed in the model are α= 0.2, ε = 0.8 at EOL, solar specular reflection coefficient = 80%.

Solar panels

Solar panels are mounted to three sides of the Orbiter (+ X, -X, +Y), with α = 0.7, ε =0.82. To limit IR flux from the planet onto the panels, these sides are tilted by 25°; moreover, to reduce the panel solar absorption, OSR have been applied on 70% of the surface area. In addition all panels are thermally connected, by heat pipes, among themselves and to panel +Z (node 200), that behaves as an additional radiator. This panel is 100% covered with OSR. High temperature MLI is interposed between the panels and the spacecraft walls.

Heat pipes

Heat pipes are used between solar arrays and between solar array and panel +Z. Heat pipes are also used to transfer dissipation of internal equipment to the radiator. Standard constant conductance heat pipes charged with ammonia or water are candidates. The number of heat pipes has to be optimised; a first estimate is 10 for each panel and 15 for the transferring internal heat to the radiator.

High Temperature Multi-Layer Insulation (MLI)

High-T MLI is used on the spacecraft side facing Nadir, on the Nadir side of the IR shield, between solar panels and spacecraft walls, and on the antenna boom. MLI with Aluminised Polyamide film and Tissuglas is assumed (α = 0.3, ε = 0.05).

10.2.2 Orbiter Thermal Analysis

The performance of the design described above was evaluated in a number of orbital cases. The results that apply to the orbit eventually selected (400 x 1500 km, polar), are summarised below.

Fig. 10.2-2 shows the internal temperatures as function of sun longitude w.r.t. the orbit plane (Ω), with two values of internal dissipation (500W and 300W). The temperature sensitivity is about 10°C/100W and highlights the importance of limiting the power dissipation inside the spacecraft. The internal temperature is maintained below 40°C in all cases with sun longitude < 135°, whereas very high temperatures are found at 135° < Ω < 180° (i.e., with the sun at perihelion, on the side of the apocentre). The cause of this behaviour has been traced back to diffuse reflection from the IR shield into the radiator. When the sun is on the side of the apocentre, the side of the IR shield facing the radiator is illuminated by the sun 60% of the orbit period, and 20% diffuse reflection from the shield is sufficient, given the large thermal inertia, to increase the mean temperature by several tens of degrees. This is confirmed by Fig. 10.2-3, where the shield has been tilted 30° away from the radiator, reducing the diffuse reflection into it.

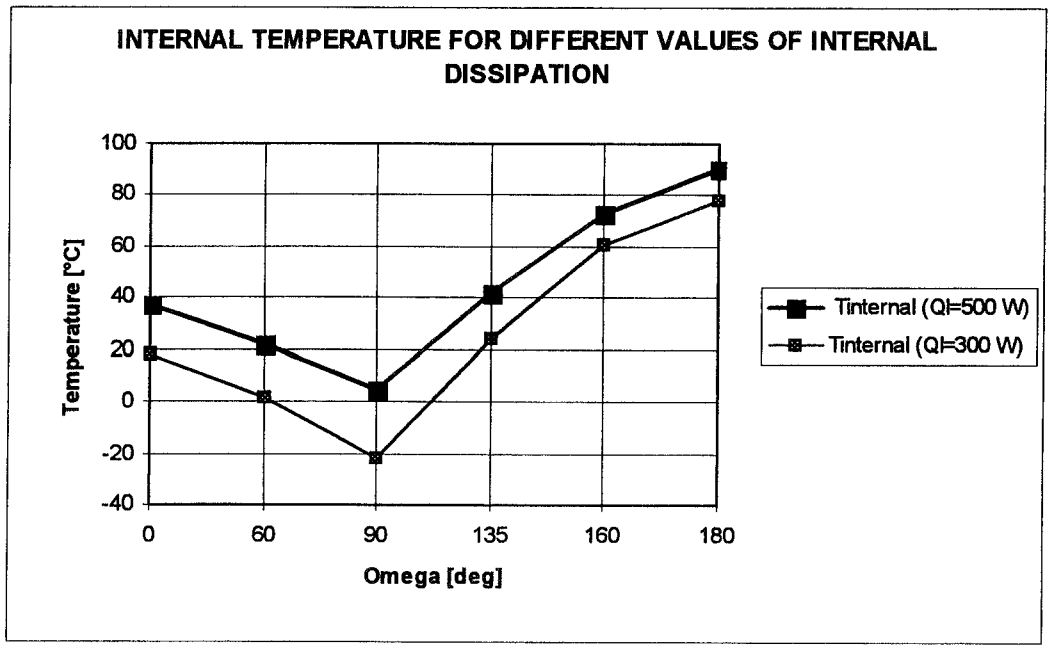

Fig. 10.2-2 Internal temperatures as function of sun longitude w.r.t. orbit plane ($\Omega = 0$ corresponds to the sun in the orbit plane, on the side of the pericentre), with 500W and 300W internal dissipation.

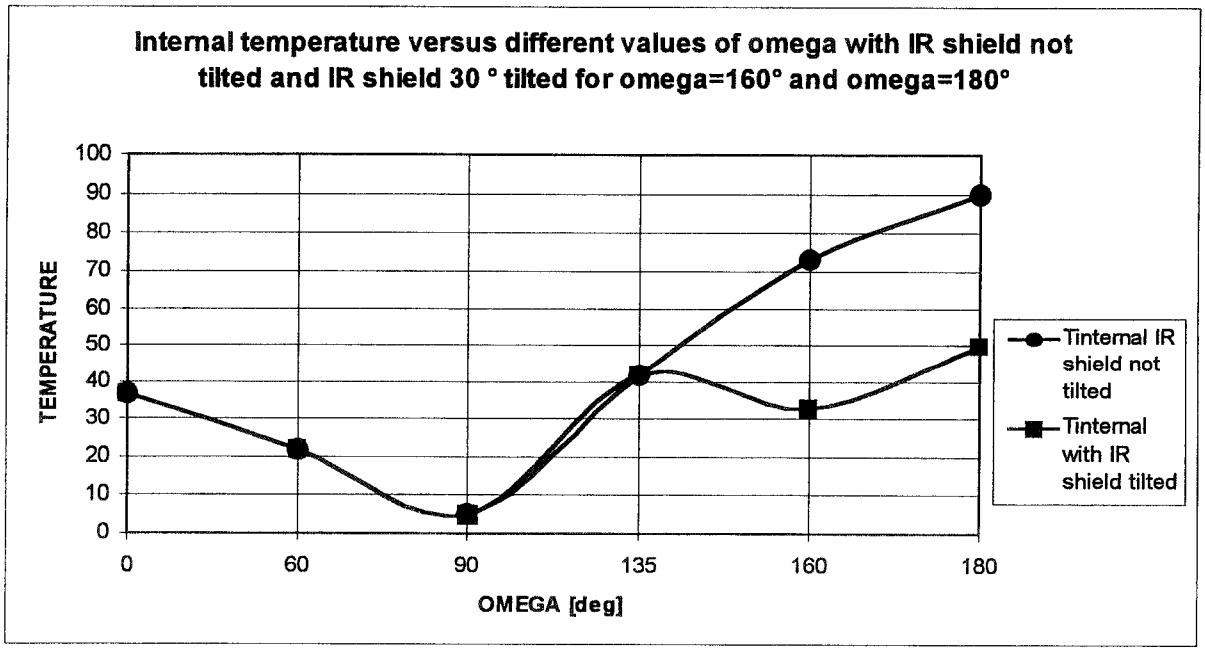

Fig. 10.2-3 Internal temperatures as function of sun longitude w.r.t. orbit plane, with 500W internal dissipation. In the lower curve, the IR shield has been tilted 30° away from the radiator.

The conclusion is that either a coefficient of specular reflection better than 80% (as currently assumed) is achieved, or the IR shield should be tilted to increase the angle between radiator and shield. The latter is, for the moment, the baseline solution. Notice that the 30° tilt angle can be maintained throughout the season in which the sun is around the apocentre (for angles higher than 30°, the diffused solar flux is even lower but IR fluxes from the planet dominate since the shield no longer protects a large part of the radiator).

The Phase 1 thermal analysis also gave important indications for the design of the solar array and antenna:

- The solar panels show large temperature variations at orbit frequency (e.g. from –50°C to 190°C at Ω= 0°) and they reach up to +280°C at 160° < Ω < 180° (near perihelion). The power produced by the panels is most of the time much greater than the requirement, which means that the OSR fraction could be further increased to reduce the maximum temperatures
- The temperatures of the high-gain antenna and its boom (modelled in 3 sections) also show large variations at orbit frequency, with upper limits around 200°C (reflector) and excursions in the booms of up to -80°C ÷ 200°C in the orbits with eclipses.

10.2.3 Conclusions on the Orbiter Thermal Design

The Phase 1 design exercise has reached its main objective, which was to show that the interior of the Orbiter can be controlled by simple, passive means to within 'normal' equipment temperatures (≤ 40°C). The design is driven by the radiator area, which is, in turn, driven by the internal power dissipation: limitation of this dissipation to no more than 300W is recommended.

The IR shield is an essential feature of the design, and its surface facing the radiator must have as large specular reflectivity and as small diffuse reflectivity as permitted by the available surface finishes (OSR). In addition, the IR shield must be tilted at times, to minimise the solar radiation component diffusively reflected onto the radiator.

The temperature of the solar panels in the perihelion cases must be reduced, perhaps by increasing further the OSR fraction. The maximum temperatures found for the antenna reflector are not extremely high (200 °C) but the large temperature variations at orbit frequency of the reflector and, above all, the booms are a cause for concern given the tight pointing requirements.

All results are valid within the limits of a preliminary thermal design and analysis exercise. More detailed analysis and improvements of the design will be the subject of the Phase 2 exercise, where the thermal requirements of the individual payload elements will be addressed.

10.3 Subsatellite Thermal Control

The design principles of the Subsatellite thermal control are in Chapter 6.4. A thermal mathematical model was prepared and analyses were run (Ref. SN4), with the environmental models described in sect. 10.1, for the cases of $\Omega = 0°$ (aphelion, periherm at noon), $\Omega = 90°$ (sun orthogonal to orbit plane), $\Omega = 180°$ (perihelion, periherm in eclipse). The orbit assumed was polar, 400 x 16800 km (the altitude of apoherm was later reduced, see Chapter 2.2, but the results of the thermal analysis can be considered valid within the limits of a preliminary exercise). The objective was to obtain preliminary results in terms of temperatures of the Subsatellite items and the electric power produced by the solar panels (as a function of their temperature-dependent photovoltaic conversion efficiency and Sun illumination).

Under conservative assumptions (reduced thermal inertia), the main results are as follows.

- the main body structure elements under the MLI remain limited within $T_{max} \approx 90°C$ and $T_{min} \approx 5$ to 10° C
- the external MLI undergoes a wider oscillation: from – 164 C to + 190 C, and even more for the IR MLI in the conical segments: T_{max} 349 C, in the sectors not masked by the solar panels. The area behind the back-side of the solar panels and the body-mounted PLEs is the hottest, on the average, of the Subsatellite, due to its radiation trap configuration.
- the body-mounted PLEs see a substantially similar thermal environment as the body internal structural nodes. The internal cavities of the external boxes show a slightly hotter peak: 105 C.
- the radiators oscillate between 30 and 60 C at $\Omega = 180°$, between 20 and 45 C at $\Omega = 90°$, but reach – 10 to +100 when $\Omega = 0°$
- the internal elements, including 4 equipment boxes (with internal power dissipation and conductively connected in an indirect mode to the radiators) and the tank, remain limited between 10 to 95 C and 0 to 75 C (the tank), at worst
- the boom-mounted PLEs show practically constant behaviour (in terms of internal cavity, not of external MLI), due to the tight and almost complete insulation: the large MAG cubical box stays at temperature values between a maximum of + 240 C ($\Omega = 180°$) and a minimum of + 190 C ($\Omega = 0°$); the smaller RPW-H boxes between + 145 C ($\Omega = 180°$) and + 85 C ($\Omega = 0°$).
- the solar panels, modelled as 2 x 8 solar panels, with 100% cells (no optical surface mirrors) oscillate from a cold limit of – 45 C to a hot one of + 200 C, with corresponding efficiency excursions from 19% nominal @ 25 C, down to 12 %. The average electric power generated on the orbit is from 95 (aphelion) to 206 W (perihelion) , with 300 W peak.

Introducing a "full thermal capacity" leads to oscillations peaks damping, from a few degrees to a few tens of degrees C; for instance: equipment boxes oscillation shrinks to 20 to 45 C.

The above described results would suggest, for the next study phase, together with an updating of design concept geometry and parameters, and after a verification vs the requirements, as areas of possible modifications, if necessary:

- limitation of internals cold excursions, using heaters fed by excess solar power/energy.
- further radiators area increase (+25%) to counter hot peaks (present radii = 250 mm).
- limitation of excessive internal boom-mounted PLEs temperatures (local Radiators on top/bottom faces of the boxes).
- reduction of cells percentage below 100% (by spreading of second surface mirrors) to curb hot excursions, above all at perihelion (an efficiency rise is a consequence).
- extension from 2 x 8 to 2 x 12 panels to counter power decrease, if necessary, and achieve a better protection of the 45° tilted surfaces behind the panels from visible radiation (causing high temperatures due to simultaneous low IR emissivity).

11. SATELLITE AVIONICS AND ELECTRICAL DESIGN

11.1 Electrical System Survey

The electrical architecture of the Mercury Orbiter, the Capture stage, and the Cruiser stage is composed of the following subsystems and elements:

- the Avionics system, composed of Command & Data Handling (C&DH) and AOCS
- the Power subsystem with Solar Generators
- the Orbiter Radio Frequency Communication System (RF COMS) with Earth stations
- The Sub-Satellite Telecommunication system and the Lander/Penetrator Receiver system (Subsat & Lander COMS)
- Thermal Control electrical equipment
- Dedicated functional/electrical interface to the S/C bus equipment, the Experiments, the Lander check-out Package, and a VMC Camera (as a standard item of future ESA missions).

The Operations interfaces will be applied via the Command and Data Handling System (C&DH) of the Avionics system.

The RCS (and its electrical I/F), the Power S/S with the Solar Arrays, the Sub-Satellite and the Lander/Penetrator electrical check-out and eject interfaces shall be able to cope with the Orbiter, the Cruise stage and the Mercury orbit Capture stage, both stages shall be jettisoned after usage.

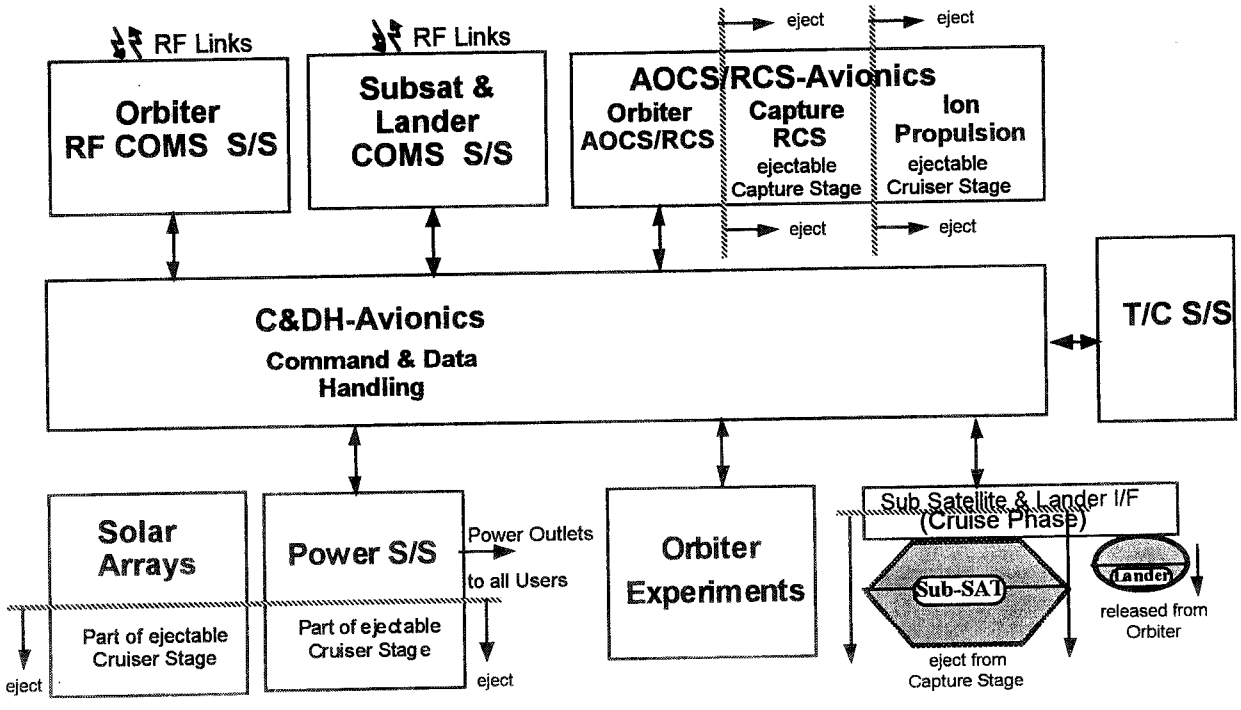

Figure 11.1 - 1: Mercury Orbiter, Cruiser, and Capture Stage Electrical Configuration Survey

11.2 Electrical System Architecture

The Electrical System Architecture is depicted in Fig. 11.2-1 for the functional and information signal flow. The electrical Architecture is composed of state of the art subsystem designs and some heritage of ROSETTA and the DSS MARS EXPRESS proposal.

The Avionics system comprises the classical Command & Data Handling System (C&DH) and the AOCS subassembly with all sensors and actuators. The Avionics system is applying an integrated avionics processor system sharing the processor for the C&DH and the AOCS/RCS tasks.

The Power discipline is realised by a Power Conditioning and a Distribution unit, Batteries and the Solar Arrays, with a dedicated cruiser stage for Ion thrust power supply.

The Orbiter Telecommunication system will transmit TM and receive TC in X-Band. For the Radio Science Experiment a dedicated Ka-Band feed will be applied to the HGA (TBC).

The Sub-Satellite Telecommunication system will receive TM and transmit TC in UHF-Band. The Sub-Satellite orbital position is to be tracked from the Orbiter. This requires (continuous) Doppler measurement. A stable link to/from the Sub-Satellite is achieved after appropriate carrier frequency sweeping. This is necessary to lock the Sub-Satellite Receiver on to the receiving carrier frequency of the Orbiter which is doppler shifted from the nominal receiver frequency. The Lander/Penetrator TM is assumed to be also received at the Orbiter via the same UHF receiver as used for the Sub-Satellite (assumption to be reviewed in Phase 2).

Thermal Control electrical items are the heaters and potentially electrically controlled roller blinds (TBC), thermistors, T/C power outlets in the PDU and thermostats for survival heater powering. Nominally the temperature control is performed via S/W control circuits.

Dedicated external functional/electrical interface to the S/C bus equipment, the Experiments, the Lander check-out Package, and the VMC Camera is controlled from the C&DH. The MIL-STD-1553B is a promising candidate for a serial Data Bus system. Remote Terminals of the Data Bus will be applied at users side as far as it will be available in the design phase. A limited number of Standard RTU channels as serial lines, Pulse Commands, and Analog & Digital inputs will certainly be necessary according to recurring units and for autonomous switching capabilities for configurations.

Fig. 11.2-2 is depicting the Electrical Architecture with the necessary Power switching capabilities to allow for autonomous S/C control. A major item for on-board autonomy is the classical hot redundancy of the COMS receivers and the Packet TC Decoders. These are powered by „Permanent Power“ outlets from the PDU. To perform autonomous AOCS control the AOCS sensors and actuators must be configured by the AOCS. This is indicated by the switching capability within the AOCS Interface Unit (AIU) for the primary power.

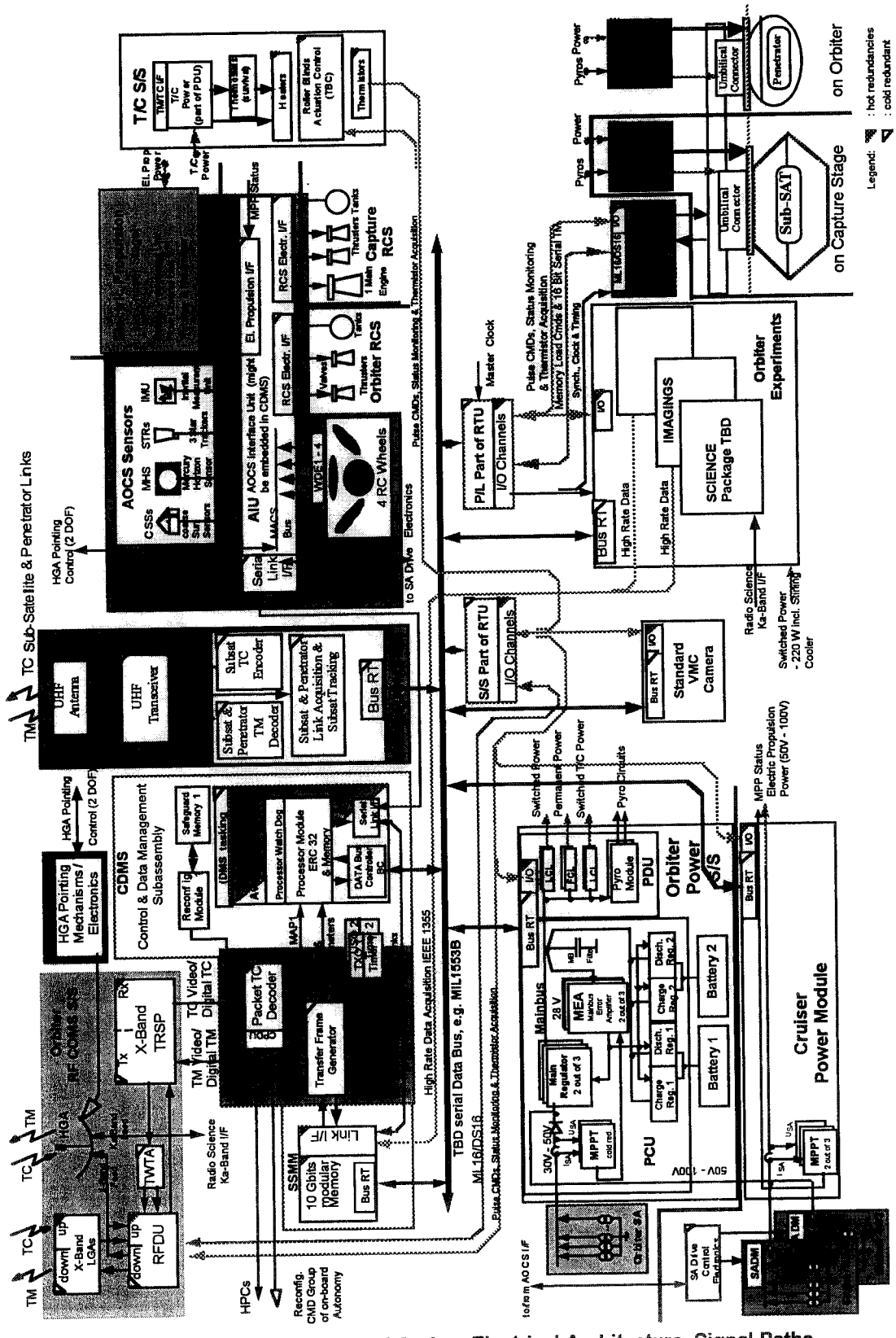

Figure 11.2 - 1: Mercury Orbiter and Cruiser Electrical Architecture, Signal Paths

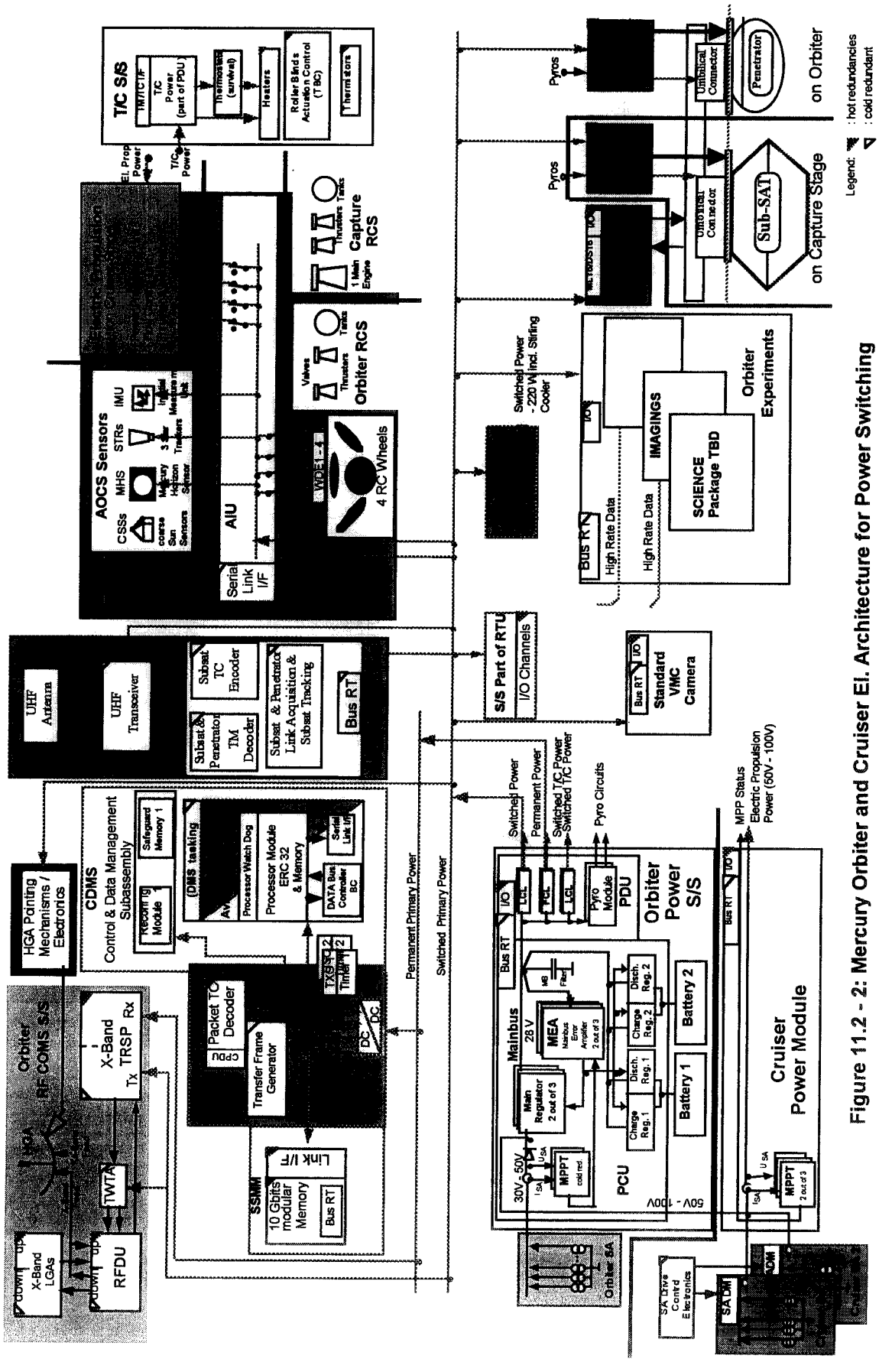

Figure 11.2 - 2: Mercury Orbiter and Cruiser El. Architecture for Power Switching

11.3 Avionics Subsystem

The AVIONICS architecture is defined as below (extracted from the System Electrical Architecture):

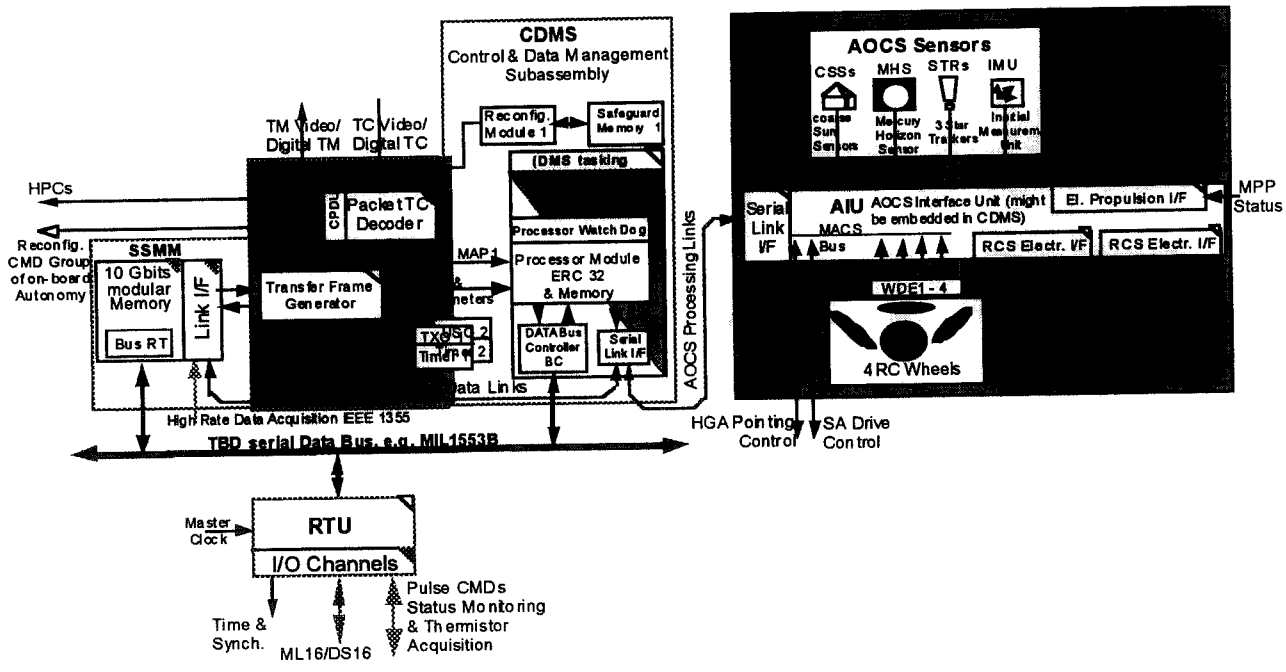

Figure 11.3-1: Avionics Subsystem

AVIONICS (advanced state of the art system) with:

Data Management System (DMS):

Control & Data Management Subassembly (CDMS); in principle 1 redundant ERC 32 Processor (SPARC) with Packet TC Decoder, Transfer Frame Generator (Packet TM), Reconfiguration Module and Safeguard Memory, System Clock, and Solid State Mass Memory (SSMM). The function of the Control and Data Management Subassembly (CDMS) is to provide command, telemetry, overall spacecraft control, and timing facilities, dedicated AOCS/RCS control, and all required memories (including SSMM) during all phases of the mission.

CDMS with Real time Operating System S/W in charge of DMS Tasking and AOCS tasking

SSMM with PALASIM concept (Parallel Access Large Silicon Mass Memory) with User I/F Switch Matrix and File Management System

TBD serial Data Bus (e.g. promising MIL-STD-1553B) with embedded Remote Terminals (RTs) at the users

Standard RTU with limited ML16 / DS16 serial channels, Pulse commands, analog and status inputs, Synchronisation, Clock and Time-reference Distribution

AOCS Avionics is composed of:

AOCS Sensors and I/F

AOCS Actuators and I/F

A common AOCS Interface Unit (AIU) with autonomous switching capabilities for Autonomy and FDIR functions. This might be embedded in the CDMS but the No. of external I/F connectors is very large. The AIU also adopts the RCS interfaces to the Orbiter RCS, Capture stage RCS, and the Cruiser Electrical Propulsion System.

AOCS Application S/W is running in the CDMS Processor.

CDMS Functional Modules

The CDMS will be composed of the following functional modules:

- Packet Telecommand Decoder
- 2 Processing Modules, cold redundant
- Local Master Oscillator with Timer Module
- Transfer Frame Generator (TFG)
- Data Bus Controller (DBC)
- Reconfiguration Module (RM)
- Safeguard Memory
- Solid State Mass Memory.

11.4 Electrical Power Subsystem

The Electrical Power Subsystem (EPS) and Solar Generator interface architecture of Fig. 11.4-1 is selected as baseline:

EPS Units:

- Large Cruiser Solar Arrays (SA1 and 2), consisting of 2 wings with Solar Array Drive Mechanisms (SADMs); (Note: the SADMs are functionally allocated to "Mechanisms", thus they do not appear in the subsystem sketch above, but in the System Architecture of section 11.2.)
- Body mounted Orbiter Solar Array, specifically designed for the Mercury environment
- Power Control Unit
- Power Distribution Unit (PCDU)
- Battery Assembly (BA), consisting of 2 single batteries of Li-ION type for one failure tolerance.

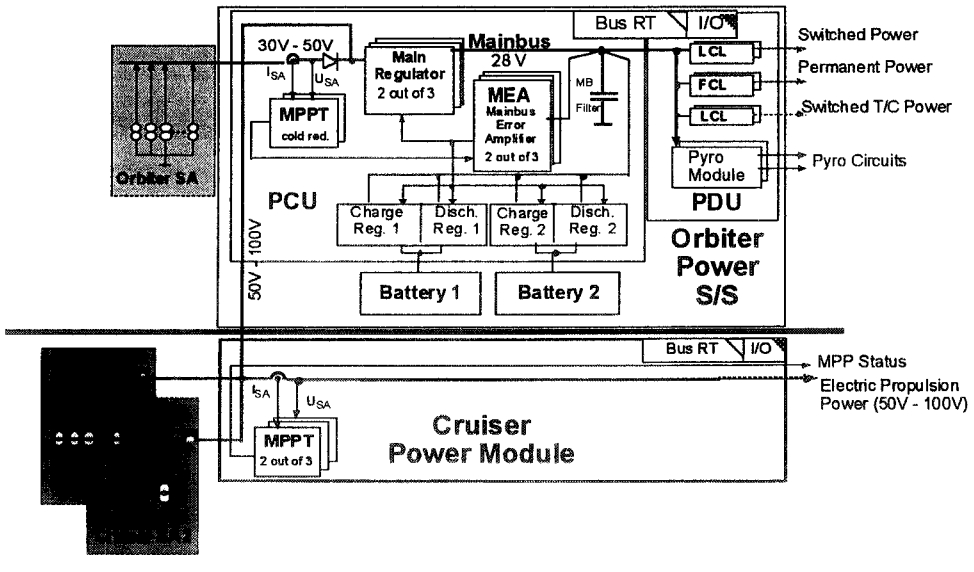

Figure 11.4-1: Electrical Power Subsystem Baseline

Major EPS Functions:

Sun tracking of the Cruiser SA by SADM, individually for each wing; applied for thermal SA control approaching Mercury. The control function is performed from AOCS S/W.

The Cruise SA delivers nearly all power to the Ion thrusters with the status of the Maximum Power Point Tracking (MPPT) indicating whether maximum thrust power is reached or not. The SA string voltage level should be > 50 V for all SA temperatures. To cope with the combined Orbiter SA operating at lower voltage level.

MPPT for accommodation of all available Orbiter SA power of 3 different SA panels at any operating mode where full power is required. At Mercury orbits the MPPT builds a closed control loop with power regulators of the buck converter type, which transfer the SA power into a 28V regulated mainbus voltage for the Orbiter. During the cruise phase SA power of the cruise arrays is converted by the main regulator at higher input voltage level that that of the Orbiter SA.

Mainbus voltage regulation, performed by a 2 out of 3 hot redundant voltage controller, including a so-called main error amplifier, which delivers the control signal of the primary power control loop, built by SA power regulators together with the battery charge and discharge regulators (BCR and BDR).

In all operating modes where the maximum power point of the SA exceeds the mainbus and battery charge power demand of the load the "surplus electrical energy" is not converted into electrical power, instead the solar flux only heats up the SA to some higher temperature. In this case the working point of the SA power characteristics is shifted closer to the open circuit point.

Battery charge and state of charge control is managed by the PCU. The design employs a highly efficient method with an extensive space proven heritage, which enables the flexibility of controlling battery charge and discharge the batteries.

The primary power distribution interface to the users must be designed that no single failure at a distributed power line can lead to a permanent shutdown of the mainbus. The PCU power bus recovers automatically from any shutdown transition if the cause of it is disappeared.

The EPS is controlled by the Data Management System (DMS) via a serial data bus and discrete command lines.

11.5 Charged Particle Radiation Issues

The basis of the radiation related conclusions is the study on Mercury Orbiter Radiation Environment (/esa/estec/ema/he/Mercury/1, Oct. 2, 1998), where the particle energy flux source term (CME coronal mass ejection component, solar protons, electrons, heavy ions GCR) and its effects have been evaluated. Fig. 11.5-1 shows the relevant data on total dose compared with the total dose curve on XMM for comparison.

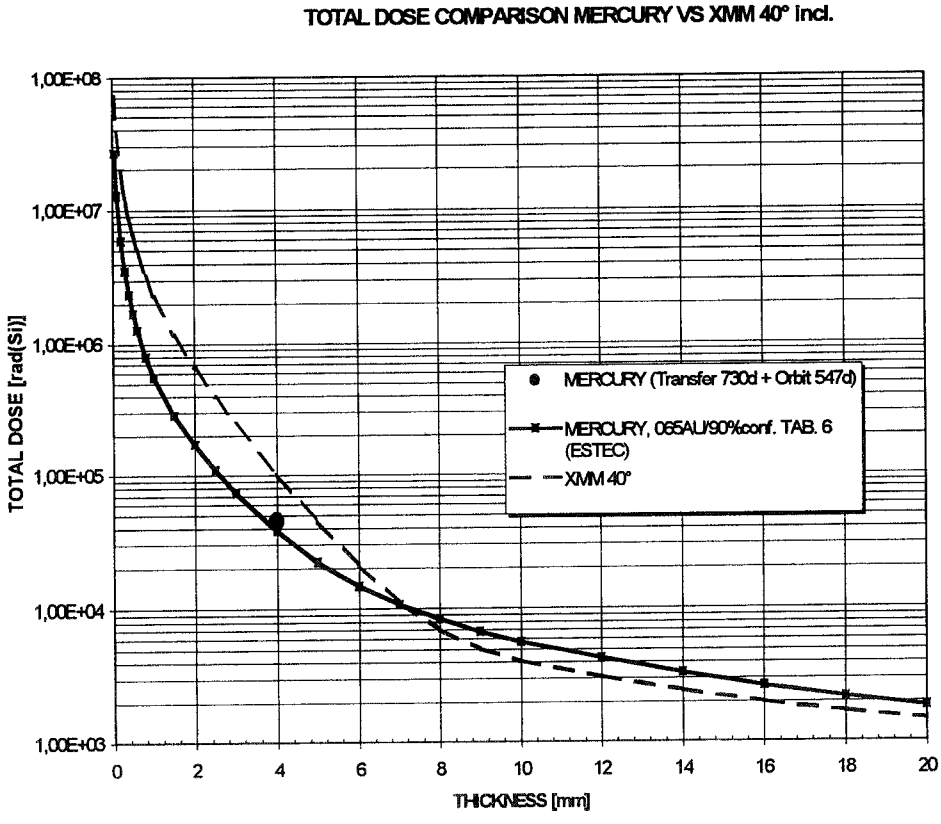

Figure. 11.5-1: Total Dose Comparison MERCURY vs XMM (XMM 10y mission)

From the above figure, the following conclusions can be drawn.

Total Dose: The resulting total dose effect on Mercury mission poses no significant problem. The values are below XMM "Standard" even if Orbiter is cruising 1.5 earth years in SOLMAX, see Fig. 11.5-1. No shielding optimisation necessary if radhard parts are implemented. A detailed sectoring analysis is necessary since the average 4 π shielding is assumed to be 4 mm aluminium equivalent. No safety factors are included.

Single Event Effects SEE (protons, heavy ions) from Solar Origin: A detailed SEU effects analysis on *proton* sensitive parts is necessary! Only few parts are already tested. (compare: SAA south atlantic anomaly problem on earth orbits).

Substantial work has to be done on reducing SEE due to protons,(the flux is a factor 10 higher than at 1 AU), some relaxation can be expected if the mission is shifted into solar minimum phase. In solar maximum phase it is questionable if ever undisturbed scientific measurements can be processed due to SEE by protons. Here it is highly recommended to have a minimised solar effect on all measurements. If high energy protons interact with matter, secondary effects can produce an undesirable background effect.

A reduction of solar proton induced effects can be expected if structure materials are selected which have a low yield of secondary effects, e. g. neutrons, see Table 11.5-1. Here we suggest materials with high carbon content, e. g. carbides, which may result in a ceramic structure.

PROTON ENERGY	NEUTRONS PER INCIDENT PROTON derived from Ref. Tesch				
E_P (MeV)	C	Al	Cu, Fe	Sn	Ta, Pb
10			1.2E-3	1E-3	2E-4
20	1.1E-3	2E-3	4E-3	1.3E-2	2.4E-3
30	1.1E-3		1.1E-2 1E-2		2E-2 1.7E-2
40	6E-3	1.5E-2	4.3E-2	4E-2	
50	7.6E-3	2E-2	2.2E-2 3.3E-2		3E-2 6.6E-2
60	1.6E-2	3E-2	8E-2	9E-2	1.2E-2
70			5.5E-2		
100	3.6E-2 3E-2	1.0E-1 1.1E-1	1.8E-1 1.6E-1	2.3E-1	2.1E-1 3E-1 3.4E-1
200	1.9E-1 2E-1	4E-1 4E-1	1.0 6.5E-1	1.2	1.2 1.5
500	1.0	1.6	2.7		4.7
1000	2.0	3.2	6	11	11 - 20

Table 11.5-1 Secondary Particle Yields (Neutrons)

GCR induced SEE: GCR effects are comparable to normal interplanetary orbits (CLUSTER, XMM) with M=3 as parameter; for the parameter M=8, significant work has to be done to reduce effects by EDAC (error detection and correction) measures, redundancy, and selection of SEU hardened parts. If an orbit is selected in solar minimum, the solar effect is only ~25% higher as in solar maximum.

Degradation effect on solar cells (coverglass characteristics): The degradation effect is due to the high fluence of expected protons not negligible, due to the proton/electron conversion factor. Diodes at the solar panel are exposed to high radiation fields depending on shielding, the wing system is more critical due to reduced backshielding.

Points for further evaluation include:

- Material selection (radiolysis of polymers & UV)
- Solar wind source term and effects (degradation of surface materials).

12. GNC/AOCS

12.1 Requirements

The driving requirements on the GNC/AOCS subsystem are:

- autonomy, because of the long distance to Earth (two way light travel time ranges from 9 minutes at closest approach to 24 minutes at 1.5 AU)
- reliability, because of the harsh environment (temperature, radiation)
- accuracy during observations in Mercury Orbit. The more stringent requirements derive from the camera observations.

From the analysis of payload camera operation (Ref. SN1), the following requirements are deduced:

- Absolute pointing error: 5 arcmin
- Relative pointing error: 2 arcsec/s
- Relative measurement error: < 1arcsec/min
- Post facto attitude reconstitution: 2 arcsec.

12.2 Disturbance Assessment and Actuator Selection

The main sources of disturbance torques are :

- thruster mismatch and solar radiation pressure during the cruise phase
- radiation pressure from the sun and the planet in Mercury orbit.

A simplified analytical model of the disturbance torques was developed (ref. SN5), in order to estimate the total angular momentum build-up and hence the requirements on the actuators. The results are in Table 12.2-1.

	Angular momentum budget (Nms)		Main axis or plane (See Fig. 12.2-1)
	total	non-cyclic component	
Cruise			
Solar flux	37000	37000	Yo
Electric thrusters	45000	45000	YoZo
Chemical thruster	20000	20000	YoZo
Total	102000	102000	
Mercury orbit (1 year)			
Solar and planetary flux	4820	2590	Xorb
Orbit eccentricity	1740	0	Yorb
Total	6560	2590	

Table 12.2-1 Angular momentum budget

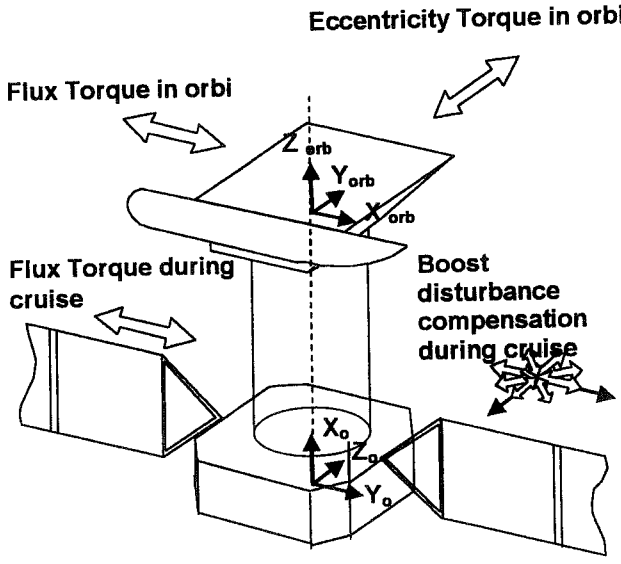

Fig. 12.2-1 Main axis or plane for each disturbance effect

The torques during the boost phases derive from assumed constant thrust misalignments (0.1 degrees for the 0.6N electric thrusters and 0.5 degrees for the 400N bipropellant thruster). They are comparable in magnitude to the solar radiation pressure torque. Angular momentum build-up is large due to the duration of the cruise (2.3 years with 6000 hours thrust assumed).

In Mercury orbit, large torques are produced by the configuration of the Orbiter spacecraft (large cross section in the radial direction and torque unbalance due to the IR shield). The solar radiation pressure has a cyclic component, whereas the planet pressure torque is non-cyclic due to the constant Nadir pointing orientation. A variable torque has to be supplied by the spacecraft to maintain Nadir pointing, since the orbit is eccentric; this component is completely cyclic and could be managed by reaction wheels without fuel expenditure.

In the electrical thrust phases, 0.6N nominal thrust can be supplied by three 200mN thrusters at full thrust, or four such thrusters, 25% throttled. The disturbance torques originate in thruster misalignments and could be managed by small-amplitude modulation in nominal cases. For single-failure tolerance, the options in Fig. 12.2-2 exist. A configuration with five thrusters can manage the failure without reduction of thrust, whereas in a configuration with four thrusters, in order not to produce a large disturbance torque, a reduction of thrust by 1/3 must be tolerated.

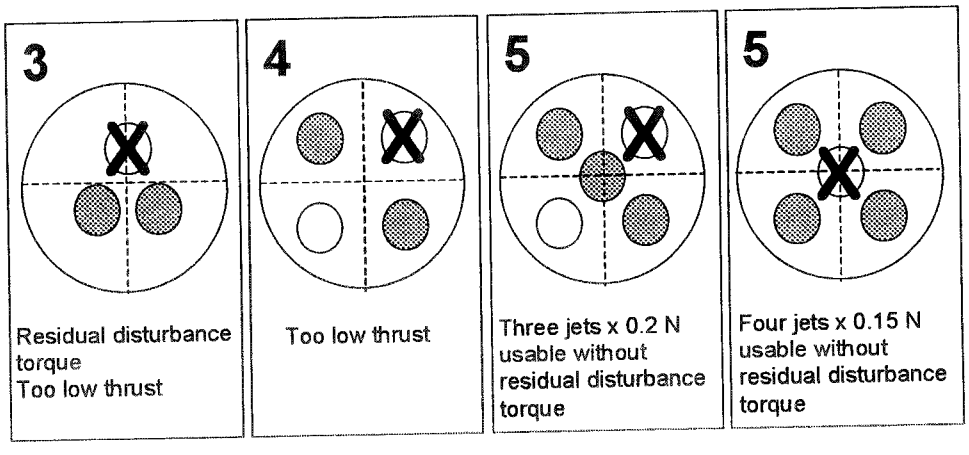

Fig. 12.2-2 Thruster failure cases and redundancy

During the boost manoeuvres with the 400N bipropellant engine, the disturbance torques are high even with small misalignment, and large AOCS thrusters must be employed. A configuration with two branches of four 10N thrusters is proposed, which can be configured such that they can also be used during the cruise and, if necessary, to perform fast slew manoeuvres.

For the Orbiter, the trade-off is between reaction wheels and a dedicated set of thrusters. Small forces and a smooth operation are required in the phases when the Radio Science payload is operated. A set of four 10 Nms reaction wheels would guarantee wide control margins and off-loading twice per day at most. However, the subsystem mass, and the power consumption, are a drawback with respect to a Nitrogen gas thruster system (the propellant mass penalty for thruster based control is only 3 kg). Therefore, a configuration with two branches of four 5 mN Nitrogen thrusters each is proposed. Despite the large power consumption, electric (FEEP) thrusters may be considered if very precise and smooth short-term control is required.

Under the assumptions made above, the propellant budget is 24 kg for bi-propellant thrusters and 6 kg for cold gas thrusters.

12.3 Sensor selection

12.3.1 Attitude Sensors for the Observation Modes

For the normal mode attitude measurement during the cruise and the Mercury observation phase, two non-orthogonal wide-field star sensors are proposed. The sensor implementation relies on the so-called Stellar Autonomous Attitude Determination System (SAADS) concept. The SAADS, in the version proposed for Mercury mission, is a system relying on three Optical Heads, two catalogues and a software package. The main features of the system are:

- rate estimation capability up to 5 deg/s;
- refined stars centroiding and magnitude computation;
- multiplexed handling of several Optical Heads;
- continuity of operations through continuous selection of the active OH configuration;
- capability of surviving to short occultations;
- possibility of exclude one OH from the active configuration because of detected failure;
- attitude initialisation using pattern recognition techniques through on-board image catalogue;
- attitude and rate estimates up to 10 Hz frequency through on-board guide star catalogue.

The system outputs high accuracy attitude and attitude rate information in inertial co-ordinates, without any support from the ground (apart from orbit updating when around Mercury) or other embarked sensors, after on-board processing of the data provided by a set of optical heads, rigidly mounted on the spacecraft body.

The system implements a fully autonomous gyroless system that is able to recover from the "lost in space" condition without any external initialisation. The SAADS package includes two embedded compressed star catalogues (an "image" catalogue, to recover from any "lost in space" condition, and a "reference star" catalogue, for the normal mode operation, to support pointing and slews), image recognition and prediction correction algorithms. It is able to handle partial or total occultations, to reconfigure itself between different operating modes and is insensitive to extended objects inside the frame.

The system is conceived in a modular way, allowing application of the on-board software to different camera configurations (in terms of number, field of view and other working parameters), according to the mission profile and requirements. For the Mercury application, three optical heads are implemented, ensuring full single-failure redundancy.

In the event that the baseline satellite configuration includes a Control and Data Management Unit (CDMU) with a powerful ERC32 based computer, the SAADS software can be executed in the CDMU computer. Assuming the following computation load budget for each of the CDMU tasks:

- Data Handling (1 MIPS)
- AOCS and FDIR (1 MIPS)
- SAADS (5 MIPS)

the CDMU computer budget should be at least 10 MIPS, so guaranteeing 30% spare. The SAADS software manages the processing of the CCD frames as well as the attitude and rate determination, so autonomous star trackers are not required, and three simpler (and cheaper) Optical Heads are sufficient.

The performances expected of the SAADS are in Table 12.3-1. Using two Optical Heads with separation angle of 60° (or 120°), as requested to avoid direct sun light (and Mercury limb) in the FOV, the expected accuracy figures are the ones declared by second and respectively fourth column for the two axes normal to the sensor Line of Sight (LoS) and 1.15 times worse for the LoS axis. Thus accuracy in ACA frame is expected to be almost the best one on whichever axis. The lay-out of the three OHs is sketched in Figure 12.3-1.

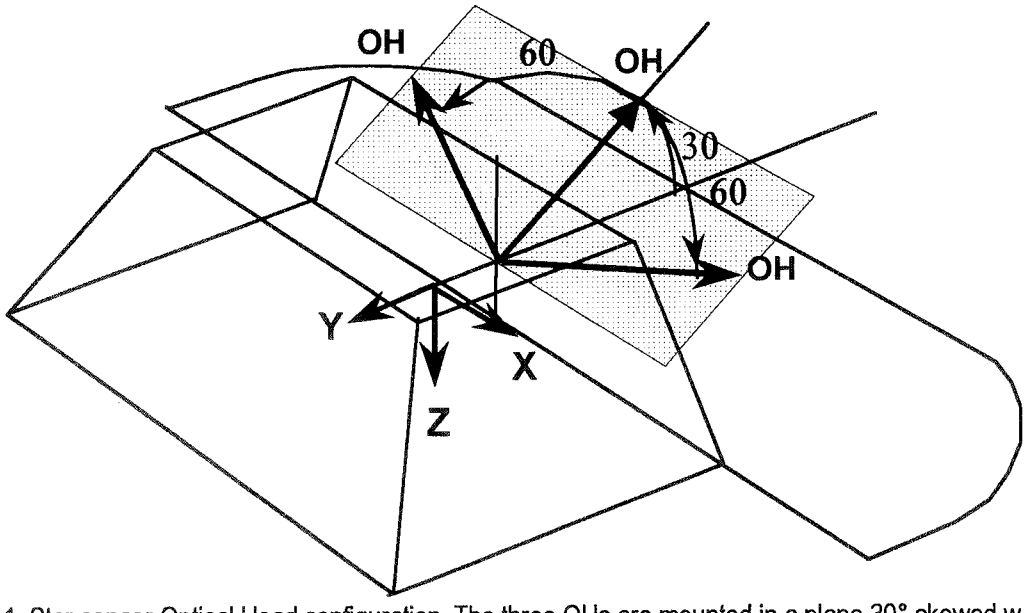

Fig. 12.3-1 Star sensor Optical Head configuration. The three OHs are mounted in a plane 30° skewed w.r.t the XY plane. Two Line of Sight axes are rotated ± 60° w.r.t. the YZ plane, the third lies in that plane

Turning rate (degrees /s)	Attitude (arcsec)		Rate (arcsec/s)	
	σ (roll)	σ (roll) = σ (yaw)	σ (roll)	σ (roll) = σ (yaw)
0	16	1.6	9	2.6
0.5	18	1.8	9.4	2.7
0.75	24	2.5	11	3.3
1	33	3.5	26	4.4

Table 12.3-1 SAADS expected performance based on SETIS heritage

12.3.2 Attitude Sensors for the Safe and Emergency Modes

Two different emergency modes are envisaged for the Mercury mission, the first for the cruise and the second for the scientific observation phase around the planet. The former is based on Sun Analogue Sensors (SAS) and Ring Laser Gyros (RLG); the latter relies on a (still to be developed) Mercury Horizon Sensor (MHS) and again Ring Laser Gyros. The need for a MHS during scientific operations arises from the on-orbit thermal constraints. Due to the high Mercury infrared flux, the satellite is obliged to maintain the nadir pointed attitude; as the mode must work in case of prolonged ground link outage, the only way to guarantee the mentioned attitude is to provide the satellite with a sensor able to compute the roll and pitch angles in a Mercury centred Local Vertical – Local Horizontal (LVLH) frame. The safe mode in the cruise scenario can be managed with a simpler approach where two axes are observed by using SAS measurements while the third is only observed in rate via RLG information. A summary description of the envisaged sensors is provided below.

Analogue Sun Sensor (SAS). Complete coverage of the sky is requested to permit single-failure tolerance in case of RLG partial failure. Due to the variable attitude of the thermal shield (besides safe modes, SAS units are used in the early mission phase to acquire Sun when the thermal shield is still stowed), 3 sensors are required (see Fig. 12.3-2). Medium Accuracy (0.25-0.5°/s) should be sufficient to cope with the relaxed safe mode pointing requirement.

Ring Laser Gyro (3 axis). RLG is used to damp rate at launcher separation and to manoeuvre the spacecraft into a safe attitude after a fallback. Then they are actively used until nominal operating modes are enabled from ground. The main features of RLG are: Readout noise 1"; Bias stability < 0.01 °/hr over 1 month; Angular random walk < 0.01 °/ $\sqrt{}$ hr; Scale factor error < 5.10^{-6}.

Linear Accelerometer (3 axes). A linear accelerometer is integrated inside the Inertial Measurement Unit (IMU) together with the RLG. During main engine boost or in orbit correction manoeuvres, it signals when the measured ΔV reaches the prescribed value commanded by ground. Its usage during nominal operations to monitor the small orbit perturbations induced by attitude control thrusters is under evaluation as this sensor seems too rough for the task. The payload accelerometer information could be used to supply this measurement.

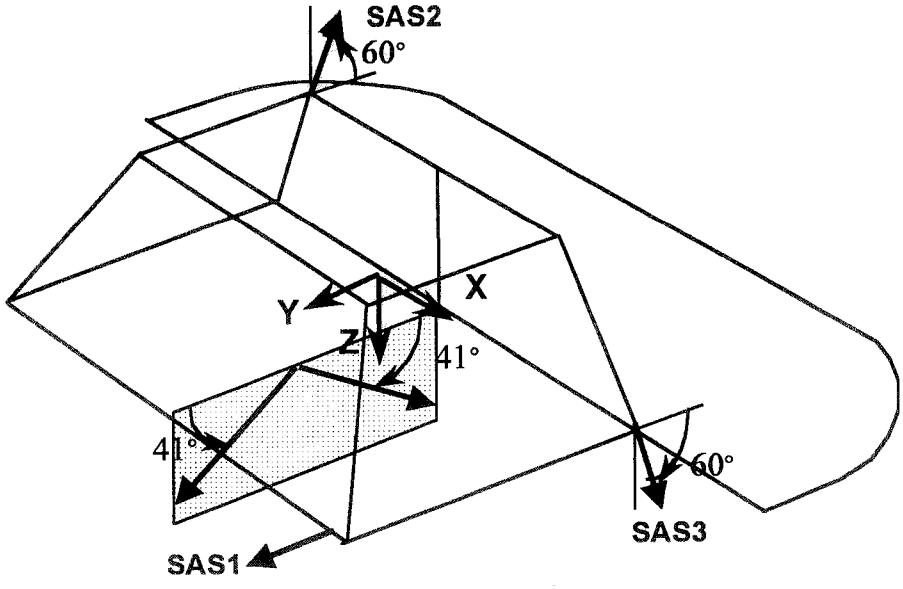

Fig. 12.3-2 Layout of Mercury Horizon Sensor and Sun Sensors. The MHS is formed by two telescopes, each tilted 41° w.r.t. the ±Y axes; the telescope axes lie in the YZ plane. One SAS is mounted with the LoS axis along Y on a bracket in a corner of the lower platform; the other two have LoS tilted by 60° and lie in planes parallel to the YZ plane

Mercury Horizon Sensor (MHS). MHS is devoted to manage safe mode (accuracy ≈ 1°) when orbiting around Mercury. Usage during scientific observations to improve orbit parameter estimation is to be evaluated in case orbit reconstruction from ground should result too inaccurate. The sensor, which is derived from the low altitude conical Earth sensor, is formed by two telescopes (FOV = 22°) mounted in half-plane Y-Z, 41° skewed w.r.t. +Y and –Y (see Fig 12.3-2), to permit operative altitude in the prescribed range (400-1500 km). The combination of the measures from the two telescopes permits the measurement of roll and pitch angles during the whole orbit: in safe mode, MHS outputs are used to correct attitude estimates; in nominal modes (if used) several roll and pitch measures would feed a filter (Least Square type) to compute updated position and velocity vectors (i.e. orbit parameters) for a prescribed point in the orbit.

12.4 Operational Modes and AOCS Logic

12.4.1 Nominal Operative Sequence

After separation from launcher, Safe Acquisition and safe Mode (SAM) is enabled to damp rates and acquire the sun. As star sensor optical heads are still occulted by the thermal shield, this phase is managed using SAS and RLG measurements. When Sun is acquired, solar arrays and thermal shield are deployed. After thermal shield deployment star sensor optical heads are available and Initial Attitude from Stars (IAS), based on SAADS pattern recognition mode, can be enabled to initialise attitude.

When attitude is initialised, Nominal Operative Mode (NOM) is activated; satellite is rotated to the prescribed orientation. Attitude is estimated via stellar sensor both in pointing and in slew phases. During cruise control reference is computed via interpolation of Sun and Earth locations contained in a time-tagged table, during Mercury observation it is obtained by propagating orbit on-board. Orbital parameters are computed on-ground, based on tracking and Doppler measurements. Use of MHS for this computation has to be evaluated.

In case of failure Rate Damping Mode (RDM), based on stellar sensor rate mode, is enabled (first-level fallback). Double failure (Normal mode and Rate mode) determines fallback to SAM or Safe Mercury Mode (SMM). After fallback, restart of the nominal sequence (IAS, NOM) shall be enabled from ground.

12.4.2 Orbit Control Modes

High Boost Mode (HBM) is enabled from NOM, after cruise separation, to insert the spacecraft into Mercury orbit and change the orbit plane. HBM requires integrative compensation to remove the bias due to step disturbance at main engine switch-on and switch-off. Attitude control cycle during boost must be as low as possible to permit fast reaction to high disturbance torque. A control rate of 10 Hz (cycle of 0.1 s) should be sufficient. At the end of ΔV boost the transition to NOM is activated.

Orbit Correction Mode (OCM) is enabled to correct orbit when requested by ground control. Before thruster activation, the spacecraft is rotated to the proper attitude. At the end of correction the transition to NOM is activated.

12.4.3 Safe Modes

Safe mode during the Cruise

Safe Mode during cruise is managed by enabling SAM based on RLG and SAS measurements. When a fallback occurs and at initial Sun Acquisition the following steps are performed to bring $+Z_o$ pointed to the Sun:

- reduction of rate below a prescribed safety threshold by using gyro information and thrusters;
- rotation of the spacecraft (using again gyro and thrusters) to align $+Z_o$ axis toward the Sun. Attitude at manoeuvre start is roughly initialised by Sun sensors;

- maintenance of Sun pointing with the $+Z_o$ axis until Ground Control restarts nominal modes. Attitude around Z_o axis is only controlled in rate, using gyro measurements; the spacecraft rotates around this axis as a consequence of the gyro drift, which is however low, $\approx 0.01°$/hour, for RLG.

In case one or two gyro axes fail, the target is achievable as the three SAS permit a complete sky coverage and separation from launcher is expected to not be done in eclipse.

In-orbit Safe Mode

Around Mercury the spacecraft is compelled to maintain the Nadir pointing attitude for thermal reasons. A gyro-compassing strategy (RLG based propagation, MHS based correction) is suitable to manage safe mode in this scenario. Safe Mercury Mode (SAM) recovery sequence is composed by the following steps:

- using gyro information the rate is damped and the spacecraft is rotated up to Mercury limb entry into MHS FOV;
- in orbit, RLG measures incremental angles and then permits to propagate attitude, MHS measures roll and pitch angles; based on gyro-compassing strategy roll angle is used to correct both roll and yaw estimates.

Note that as gyro-compassing filter is function of the current orbit rate (variable in an elliptic orbit), this parameter shall be computed or interpolated (simplest and more robust implementation) on board.

12.4.4 AOCS Logic

Fig. 12.4-1 shows the envisaged attitude control logic. A description of the control approach is in Ref. SN4.

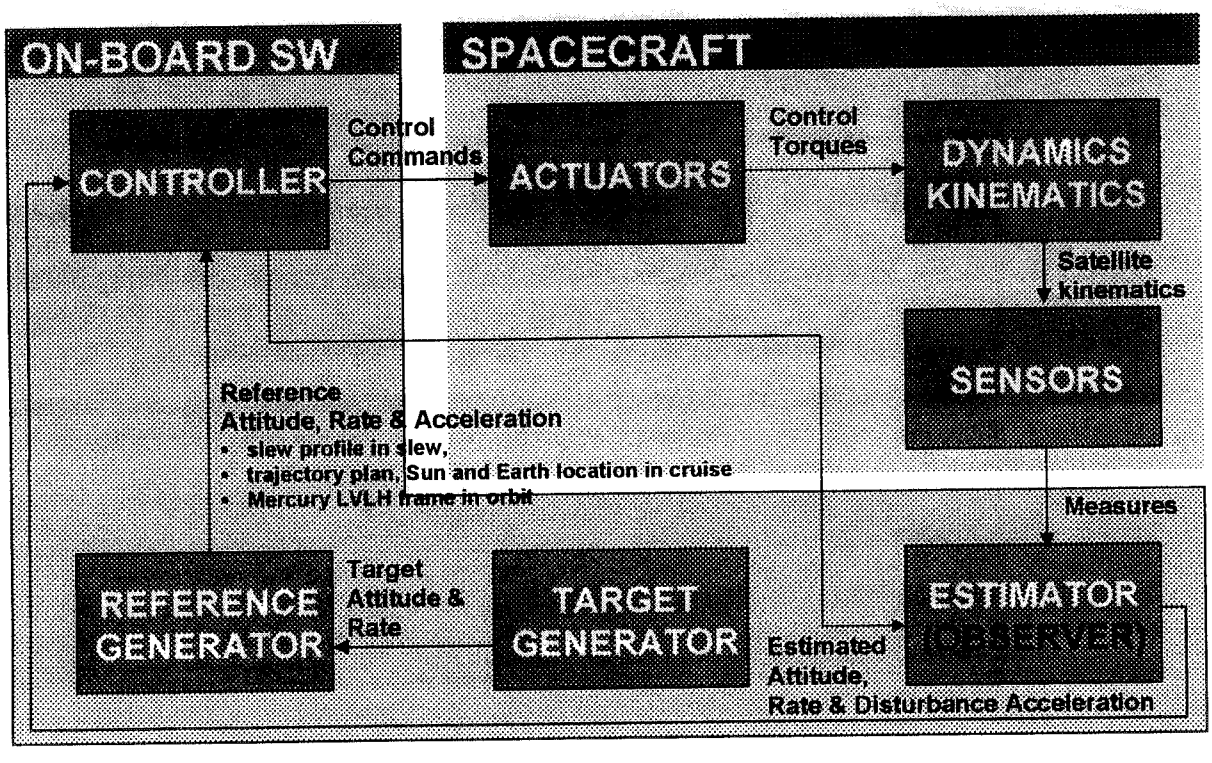

Fig. 12.4-1 AOCS Control Logic

12.5 *Subsystem Budgets*

Table 12.5-1 shows the mass and power budgets. The table does not include a dedicated electronic unit, under the mentioned assumption that the central CDMU computer is sufficiently powerful to perform optical heads management, image processing and state vector estimation. For the Orbiter actuators, the option with cold gas thrusters is provisionally selected.

Hardware	Units	Mass /Unit [kg]	Total Mass [kg]	Power/ Unit [W]	Total Power [W]	Remarks
IMU	1	3.65	2.65	33.00	33.00	
SAS	3	0.23	0.70	0	0	Internally redundant
MHS	1	0.15	0.15	2.00	2.00	
STR Optical Heads	3	1.50	4.50	1.00	2.00	Two units active
CDMU, RTU & RCS			TBD		TBD	Not included in AOCS Equipment
Total			**9.00**		**2.00** **33.00** **35.00**	Normal mode Sun Acquisition Mode Mercury Safe Mode
Cold gas			6.40			
AOCS Bi-Propellant			24.00			Including 5%Δ-V margin

Table 12.5-1 Mass and Power Budget

12.6 Conclusions and Open Points

Disturbance budgets : For the Orbiter, the maximum disturbance torque ($<1.10^{-3}$ Nm) is due to the combination of solar and Mercury fluxes; the torque needed to follow orbit rate is one order of magnitude lower. Gravity gradient is absent thanks to the LVLH reference attitude. During the cruise, the spacecraft is subjected to growing solar flux. However the maximum disturbance effect on the spacecraft is due to the compensation of unbalanced spurious torque associated to the thrust systems: electrical for the transfer from Earth to Mercury (about 2. 10^{-3} Nm worst case) and chemical for orbit insertion (about 12 Nm worst case).

Attitude determination and sensors : Attitude determination is based on a stellar autonomous sensor, which is, in principle, able to support the whole nominal mission. For emergency modes the spacecraft is provided with an inertial measurement package (containing Ring Laser Gyros and Linear Accelerometers), three Sun Acquisition Sensors and a Mercury Horizon Sensor, which is still to be developed as a derivation of the Conical Earth Sensor. Linear Accelerometers are used in orbit control modes, to monitor ΔV.

Actuators for Attitude and Orbit Control : Due to the LVLH reference attitude, reaction wheels are not convenient to control the spacecraft unless they are strictly needed to cope with the stringent RPE and RME requirements during the scientific phase. Control authority, for the cruiser actuators, is driven by the unbalanced torque during main engine activation. 8 Bi-propellant jets with a 10 N thrust (only four used at the same time) are suitable. During the cruise, thanks to the high spacecraft inertia, the control deadband would remain in the order of the arcminute, an accuracy acceptable for this phase. A total mass of 25 kg would be sufficient to perform AOC tasks. In the Orbiter, 8 cold-gas jets with a 5 mN thrust (only four used at a time) are sufficient to guarantee the satellite control.

Budgets : A total mass of 9 kg and a total power of 2 W for nominal modes and 35 W for safe modes has been evaluated. In case wheels are included, an increment of about 9 kg and, respectively 20 W is expected.

The following points are identified for detailed study in Phase 2:

- Definition of control law in the different operative modes;
- Analysis of dynamic performances and preliminary tuning of controller and estimator;
- Evaluation of control performances (taking into account flexibility features of the antenna);
- Design of orbit reconstruction and propagation;
- Requirements for orbit maintenance.

13. TELECOMMUNICATIONS

13.1 Earth Telecommunications Scenario

Communication to Earth are constrained by the variable distance between the planets, by occultations and by radio blackouts.

Fig. 13.1-1 shows a time profile of the Earth-Mercury distance. The minimum distance is 0.53 AU ($79 \cdot 10^6$ km) and the maximum distance is 1.47 AU ($219 \cdot 10^6$ km); the ratio of maximum to minimum distance is about 2.8 and the time from a maximum to the next minimum is about 58 days (half a synodic year). Therefore, about 8 times more data can be transmitted at closest approach than at maximum distance; hence, the data return strategy must be planned over a synodic year of 116 days.

Radio blackouts occur when Mercury is aligned with the Earth and sun, such that the ground antenna sees the spacecraft with the sun either in the background or the foreground. This condition occurs regularly, every 58 days. The angular separation between Mercury (the spacecraft) and the sun takes minimum values that depend on the epoch, as shown in Fig. 13.1-2. The minimum angular displacement for telecommunications has been calculated as $\approx 2.8°$ (Sun between Mercury and Earth), and 0.33° (sun behind Mercury).

Occultations occur when the earth is close to the plane of the spacecraft orbit around Mercury. This condition repeats regularly, every half Earth year, for a time span (in Earth days), and a fraction of the orbit period, that depend on the orbit altitude. Fig. 13.1-3 shows the occultation pattern for the nominal 400 x 1500 km orbit.

Telecommunication with the Earth can take place when the ground station is available, and in absence of radio blackouts or occultations. Assuming for the ground segment the Perth station, 32m dish, available for 8 hours out of 24 with spacecraft elevation > 10°, then the time per day available for communications in the 400 x 1500 km orbit is :

- 33% (station availability)
- 23% (worst case) ÷ 29% (average)
- 0 % (radio blackouts of a few days).

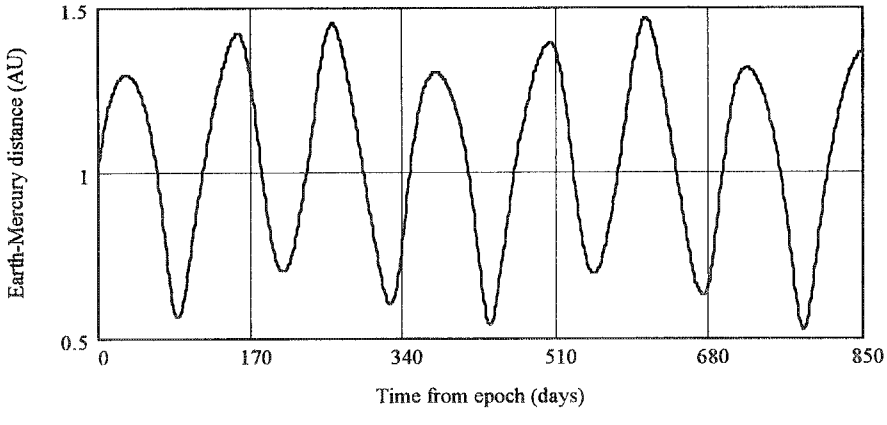

Figure 13.1-1 Profile of Earth-Mercury distance (AU). Time from epoch 2013/1/13

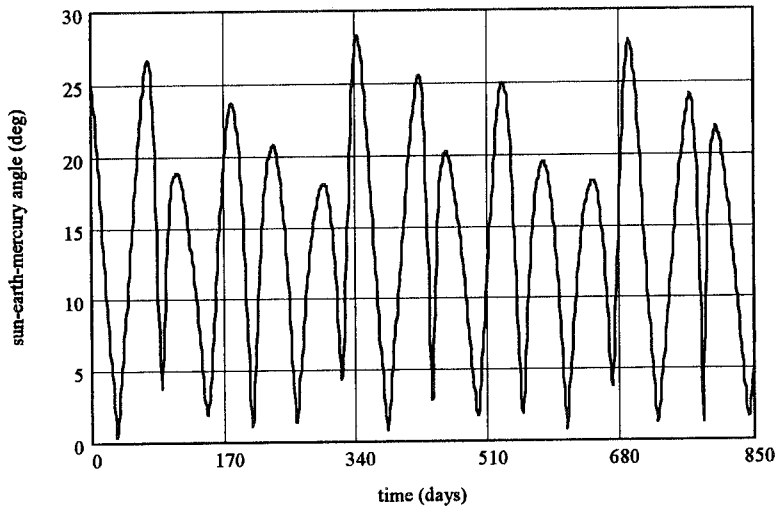

Figure 13.1-2 Evolution of sun – earth - spacecraft angle. Time from epoch 2013/1/13

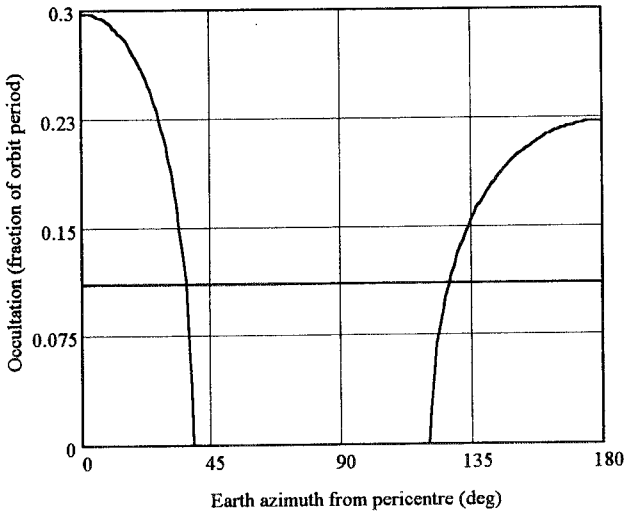

Figure 13.1-3 Pattern of occultation by the planet. The average per year is 11%

13.2 *Earth Telecommunications Subsystem*

The telecommunications subsystem shall establish and maintain the telecommand and telemetry link with the Earth station in all mission phases. The minimum telemetry rate will be determined as part of the study, as a compromise between scientific needs and engineering constraints. Two options are to be traded-off:

- X/X system (X up – X down)
- X/Ka system (X up – Ka down)

as mentioned in Chapter 2.5. The Phase 1 study has mainly concerned the X/X system; the X/Ka band system will be studied and the trade-off will be concluded in Phase 2.

An important factor in the trade-off is the Radio Science experiment on board. The Radio Science requires ranging and Doppler tracking in two frequency bands; hence the on-board system must be dual-band anyway. The payload will provide the Ka part of the system unless the X/Ka option is selected at system level (see the block diagram in Fig. 3.1-1); common elements such as the high gain antenna reflector and the Ka band feed will be provided by the system anyway. The experiment needs a radio-quiet environment [see e.g., CASSINI, for which SNR = 30 dB/Hz was required on the unmodulated carrier (Doppler)]; this means that the experiment will most probably get dedicated time slots at convenient times in the mission.

Fig. 13.2-1 shows a block diagram of the X/X system. The architecture includes a redundant X band transponder (mass = 3 kg, power = 12 W), an X band TWT Amplifier with 20 W RF output power (mass = 3.1 kg, power = 48 W), a high gain antenna (HGA) and two Low gain antennas (LGA). For the HGA, a 1.5 m reflector in a Cassegrain configuration, with the X-band feed in primary focus is proposed. The LGA is an X-band horn with 9.5 dB boresight gain; Fig. 13.2-2 shows the gain pattern.

Standard environmental requirements apply to the units inside the spacecraft, such as temperature between 0-50°C at the baseplate and 20 krad radiation at component level. For SEU immunity, a trade-off between hardware and software immunity is planned (the latter implies automatic reset and restart capability). The reflector, feeds and articulation mechanisms are exposed to the severe external environment of Mercury orbit, and special provisions have to be taken (see below).

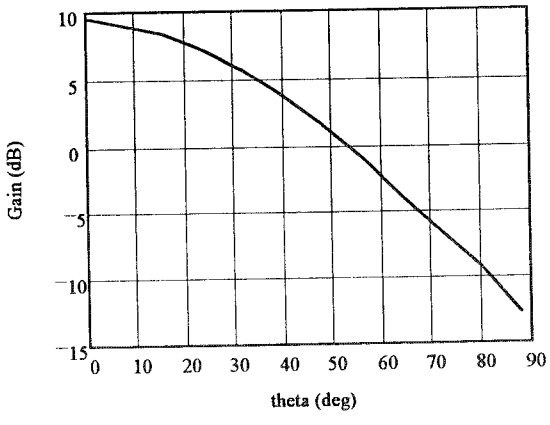

Fig. 13.2-2 Low Gain Antenna Pattern

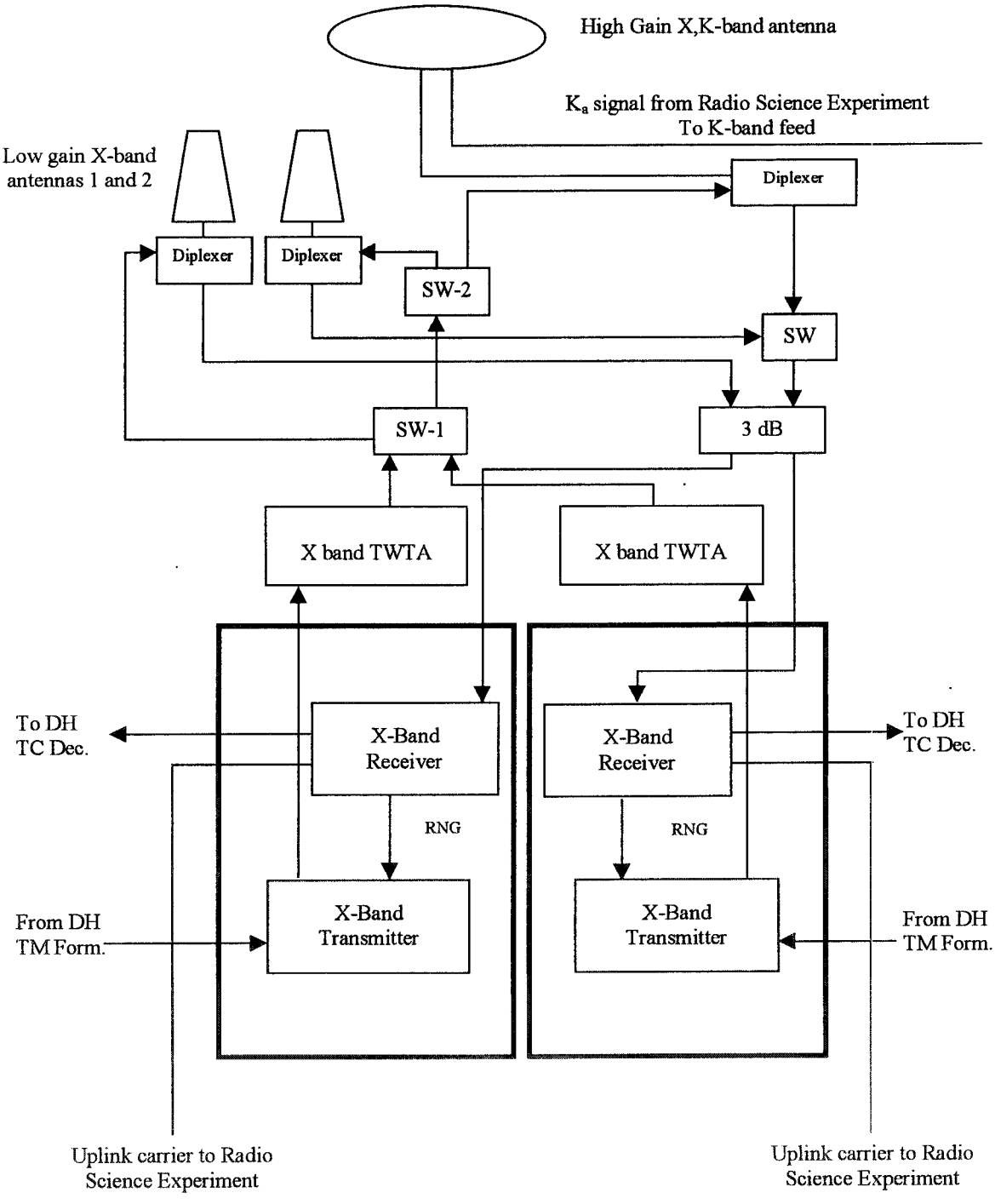

Fig. 13.2-1 X/X Telecommunication system block diagram

13.3 *Operating Modes and Telemetry Rates*

Four high-level telecommunications modes are envisaged:

- LEO mode
- Deep Space HGA mode 1
- Deep Space HGA mode 2
- Deep Space LGA mode

with the characteristics in Table 13.3-1.

	Telecommand	Telemetry	
LEO mode	2 kbit/s	4 kbit/s	standard ranging allowed
Deep Space HGA mode(s) 1	2 kbit/s	27 - 190 kbit/s [1]	Doppler ranging only
Deep Space HGA mode(s) 2	2 kbit/s	12 - 90 kbit/s [1]	standard ranging allowed
Deep Space LGA mode	1-7 bit/s [1]	1-12 bit/s [1]	

[1] 1.48 ÷ 0.55 AU

Table 13.3-1 Telecommunications modes

Deep Space HGA mode 1 is a suppressed carrier mode which could allow a substantial increase of data rate, since high data rate payloads (e.g. cameras) are on board. Only Doppler ranging is possible with this modulation. Deep Space LGA mode is entered in case of on board failures that can affect the orbital attitude. In this case the mode transition shall be commanded by the on board control computer. Otherwise, mode transitions are commanded by the Earth station via immediate or time tagged commands.

As noted, telemetry rates are variable with distance. Fig. 13.3-1 shows the telemetry rate as function of mission time, achievable at X band (8.4 GHz) assuming 20W RF power and 1.4m antenna reflector.

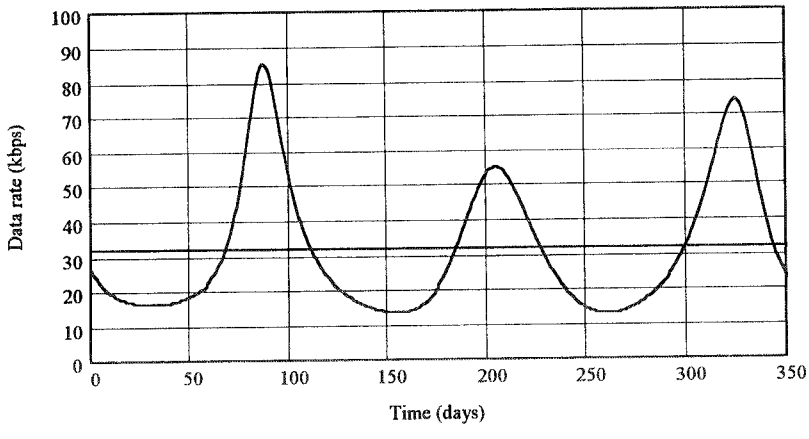

Fig. 13.3-1 Telemetry rate as function of mission time at X band (with residual carrier). The average per year is 31.6 kbps

Ka band telemetry (32 GHz) could allow a substantial increase of data rate. Using a 1.4 m reflector, the data rate could reach 40-300 kbit/s, provided that the receiving antenna is placed in a good site from the meteo point of view. Note that the Ka band telemetry link budgets have been calculated using the data sheet provided by ESA (Ref. 12); significantly better rates could be obtained if the ground antenna G/T is improved with respect to the assumed 56 dB/K.

Table 13.3-2 shows the average data return per year under a number of assumptions as to the communications mode, frequency band, and antenna reflector size, with one and two ground stations. Ka band improves the data return by a factor of at least 3 and could allow implementation of a smaller antenna dish (which could help solve some of the accommodation and articulation problems).

1 Station

	Average Transmit Rate kbit/s	Station Availability %	Occultation %	Total Data Return Gbit	Equivalent Continuous Rate (kbit/s)
X band, 1.4m	31.6	33	11	293	9.3
Ka band, 1.4m	105	33	11	970	31
Ka band, 1.2m	77	33	11	710	23

2 Stations

	Average Transmit Rate kbit/s	Station Availability %	Occultation %	Total Data Return Gbit	Equivalent Continuous Rate (kbit/s)
X band, 1.4m	31.6	66	11	586	18.6
Ka band, 1.4m	105	66	11	1945	62
Ka band, 1.2m	77	66	11	1420	46

Note: 20W RF transmitter power, residual carrier

Table 13.3-2 Average data return per year

13.4 High Gain Antenna Configuration and Design

The proposed antenna configuration is based upon a Cassegrain centred geometry having the X-band feed placed in the reflector primary focus (Fig. Fig. 13.4-1). The optical parameters are :

- Circular Reflector Diameter 1.5 m
- Focal Length 0.63 m
- F/D ratio 0.42 m

The feed aperture is about 60 mm and the overall length (Horn + Septum Polariser) is about 180 mm. The feed is supported in the focal point by means of four struts converging at the feed interface flange. A suitable backing structure is provided to properly support both main reflector shell and feed supporting structure.

Assuming the above mentioned geometrical parameters, the peak directivity is evaluated as D = 41.00 dBi, and the peak gain after losses is G = 38.25 dB (see Table 13.4-1).

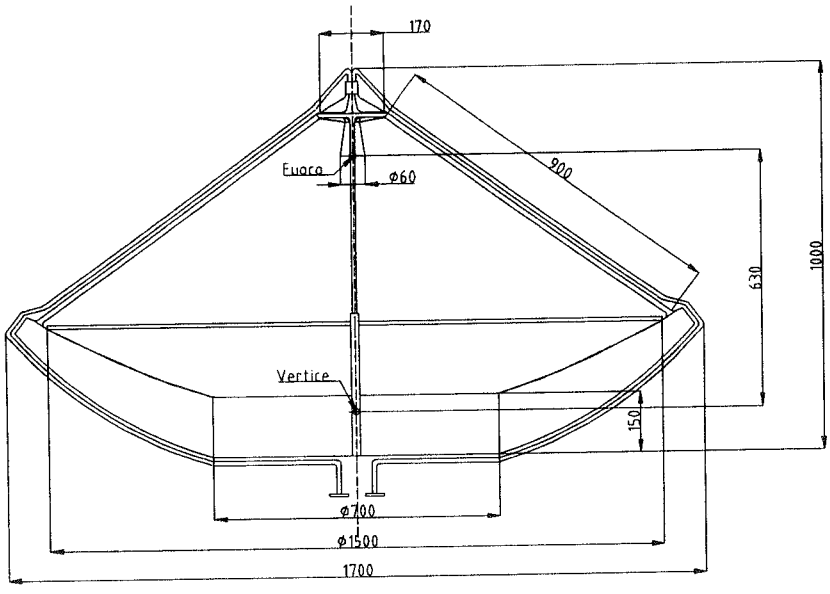

Fig. 13.4-1 Antenna reflector configuration

Peak Directivity	**41.00 dBi**
Efficiency Losses	1.40 dB
Blockage Losses	0.70 dB
Transmission Lines Losses	0.40 dB (WR112-RH)
Feed Ohmic Losses	0.10 dB
Reflector Ohmic Losses	0.05 dB
Thermal Distortion Losses	0.10 dB
Total Losses	**2.75 dB**
Peak Gain	**38.25 dB**

Table 13.4-1 First estimation of reflector losses

The proposed antenna mechanical design is based upon a reflector backing structure essentially made by:

- circular sandwich drum
- four radial sandwich ribs
- reflective sandwich shell
- interface points to antenna steering mechanism
- interface points to antenna hold down and release mechanisms

The feed supporting structure is made of four hollow struts connecting ribs edge sections toward the feed mechanical interface flange. Two wave guides WR112-RH (reduced height) will run from the feed polariser interface toward the reflector back side along the struts and along the radial ribs (structural support to wave guide path). Composite materials will be extensively used for main reflector and backing structure as well as struts; RF components will be manufactured from Aluminium alloy AC061/Alodyne)

The selection of technology and materials to be finalised based on temperature and thermal distortion analysis (Phase 2).

Assuming Carbon Fibre reinforced plastics for composite parts and Aluminium alloy for RF components, using the CASSINI HGA/LGA1 qualified HINCOM white paint protective coating, a preliminary mass budget can be made as shown in Table 13.4-2.

Item	Mass [kg]
Reflector Dish	2.20
Backing Structure	1.02
Reflector/backing Structure Joints	0.80
I/F to Hold Down	0.60
I/F to Steering Mech.	0.35
Struts & Fittings	1.00
I/F to Feed	0.30
Feed	0.35
W/G & Flanges	0.54
Thermal H/W	0.45
Miscellanea	0.75
SUBTOTAL	**8.36**
Uncertainty (10%)	0.84
TOTAL	***9.20***

Table 13.4-2 First estimation of reflector mass budget

Due to the severe deep space mission requirements, special care will be devoted to properly select materials able not only to survive at the high temperature and radiation environment of Mercury but also to guarantee the required performance and operational lifetime.

Alenia Aerospazio has extensively qualified advanced carbon fibre materials and white paint technologies in the frame of CASSINI HGA/LGA1 programme. The thermal range of the CASSINI mission was driven by the distance from Sun (from 0.61 AU to 10 AU) and by mission requirements to adopt the HGA as spacecraft sunshade during Venus flyby (0.61 AU). CASSINI Materials and Processes are qualified from + 180 °C until -238 °C.

In the case of the Mercury Orbiter, higher temperatures are expected and for this reason high Tg materials have to be selected as required by the thermal design. Examples of available resins are shown in Table 13.3-4. The technological investigation will continued and completed in Phase 2 when appropriate resin systems will be selected.

RF components will account for temperature extremes by an analytical evaluation of thermal bandwidths at which components will be operative.

944 Resin System (Cytec-Fiberite) **315 °C Service temperature**

Typical Properties of Cytec-Fiberite 944 Comp. Laminate (8 Harness Satin Fabric)		
	RT	315 °C
Strength MPa	655	NA
Modulus GPa	76	NA

966C Resin System (Cytec-Fiberite) **288 °C Service temperature**

Typical Properties of Cytec-Fiberite 966 C Comp. Laminate (Unidirectional Tape)		
	RT	288 °C
Strength MPa	1400	1400
Modulus GPa	138	124

Table 13.3-4 Examples of high temperature curing materials properties. Processes are, for 177 °C Curing Materials: Standard 121/177 °C Primary Curing Cycles and 220/280 °C Secondary Curing Cycles; for HT Curing Materials: 330 °C one step Curing Cycle

13.5 Subsatellite-Orbiter Data Relay

During the Mercury mission, the Orbiter acts as relay for transmission of Subsatellite data to Earth and reception and forwarding of commands to the Subsatellite. The design of the Subsatellite-Orbiter relay link is subjected to configurational and orbital constraints. The miniaturised Subsatellite allows for limited RF power and small accommodation room; steerable antennas are to be avoided. The Orbiter thermal design does not permit pointing manoeuvres; steerable antennas are a possibility that will only be resorted to if no other solution is found.

A preliminary exercise on the geometry of the inter-satellite link has been performed to determine the mutual distance and viewing pattern. The distance depends on the orbit definition and the initial conditions. For the purposes of the exercise, it was assumed that the ratio of Subsatellite to Orbiter periods of revolution is exactly 1:4, so that the pattern repeats every four revolutions of the Orbiter and one revolution of the Subsatellite. Such a repeat condition could be imposed to make the planning of the communications easier (the 1:4 ratio would follow, for example, if the Subsatellite initial apocentre altitude was taken 400 km lower than in the nominal orbit definition, i.e., 11800 km).

A condition of near-simultaneous periherm passes was also imposed, which appears well suited to the mission profile where the Orbiter is injected into its orbit by a thrust manoeuvre near the pericentre of the Subsatellite orbit. The results of the exercise (duration of communications windows) depend on the assumed phase lag at pericentre. In the exercise, a minimum distance of 100 km at pericentre was arbitrarily taken.

With the above assumptions, the pattern repeats exactly every 9.2 hours, and the max/min distances are 17,000 km / 100 km, as shown in Fig. 13.5-1. Occultations by the planet also occur regularly, in the regions where the distance is maximum.

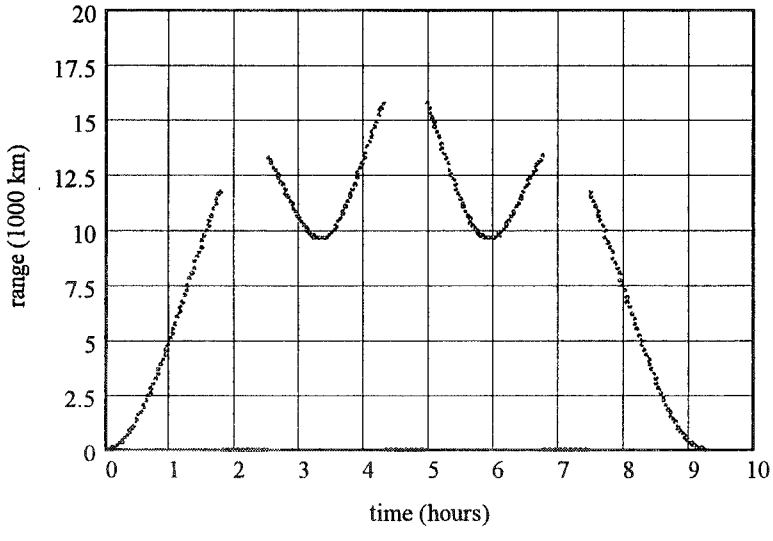

Fig. 13.5-1 Example of distance pattern and occultations

It was assumed that the Subsatellite generates data at 6 kbps constant rate, and all data (including data generated during occultations) must be transferred to Orbiter in 1 Subsatellite revolution. Favourable windows for communications occur when (a) the distance is small and (b) each antenna sees the other close to its peak directivity axis. For the antennas, the following assumptions were made:

a) the same system is implemented on both the Subsatellite and the Orbiter.

b) The Subsatellite has 1 antenna on the North side, and 1 on the South side, with patterns centred on the N-S direction. The Orbiter has 1 antenna on the Zenith side with pattern centred on the Zenith direction.

c) A 'high'-gain UHF (400-430 MHz) antenna is implemented. The peak gain was taken to be 6 dB, with a wide pattern (0 dB at 50°). Antennas of this type are described in the literature (4 dipoles or rail antenna on a 1λ ground plane).

Notice that since the Subsatellite spins about the N-S direction, the antenna pattern must have cylindrical symmetry about that axis; a pattern symmetry axis in any other direction would result in the gain being modulated at the spin frequency.

Under the assumptions described above, two windows are found meeting the conditions of small distance and antenna pattern alignment. The windows are not symmetric because of the assumed phase lag at pericentre; with our assumption the durations are 10' and 20'. Notice that the North and South antennas on the Subsatellite are used in turns. Fig. 13.5-2 shows the first window. With 5W RF power, and if the useful interval is restricted to that with d < 1000 km, a data return ≈1 is obtained provided that a data rate of 110 kbps can be achieved.

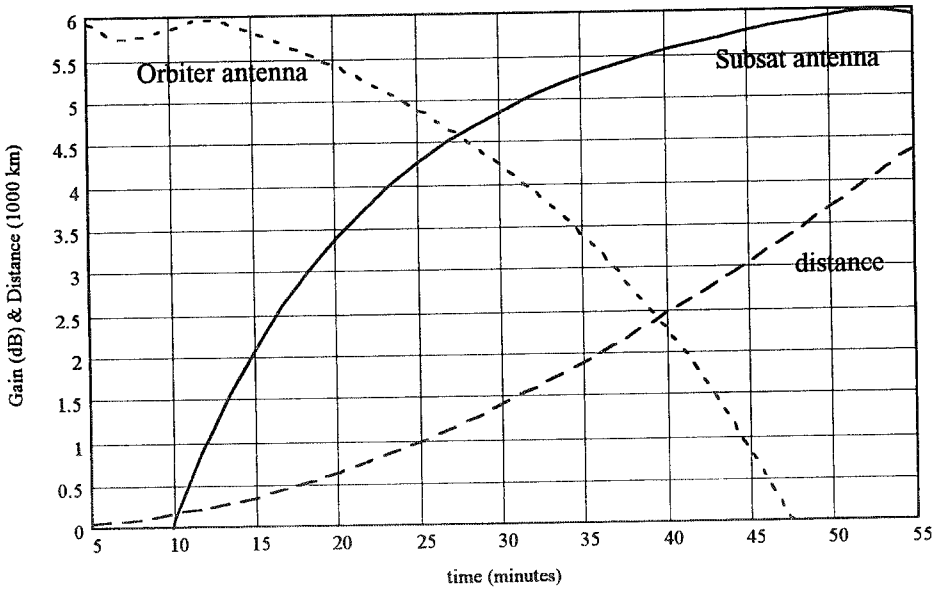

Fig. 13.5-2 Example data relay window

It is concluded that a data return =1 appears possible, with small RF power, provided that

- antennas with sufficient directivity and a large pattern are employed
- data are stored and forwarded to the Orbiter at high speed for short periods.

A repeat condition between Orbiter and Subsatellite periods of revolution will be necessary for communications scheduling. This needs not be 4:1; different ratios could be looked for to meet orbit altitude criteria.

The data relay assembly on both the Subsatellite and the Orbiter would be made up of (Fig. 13.5-3):

- Directive UHF antenna (one on Orbiter, two on Subsatellite)
- UHF Transceiver (Receiver / Demodulator / Transmitter, integrating in a single box all RX and TX functions and the interface with the Data Handling subsystem).

Commonality between Orbiter and Subsatellite units is recommended for cost saving; commonality with other planetary missions is a possibility to be explored.

Antenna and Transceiver designs are to be identified and developed in Phase 2, with particular regard to Subsatellite constraints : small transmit power, configuration. For example, directive UHF antennas will require 1λ-diameter ground plane, that is about 70 cm, nearly as large as the Subsatellite cross section.

Another possibility is an active array antenna on the Orbiter whose direction (and polarisation) is changed as function of time according to a pre-defined profile : both more expensive and more complex, this option will be considered as a last resort.

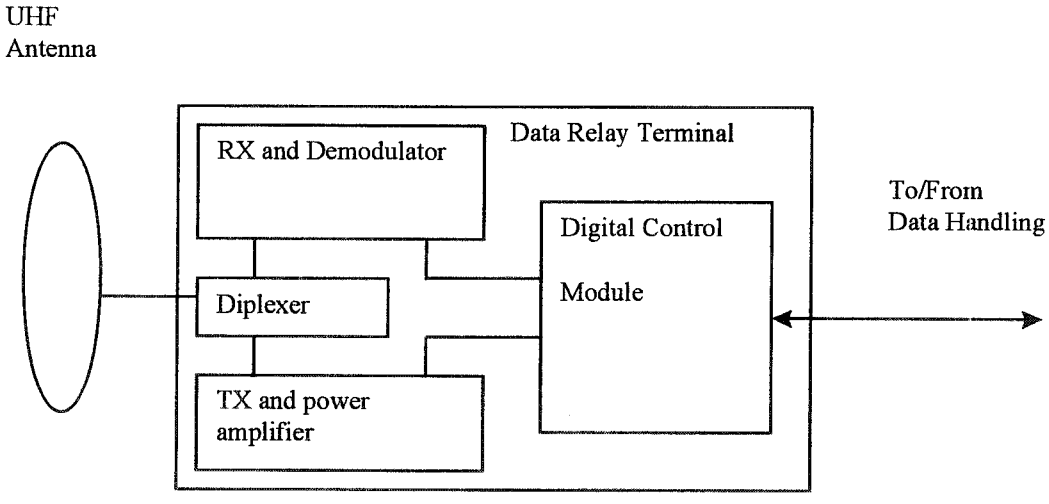

Fig. 13.5-3 UHF system block diagram

14. SYSTEM BUDGETS

14.1 Mass Budgets

The launch mass budgets of the 2010 opportunity, with ion thrusters and SPT thrusters, are presented in Table 14.1-1. The dry mass estimates are taken consistent with the current design assumptions. The system margins are allocated in such a way that the assumptions made in the mission analysis (Table 4.1-1 of Chapter 4) are respected, and the launch mass limit of 2100 kg is not exceeded.

The system margin of the option with ion thrusters is about 10%. This is below the contingency usually requested by ESA at feasibility study level (20%); however, many worst-case assumptions have been made (see for example the remarks in Chapter 5.2.1) and this mass budget should not be considered, at this stage of the study, particularly critical. In the SPT option, 2010 launch, on account of the large Xenon propellant mass, the system margins are smaller (5%), and this case is somewhat more critical.

Margins larger than 20% exist in the 2012 launch option, with either type of thruster, despite the larger Δ v, on account of the Ariane 5 launch performance of 3000 kg. In order to produce a consistent launch mass statement, the mission analysis (see Table 4.1-1, column 3) ought to be updated by introducing the current dry mass estimates, plus 20% system margin.

Item	Total Mass [kg]	
	Ion Thrusters	SPT Thrusters
Subsatellite [1]	59	59
Surface Package [1]	42	42
Orbiter	548	548
Bipropellant Stage Dry	91	91
System margin 1	74 (10%)	37 (5%)
Subtotal 1 (dry mass at Mercury)	**814**	**777**
Bipropellant	286	273
Subtotal 2 (mass after jettison)	**1100**	**1050**
Cruiser Dry	652	571
System margin 2	65 (10%)	29 (5%)
Subtotal 3 (mass before jettison)	**1817**	**1650**
Cruise Propellant	303	460
Launch mass minus adapter	**2120**	**2110**

[1] 20% mass margin taken on raw estimates

Table 14.1-1 System Mass Budget for the 2010 launch opportunity

14.2 Power Budgets

The power budgets of the Orbiter and Subsatellite are in chapters 5.3.2 and 6.13. The cruise phase power allocation, including the spacecraft subsystems power demand, is 10 kW in the option of ion thrusters with grids, and 6.5 kW in the SPT thrusters option.

15. IDENTIFICATION OF TECHNOLOGY DRIVERS

As part of the system study, about 30 items requiring technology development at some level have been preliminarily identified. To set the requirements in perspective, the following tentative classification is proposed:

- Level 1A : Items that are new, or must be substantially re-developed for the Mercury environment, and are critical for mission success according to the design concepts developed up to now
- Level 1B : Items that are new, or must be substantially re-developed for the Mercury environment, but are not critical (alternatives exist) and/or not (yet) part of the current design concepts
- Level 2 : Items with a high degree of inheritance from existing designs, but needing dedicated testing and possibly upgrading to Mercury environment requirements
- Level 3 : Items that do not yet exist as standard qualified equipment, but will emerge anyway (or are likely to) outside of the Mercury project.

Table 15-1 shows the identified items; summary forms with an initial specification of the requirements have been produced. The list is preliminary and the exercise in identification and specification of the requirements will continue in Phase 2.

Subsystem	Item	Category			
		1A	1B	2	3
Thermal	High-Temperature (HT) insulation	•			
	HT Thermal coatings	•			
	Variable surface radiators (Subsatellite)	•			
	HT louvers		•		
	Active cooling systems		•		
	High specular reflectivity OSR		•		
	(Thermal test chamber)				
	(Thermal analysis software)				
Structure and Mechanisms	Two-axis, large amplitude antenna articulation mechanism	•			
	HT boom joints (Subsatellite)	•			
	Structural materials for radiation protection	•			
AOCS	Mercury horizon sensor	•			
Electrical power	HIHT solar cells	•			
	HIHT solar panel	•			
	Solid state thermoelectric converter		•		
	HT battery cells			•	
Electronics	Miniaturised integrated electronics for HT environments (Subsatellite)	•			
Radiofrequency	X/Ka high gain antenna reflector and feeds for HT environment	•			
	Ka band rotary joints	•			
	UHF 'high' gain antenna for HT environments	•			
	X/Ka band transponder				•
	Ka band high power amplifier				•
	UHF transceiver				•
Electric Propulsion	System			•	
	Power conditioning and control			•	
	Thrusters			•	
	Propellant storage and feed system			•	

Table 15-1 Identification of candidate technology development items

16. REFERENCES

16.1 ESA Documents

1. Mercury Orbiter Assessment Study, ESA SCI(94)3, May 1994
2. R. Grard, G. Scoon, M. Coradini, Mercury Orbiter : an Interdisciplinary Mission, ESA Journal Vol. 18, 1994
3. Mercury Cornerstone Interim Report, ESTEC Memorandum ESA/PF/1462.97/GR, August 1997
4. Mercury Cornerstone System and Technology Study, Statement of Work, Appendix 1 to AO/1-3286/97/NL/MS, September 1997
5. M. Hechler, Mercury Orbiter Mission Analysis: On Mission Opportunities with Chemical and Solar Electric Propulsion, ESOC MAS Working Paper No. 389, October 1996
6. Y. Langevin, Ion Propulsion to Mercury: Trade-offs with Gravity Assists, document presented at PM2, 2 July 1998
7. Y. Langevin, PM3 presentation, Sept. 8, 1998
8. M. Hechler, Mercury Orbiter Assessment Study Mission Analysis, ESOC MAS Working Paper No. 345, March 1994
9. M. Hechler, Mercury X/Ka-band from Perth 32 m Antenna, e-mail, Oct. 2, 1998
10. Y. Langevin, M. Hechler, Mercury Orbiter Mission Analysis, Phase 1 Presentation, Oct. 15, 1998
11. H. Evans, Mercury Orbiter Radiation Environment, ESA/ESTEC/ema/ha/Mercury/1, Issue 1, October 2, 1998
12. G. Scoon, Data Sheet on Perth 32 m Antenna, e-mail, April 5, 1998

16.2 Study Notes

SN1 A. Ferri, Mercury Orbiter Payload Assessment, Alenia Technical Note SD-TN-AI-0572, Issue 1, 29 October 1998

SN2 P. Martella, Mercury Cornerstone GNC/AOCS, Alenia Technical Note SD-TN-AI-0601, Draft, 30 October 1998

SN3 D. Rapetti, Mercury Orbiter Thermal Mathematical Model Description and Analysis Report, Alenia Technical Note SD-TN-AI-0600, Issue 1, 29 October 1998

SN4 M. Briccarello, Mercury Subsatellite Thermal Analysis Report, Alenia Technical Note SD-TN-AI-0599, Issue 1, 4 November 1998

SN5 H. Faulks, Mercury Subsatellite Configuration Concepts, Dornier Technical Note MERICS-DSS-TN-001, Issue 1, November 1998

SN6 R. Collina, C. Bruno, Mercury Telecommunications Systems, Alenia Technical Note, in preparation

SN7 R. Campesato, C. Flores, Mercury Orbiter Study Consultancy on GaAs Solar Cells, ENEL Test Report SRI-PDM-LPI-98-3, 24 September 1998

SN8 J. Farrow, MMS-UK Consultancy on Mercury Orbiter Study: Response to Request for Data on UK Ion Thrusters, Merc/JF/1, July 1998

SN9 E. Klinger, Thruster data for Application to Mercury Orbiter Mission, SEP Consultancy Report DI/P/13452/98, 11 August 1998